EARLY CHARACTERIZATION AND PERFORMANCE OF A FLEXIBLE THICK LIFT PAVEMENT

by

Caroline Anne Ellsworth McCarty

A thesis submitted to the Graduate Faculty of
Auburn University
in partial fulfillment of the
requirements for the Degree of
Master of Science

Auburn, Alabama
May 2, 2020

Keywords: Thick lift pavement, Asphalt instrumentation

Approved by

Dr. David Timm, Chair, Brasfield & Gorrie Professor Pavements and Materials
Dr. Benjamin Bowers, Assistant Professor Pavements and Materials
Dr. Adriana Vargas, Assistant Research Professor National Center for Asphalt Technology

THESIS ABSTRACT

Early Characterization and Performance of a Flexible Thick Lift Pavement

Caroline Anne Ellsworth McCarty

Master of Science, May 2, 2020

140 Typed Pages

Directed by Dr. David Timm

The South Carolina Department of Transportation (SCDOT) has recently been experimenting with thick lift paving to increase construction speed and facilitate faster access to traffic. However, there has been limited research and practice with thick lift paving. South Carolina has successfully placed a pavement in two lifts of 4.5 inches thick each. However, what happens if instead of two lifts, only one thick lift is placed? Thick lift paving within this thesis is defined as pavements that were placed in one single lift of 6 inches or greater. Thick lift paving's major concerns and risks include placing a pavement with relatively unknown constructability, cooling curve predictability, and long-term structural and field performance. With such a knowledge gap in this particular construction technique, a test section at the National Center for Asphalt Technology (NCAT) Pavement Test Track was constructed to analyze whether thick lift paving is a viable alternative to conventional multi-lift paving.

There are many benefits to placing a thick lift pavement such as the rapid speed of construction, the elimination of tack between layers, the lower cost of labor with faster construction speed, not switching between mixtures while paving multiple lifts, and reducing the need to rotate construction equipment. Despite these benefits, there are still many concerns with

this procedure due to limited research and unproven implementation. Section S9 at the Test Track was designed as a thick lift pavement in an effort to address some of these concerns.

To ensure that the major benefit of rapid construction was an option, the section was subjected to temperature analysis during construction. The analysis included determining if conventional means of measuring temperature at a construction site was adequate for a pavement of this thickness, if software such as MultiCool was able to predict the cooling curve accurately, and if the cooling rates were fast enough for overnight construction and opening to traffic in the morning. The results illustrated that the best time to pave a thick lift pavement would be in evening, as the lifts laid during this time required the shortest cooling times. Also, the evening in-situ cooling results were more consistent when comparing results to the MultiCool software.

Another major concern is the performance and structural integrity of the section under traffic application. To address this concern, instrumentation such as asphalt strain gauges (ASGs), earth pressure cells (EPCs), and temperature probes were embedded into the pavement during construction. Along with these instruments, weekly field testing was done to analyze the pavement's performance. The analysis during the construction of the thick lift pavement did illustrate that controlling roughness was an issue and this problem was resolved using diamond grinding immediately following the paving. Overall, based on early data from the embedded instruments and weekly field testing, the thick lift pavement did have similar performance to conventional pavements.

Section S9 was subjected to full-scale analysis to ensure that the benefits of utilizing thick lift pavements were viable and that the associated risks could be mitigated. From all construction, cooling curve, field performance, and structural results, it is recommended that thick lift pavements be implemented when speed of construction is a concern. This method could

be utilized to place a single thick lift structure including the surface layer and use diamond grinding to control smoothness. Another strategy would be to use the thick lift construction method to place the base layers in one lift and place a thin wearing layer on top that could improve smoothness without diamond grinding.

ACKNOWLEDGMENTS

I would like to thank my husband and my family for their continuous love and support throughout this graduate program and the writing of this thesis. I am tremendously grateful to my advisor, Dr. David Timm, for his unending guidance and support throughout the writing of this thesis and all my endeavors throughout my time in the Pavements and Materials program. I would like to thank my advisory committee, Dr. Adriana Vargas and Dr. Benjamin Bowers, for their support and guidance. Lastly, I would like to thank the South Carolina Department of Transportation and National Center for Asphalt Technology for their support and assistance on this project and thesis.

TABLE OF CONTENTS

LIST OF TABLES

LIST OF FIGURES

List of Abbreviations

AASHTO	American Association of State Highway and Transportation Officials
AC	Asphalt Concrete
ANOVA	Analysis of Variance
ASG	Asphalt Strain Gauges
DATAQ	Data Acquisition System
ESALs	Equivalent Single Axle Loads
EPC	Earth Pressure Cells
FWD	Falling Weight Deflectometer
GB	Granular Base
HMA	Hot Mix Asphalt
IRI	International Roughness Index
I-FIT	Illinois Flexibility Index Test
LCA	Life Cycle Assessment
LCCA	Life Cycle Cost Analysis
MTD	Mean Texture Depth
NCAT	National Center for Asphalt Technology
NMAS	Nominal Maximum Aggregate Size
NTUA	National Technical University of Athens
NYDOT	New York Department of Transportation
RAP	Recycled Asphalt Pavement
SCDOT	South Carolina Department of Transportation
WMA	Warm-Mix Asphalt

CHAPTER 1

INTRODUCTION

BACKGROUND

Around the United States, the conventional method of constructing a flexible pavement is to have multiple lifts of asphalt concrete (AC) layers typically consisting of one to three inches per lift over a granular base (GB) on top of subgrade soil. This method typically requires different mixtures for the AC layers including a less expensive, lower quality mix for the base layers and higher quality mixtures for the intermediate and wearing courses. Also, the multiple lift system usually requires tack between the layers to ensure proper bonding to eliminate slippage between lifts. Although this method is frequently used and has the advantage of known long term performance, this construction practice also has some disadvantages.

One disadvantage is the need to move equipment frequently to place the layers and tack between lifts. This conventional construction method requires more time and results in more delays for users when utilized on existing roadways and work zones are in place. Based on the extended time it takes to construct pavements, there is a need to develop a faster method of placing pavements.

The South Carolina Department of Transportation (SCDOT) has been investigating methods to reduce pavement construction time, such as thick lift paving. Thick lift pavements speed up the construction process by eliminating the need for multiple lifts and the use of tack between layers. However, with little research into this practice, there are many concerns and unknowns including the constructability, the cooling curve, and the overall pavement performance of thick lift pavements. Questions such as if density and smoothness can be achieved with conventional construction equipment needs to be determined. Also, when traffic

can be applied after construction, dictated by the rate of cooling, is a major concern that needs to be addressed. By placing traffic onto a pavement before the entire lift is sufficiently cooled could lead to premature distresses. Lastly, the performance of the pavement needs to be verified and compared to conventional pavements to ensure this construction method does not impact the quality of the pavement. With little documented about this particular construction technique, the National Center for Asphalt Technology (NCAT) Pavement Test Track constructed a section to analyze whether thick lift paving is a viable alternative to conventional multi-lift paving.

OBJECTIVES

To address the questions and problems described above, the main objectives of this research were:

1. Describe and analyze the construction of a thick lift pavement.
2. Analyze the cooling rate of a thick lift pavement to determine if the cooling time is detrimental to the rapid opening to traffic.
3. Characterize the field performance of a thick lift pavement, both at the surface in terms of distress development and subsurface structural characteristics.
4. Determine if thick lift paving is a viable alternative to conventional construction practices.

SCOPE

To accomplish the research objectives, the SCDOT sponsored construction of a thick lift pavement in 2018 at the National Center for Asphalt Technology (NCAT) Pavement Test Track. Traffic was applied to the section by using multiple heavy triple-trailer trucks. The trucks run

five days a week for multiple hours a day to apply 10 million equivalent single axle loads (ESALs) during the two-year experimental period. For the 2018 research cycle, traffic began on November 26, 2018. This thesis included field performance information from the start traffic until August 31, 2019, capturing approximately 3.815 million ESALs.

The thick lift section, S9, was built in a single lift of 8 inches of AC and 12.5 mm nominal maximum aggregate size (NMAS) using a standard SCDOT mix design. During construction, a thermal probe was embedded to evaluate the in-situ cooling rates, which were compared to cooling analysis software known as MultiCool. In preparation for construction S9, two other trial sections, Trial S9 and N11, were used to help determine if time of day had an impact on thick lift cooling rates. A thermal imaging camera was utilized during construction to monitor the surface temperature of the sections while comparing the results to the inserted thermal probe. Section S9 included embedded instrumentation such as asphalt strain gauges (ASGs), earth pressure cells (EPCs), and temperature probes. These instruments were used to analyze the pavement's structural health over time under accelerated trafficking. Field testing with a falling weight deflectometer (FWD) was utilized to characterize the in-situ material properties. Lastly, a weekly performance measurement was recorded to determine rutting, cracking, and ride quality of the section.

ORGANIZATION OF THESIS

The thesis continues in Chapter 2 with a literature review that describes past research on pavement performance, material characterization, methods of measuring cooling pavements (MultiCool and thermal imaging), and previous work on thick lift paving. Chapter 3 describes the construction process and Section S9 instrument implementation. Chapter 4 provides a

cooling curve analysis on three similar thick lift sections, Section S9, N11, and S9 Trial. The cooling analysis includes comparing the measured cooling rates, evaluating the measured cooling rates against predicted cooling rates provided by MultiCool, and evaluating the in-situ cooling rates against measured surface monitoring temperatures. Chapter 5 discusses the field performance and material characterization as of August 31, 2019 under accelerated traffic. Lastly, Chapter 6 includes conclusions and discusses the viability and practical options of using thick lift paving as an alternative to typical paving practices.

CHAPTER 2

LITERATURE REVIEW

INTRODUCTION

The conventional method of constructing an AC pavement includes placing a multiple successive AC layers over a GB over a soil subgrade. The AC layer lifts are typically between one to three inches thick. However, the South Carolina Department of Transportation (SCDOT) has been experimenting with full-depth pavement reconstruction. This method consists of building the entire AC depth in one single thick lift. A schematic comparing the two approaches is shown in Figure 2.1.

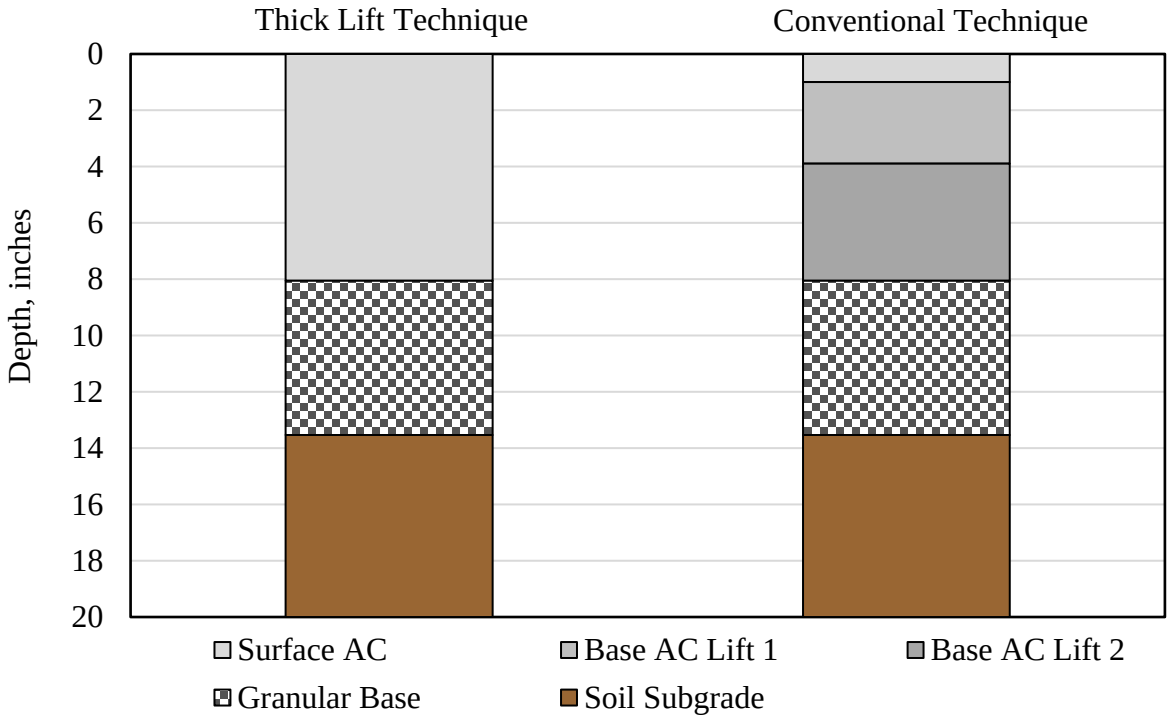

FIGURE 2.1: Cross-Section of Two Methods – Thick Lift and Conventional.

However, there has been limited research with this construction strategy, and many questions need to be answered before implementing this research into practice. The issues

include pavement compaction, mat cooling, and long-term pavement performance which will be explored in this chapter.

THICK LIFT PAVING IN THE PAST

The leading reason why the SCDOT would like to research and ultimately incorporate thick lift paving into their practice is to increase the speed of construction. This method eliminates the need for tack between the layers and decreases construction time as there is no waiting between pavement layers for the results of quality control testing before proceeding to the next lift, switching between mixtures, or need to repeatedly move equipment. The goal of this method is to be able to close down the road for one night and reopen to traffic the next morning. Thick lift paving will reduce delays and traffic caused by construction.

The SCDOT has already started to incorporate this method, successfully placing two 4.5-inch single lifts in a single night that were turned over to traffic the next morning. This allowed the contractor to avoid late penalties for not having the highway opened in time (For Construction Pros, 2016). The capability of quick turnaround to traffic offers a significant economic advantage over traditional paving methods including the reduction of traffic delays, labor expenses, amount of material such as tack, and the avoidance of late fees.

There have been a few studies that have been conducted that research the method of placing a single thick lift pavement. A case study in Germany researched the implications of replacing the multiple lifts of base layers into one thick lift base course. However, this case study placed the base and surface course simultaneously. The wearing course was approximately 0.75 inches, but the base course thickness totaled around 8.5 inches. Figure 2.2 depicts the two types of cross-sections that were compared during this experiment.

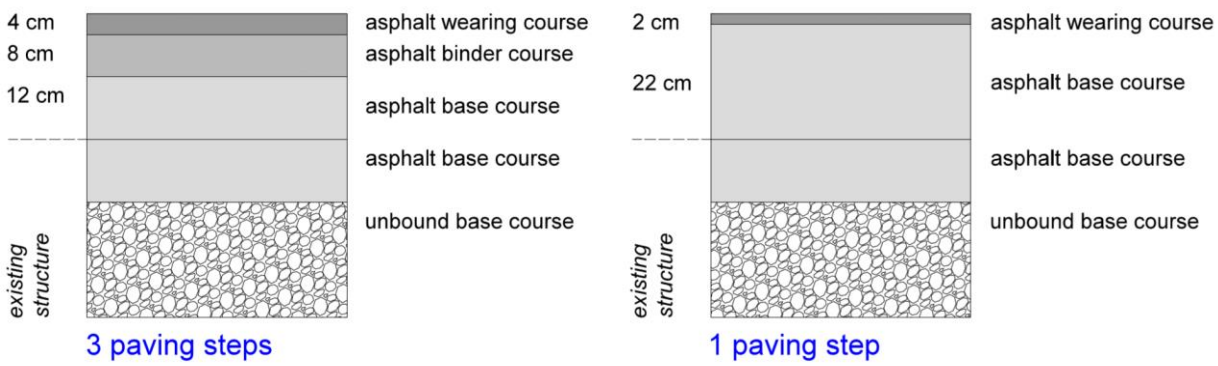

FIGURE 2.2 Cross-Sections Used with German Study (Tielmann and Böhm, 2016).

The placement of both layers required a Dynapac paver that is outfitted with two material hoppers and two screeds that are concurrently in use during construction. The first screed placed an already compacted binder course. The machine used tampers, vibrations, and a final pressure plate to compact the base course before placement. After, the second screed immediately placed the wearing course (Moore, 2011). The results of the simultaneous paving can be viewed below in Figure 2.3.

FIGURE 2.3 Thick Lift Pavement During Construction (Tielmann and Böhm, 2016).

The thick lift pavement's performance was compared to a pavement that was constructed in the conventional layered method. The results illustrated that the performance of the pavements was similar, but a large problem was identified for the thick lift pavement. With a significant

depth of mix to place at once, controlling smoothness for the thick lift pavement was difficult (Tielmann and Böhm, 2016). Shown in Figure 2.4 is the transversal roughness of the thick lift pavement. German codes specify a maximum limit of 4-6mm in any position. As seen in the results, the middle of the pavement had minimal problems. However, the edge regions of the pavements experienced considerable unevenness. Figure 2.5 depicts the edge region's unevenness after compaction.

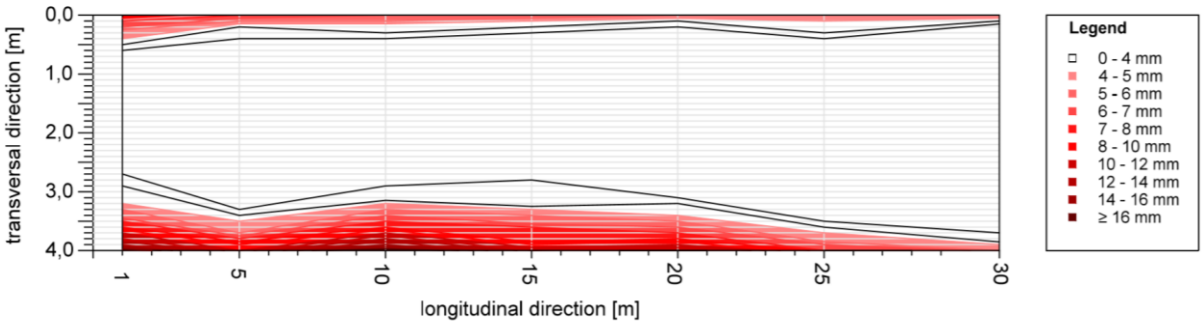

FIGURE 2.4 Transverse Evenness Results (Tielmann and Böhm, 2016).

FIGURE 2.5 Outside Region Smoothness Problem (Tielmann and Böhm, 2016).

In 1972, the New York State Department of Transportation (NYDOT) produced a thick lift pavement study for similar reasons and to answer similar questions as the current SCDOT. The reasons included increased speed of construction and determine if the NYDOT maximum AC thickness requirement of 4 inches per layer is overly conservative. This NYDOT study was

conducted on base courses and not the surface layer. This study answered major questions about thick lift paving such as the ability to acquire adequate density and if thick lift paving produces similar temperature and cooling results as conventional paving methods (Vyce et. al, 1972).

This study used a 1.2-mile interstate road to compare multiple layer paving technique and thick lift paving. The control sections included two 3-inch lifts of AC and the thick lift sections included one lift of 6 inches. Each section was subjected to a cooling analysis by embedded thermocouple dowel within the hot mat and density analysis. The temperature comparison can be viewed below in Figure 2.6.

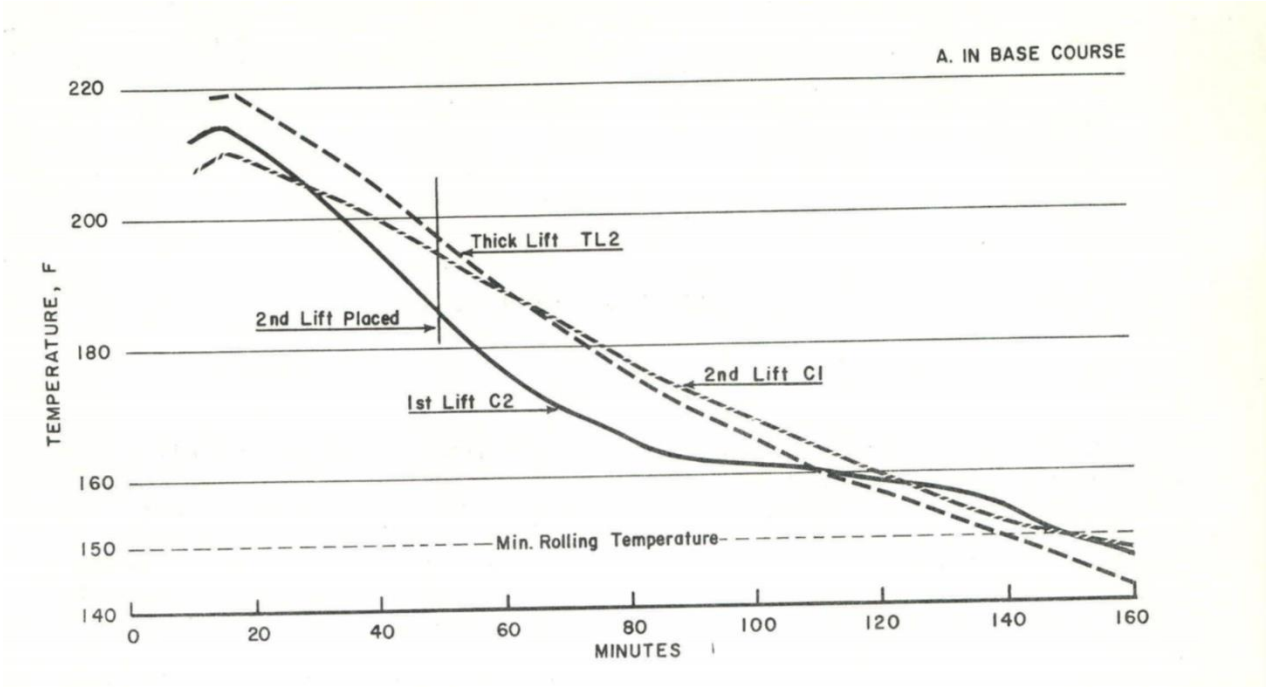

FIGURE 2.6 NYDOT Thick Lift Paving Temperature Analysis (Vyce, 1972).

As seen above, the control and the thick lift pavement produced similar cooling results. The NYDOT study specifically noted that the center of the bases maintained a temperature above 150°F for approximately 2.5 hours. This amount of time was determined to be more than adequate for sufficient rolling and compaction time. Overall, the study determined that temperature cooling time in thick lift paving should no longer be deemed a concern.

Achieving adequate density was the next major concern for the NYDOT with regards to thick lift paving. Shown below in Table 2.1 is the density results of the thick lift pavement and the control pavements. The NYDOT cut cores for the control and thick lift pavement sections. Also, it should be noted that the cores were cut into thirds to determine if the thick lift pavement was producing similar densities throughout the depth of the pavement.

TABLE 2.1 NYDOT Thick Lift Pavement Density Results (Vyce, 1972).

CORE DENSITIES

Sample	Thick-ness, in.	Bulk Density, pcf					
		Total	Top Third	Middle Third	Bottom Third	Top Half	Bottom Half
A. CONTROL							
050A	7	130.4	119.2	134.2	137.9	--	--
050B	6-3/8	136.0	--	--	--	134.2	136.7
050C	5-5/8	137.3	--	--	--	--	--
200A	7-1/4	133.5	--	--	--	--	--
200B	7	133.5	131.7	139.2	132.9	--	--
200C	6-7/16	134.2	--	--	--	134.2	136.0
350A	7-1/16	127.9	--	--	--	119.2	132.9
350B	6-1/2	134.8	--	--	--	--	--
350C	5-3/4	136.7	134.2	140.4	137.3	--	--
Average	6-5/8	133.8	128.3	137.9	136.0	129.2	135.5
B. THICK LIFT							
100A	6	137.3	--	--	--	139.2	134.8
100B	5-15/16	142.3	139.2	147.3	139.2	--	--
100C	5-13/16	128.5	--	--	--	133.5	127.9
250A	6-1/16	126.1	--	--	--	--	--
250B	6-3/4	132.9	--	--	--	136.7	131.7
250C	6-1/2	131.7	132.3	137.3	125.4	--	--
400B	6-1/8	134.2	131.0	141.6	136.7	--	--
Average	6-1/8	133.3	134.2	142.1	133.7	136.5	131.5

As seen above, the densities of the thick lift pavement and the control pavement sections were very similar. However, as seen above in Table 2.1 the middle third of the cores from both the control and the thick lift paving cores had the highest densities. Overall, the NYDOT determined that the densities achieved throughout the pavement for the thick lift pavement

sections was considered to be adequate. The findings from this NYDOT study determined that thick lift paving has the capability of achieving adequate density and provide similar cooling times as conventional pavements.

CONCERNS OF THICK LIFT PAVING

Compaction and Mat Cooling

There are three major concerns in regard to thick lift paving, including the construction and compaction of the structure, the cooling of the mat, and the long-term performance. All three concerns are interrelated and have major impacts on whether this construction method is practical. Compaction has a major influence on the long-term performance of the pavement. If the pavement is under compacted, the structure can have higher susceptibility to moisture and air damage. If the pavement is over compacted, distress such as rutting, flushing, or bleeding could occur (Plati et al., 2014; Vargas-Nordcbeck and Timm, 2011). Therefore, achieving adequate compaction is necessary to create a well-performing structure. Although there are many factors that contribute to the hot mix asphalt (HMA) density, the mat temperature has the most significant influence (Plati et al., 2014). As mix cools and the binder stiffens, it becomes more challenging to reach density even with more applied compaction effort (Vargas-Nordcbeck and Timm, 2011). Therefore, understanding the cooling curve of the structure is key to achieving well-performing pavement.

A study conducted by the National Technical University of Athens (NTUA) addressed the use of infrared thermography for assessing HMA paving and compaction. This study specifically investigated the benefits of thermal imaging. The first major benefit of thermal imaging is that this is a non-destructive method that can be viewed in real-time. Thermal imaging

provides an expansive look at overall mat temperature, helping visualize thermal segregation. Also, thermal imaging can be used in lieu of conventional temperature guns as shown in Figure 2.7.

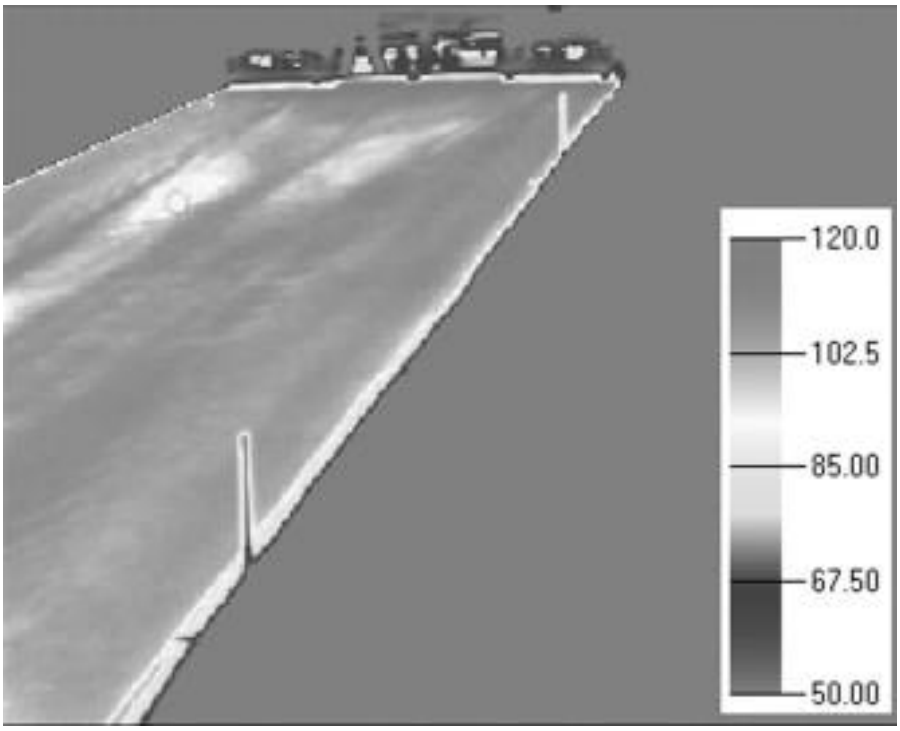

FIGURE 2.7 Thermal Image (Plati et al., 2014).

The thermal image relays a temperature that can then be used as a parameter in the MultiCool software. This research compared MultiCool simulated cooling curves to a measured cooling curve determined by a thermocouple probe (Plati et al., 2014). This experiment used a section that was 3.5-inches of AC pavement, 1.5-inch wearing course and 2-inch base course, over a GB on top of a soil subgrade. The results of this study concluded that the thermal imaging camera, along with the MultiCool software, would be a good prediction to the actual cooling rates as shown in Figure 2.8. However, this experiment was performed on a typical mixture placed with conventional construction methods.

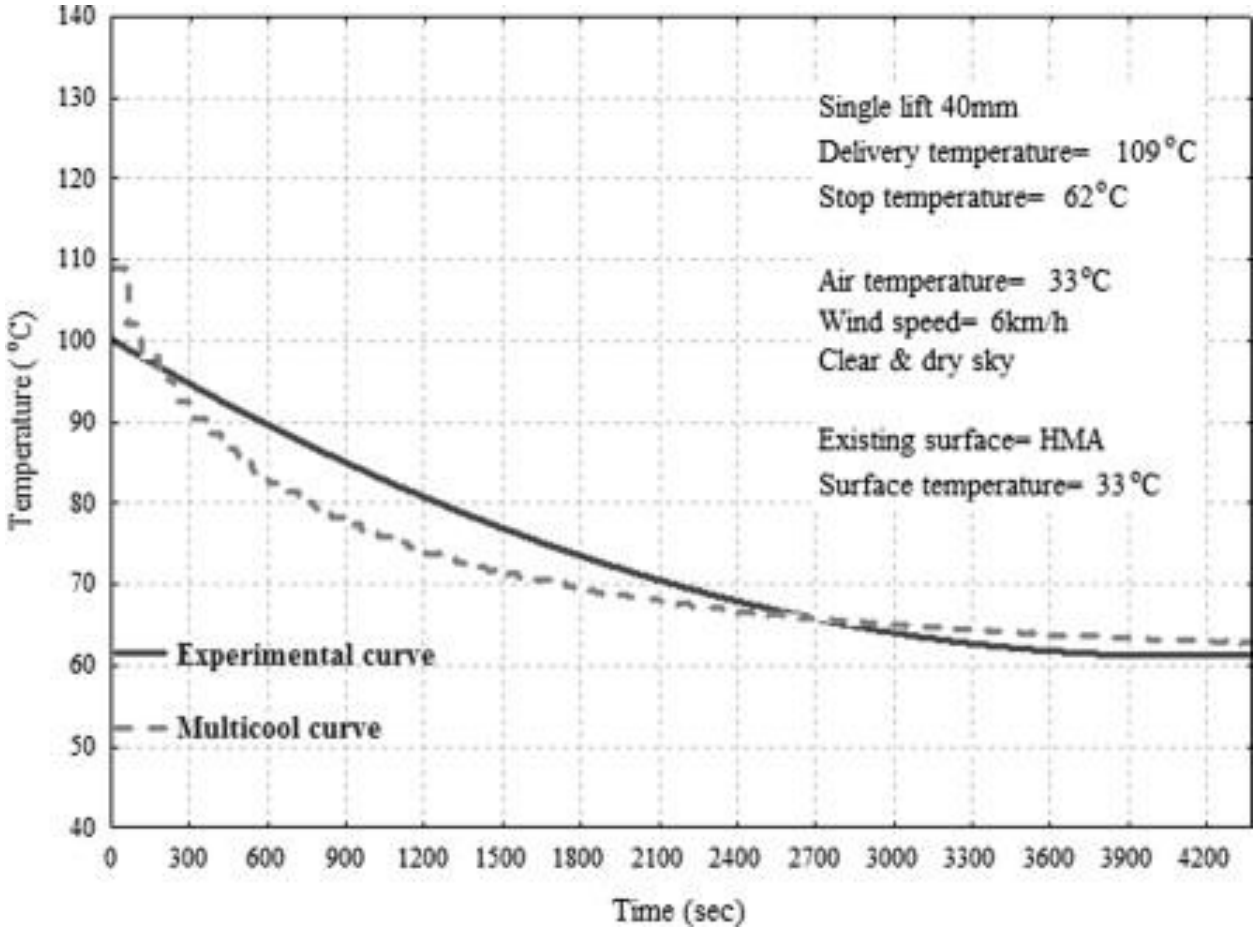

FIGURE 2.8 MultiCool versus Measured Cooling Curves (Plati et al., 2014).

NCAT conducted a study to look at the validity of the MultiCool software when dealing with unconventional mixtures, including warm mix asphalt (WMA) and high reclaimed asphalt pavement (RAP) mixtures as shown below in Table 2.2 (Vargas-Nordcbeck and Timm, 2011).

TABLE 2.2 NCAT MultiCool Verification Test Sections (Vargas-Nordcbeck and Timm, 2011).

Section Number	Description
N5	Shell Thiopave—sulfur-modified WMA
N6	Shell Thiopave—sulfur-modified WMA
N7	Kraton—7.5% styrene–butadiene–styrene modified asphalt
N10	50% RAP HMA
N11	50% RAP WMA
S8	Control with permeable surface
S9	Control
S10	Foamed WMA
S11	Additized WMA
S12	25% asphalt replacement with Trinidad Lake Asphalt pellets

The unconventional mixtures were all placed in three separate lifts that had a maximum lift thickness of three inches. The results demonstrate that MultiCool can be a good predictor of the cooling curve for conventional and unconventional pavements as shown below in Figure 2.9 and Figure 2.10. Figure 2.8 illustrates a control conventional section MultiCool comparison and Figure 2.10 depicts a section that had two components of unconventional pavements including high RAP and the WMA technology.

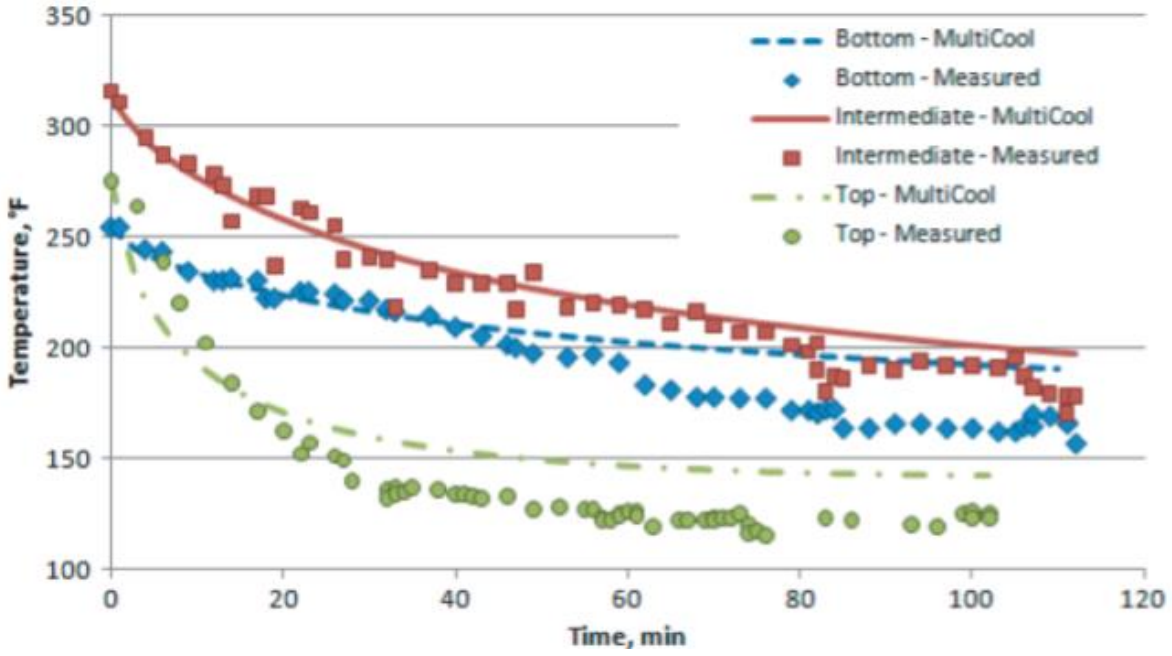

FIGURE 2.9 NCAT Conventional MultiCool Comparison (Vargas-Nordcbeck and Timm, 2011).

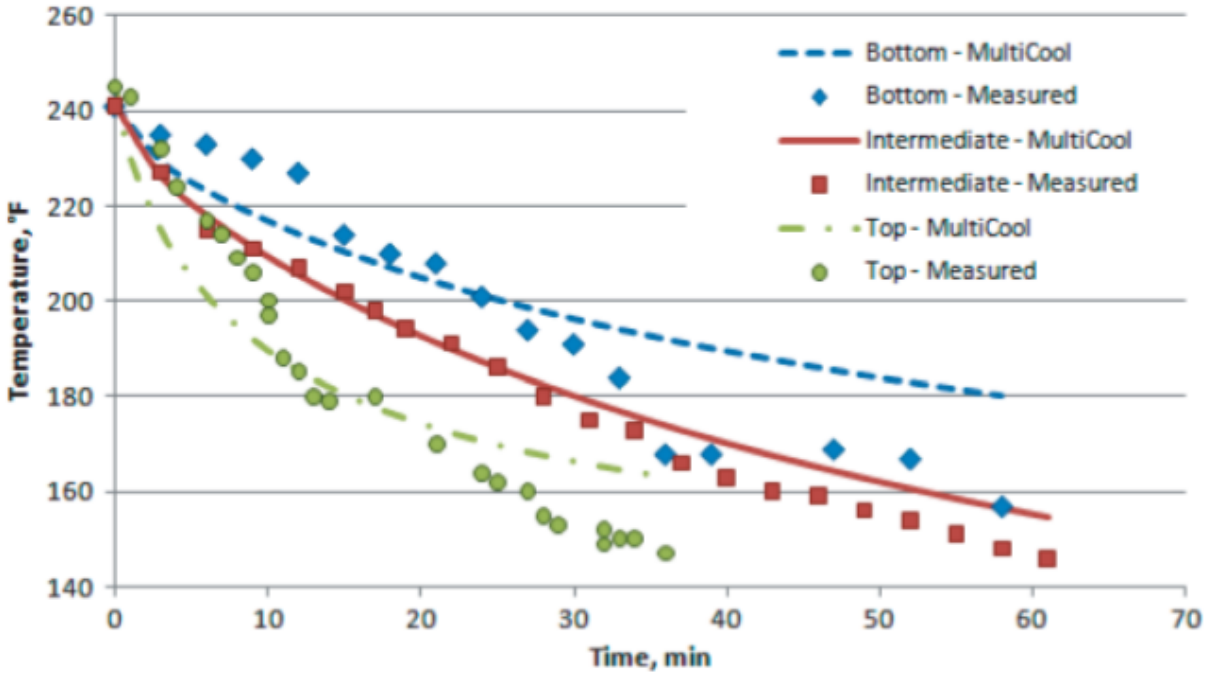

FIGURE 2.10 NCAT Unconventional MultiCool Comparison (Vargas-Nordcbeck and Timm, 2011).

However, the results also determined that the lift thickness and initial mix temperature are the most influential factors to cooling curves (Vargas-Nordcbeck and Timm, 2011). This study determined that MultiCool over predicted the mix temperature. Shown below in Figure 2.11 is the temperature differential results discovered during this experiment. The maximum temperature differential was determined to be 18°F.

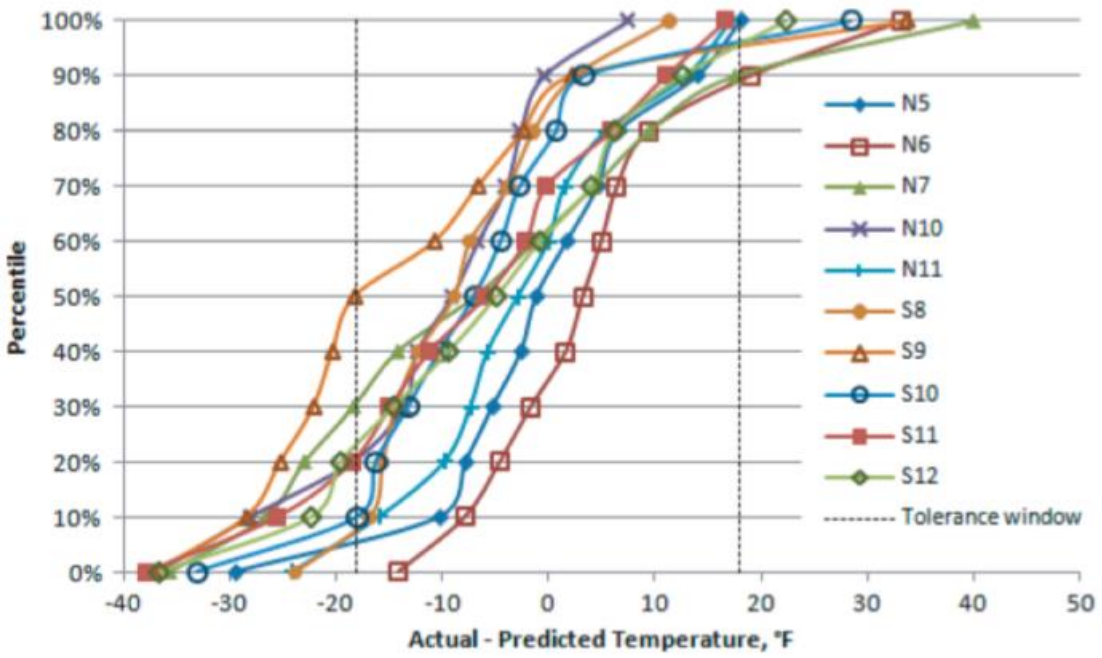

FIGURE 2.11 NCAT MultiCool Verification Temperature Differential (Vargas-Nordcbeck and Timm, 2011).

Based on the two cooling curve studies, the MultiCool was determined to be successful for predicting cooling curves for unconventional and typical pavements. As stated previously, thickness is a major component to the effectiveness of MultiCool. Therefore, a major question that needs to be answered is: How will a pavement that is two to three times the thickness compare to the positive thermal imaging and MultiCool results from the two case studies?

Long-Term Performance and Field Characterization

The last major concern when looking into a new pavement implementation method is how the final structure will perform long term and will it act similar to conventional pavements? To analyze the performance of the pavement, a structural characterization analysis and field performance surveys should be incorporated into the full-scale research study. At the NCAT Test Track, structural analysis and field characterization has been a major research subject since the second research cycle in 2003. The Test Track began a structural experiment in 2003 to investigate two major components. The first was to study the dynamic pavement response of emerging and promising technologies, methods, or mixtures under live truck loading (West et al., 2018; Timm et al., 2006). The second consideration was to determine if the sections also "support the evaluation, calibration, and validation of mechanistic-empirical pavement design methodologies" (West et al., 2018).

The mechanistic design experiments utilized embedded instrumentation such as ASGs, EPCs, and temperature probes to analyze the pavement responses under accelerated traffic (Timm et al., 2006). There are two critical locations that are correlated to two major distresses of fatigue cracking and rutting. Cracking can be correlated to the strain at the bottom of the AC layer (Timm et al., 2006), while rutting corresponds to the compressive stress at the top of the GB layer.

During each test cycle that studied structural health of the sections, the ASGs were used to monitor the strain level and the EPCs were utilized to observe compressive stresses. Figure 2.12 and Figure 2.13 are typical AC pavement's seasonal trends in regards to tensile microstrain and compressive stress, respectively. The results are taken from 2012 Test Track cycle. The expectation, as shown below in the following two figures, is that the microstrain and the

compressive stress will be temperature dependent (West et al., 2012). The exponential relationship between temperature and microstrain and temperature and compressive stress is determined from the power function equation shown in Equation 2.1.

$$\varepsilon_T = k_1 e^{k_2 T} \qquad \text{(Equation 2.1)}$$

Where,
ε_T = measured tensile microstrain or compressive stress
k_1, k_2 = regression coefficients (see values in Figure 2.11 and Figure 2.12)
T = mid-depth pavement temperature, ^oF

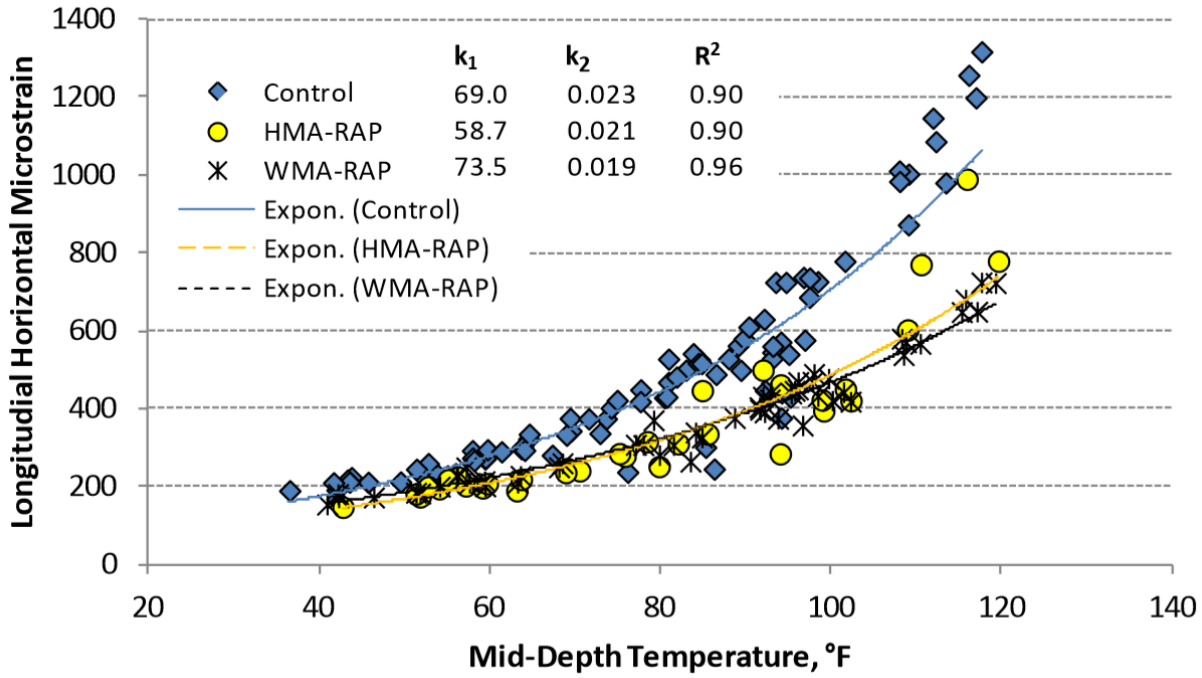

FIGURE 2.12 Past NCAT Microstrain Trends (West et al., 2012).

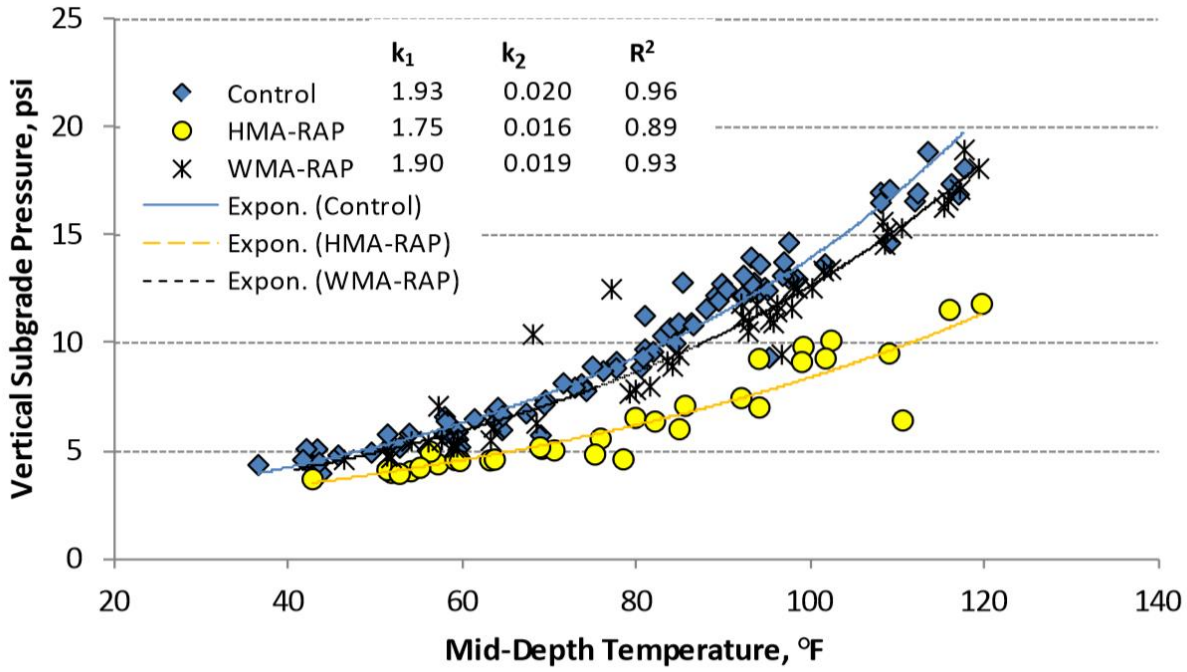

FIGURE 2.13 Past NCAT Compressive Stress Trends (West et al., 2012).

NCAT also utilized weekly field characterization tests within the structural analysis. The weekly field characterization includes visual crack inspection, determining the average rut depth, and determining the International Roughness Index (IRI). Shown below in Figure 2.14 a, b, and c, are examples of crack mapping, rut depth over time, and the display of IRI over time. It should be noted that mean texture depth (MTD) was also included in the past Test Track cycle analysis (West et al., 2012).

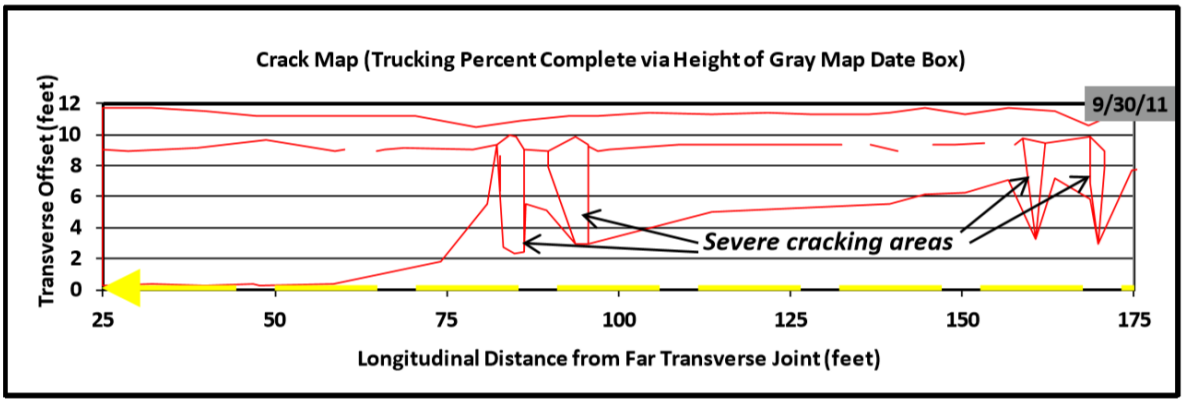

a) NCAT Crack Map

b) NCAT Rut Depth Chart

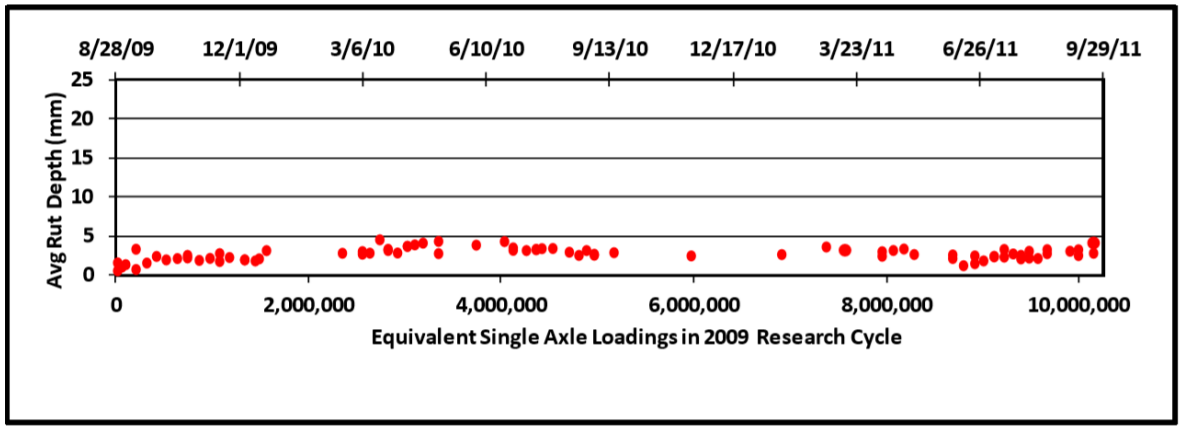

c) NCAT IRI Chart

FIGURE 2.14 Weekly Field Test Monitoring Charts (West et al., 2012).

Lastly, routine FWD testing concluded the in-situ structural characterization. The FWD was used for a few reasons including analyzing how seasonal trends and temperatures impact the AC stiffness and how pavement damage effects the AC modulus (Timm and Priest, 2006). Shown below in Figure 2.15 is an example from the 2012 Test Track cycle of typical FWD data that illustrate AC modulus-temperature dependency and the typical AC modulus patterns. Similar to the microstrain and compressive stress relationship with temperature, the AC modulus utilizes an exponential power function to portray the correlation with temperature shown below in Equation 2.2.

$$E_{AC} = k_1 e^{k_2 T} \quad \text{(Equation 2.2)}$$

Where,
E_{AC} = asphalt concrete modulus, ksi
k_1, k_2 = regression coefficients (see values in Figure 2.14)
T = mid-depth pavement temperature, °F

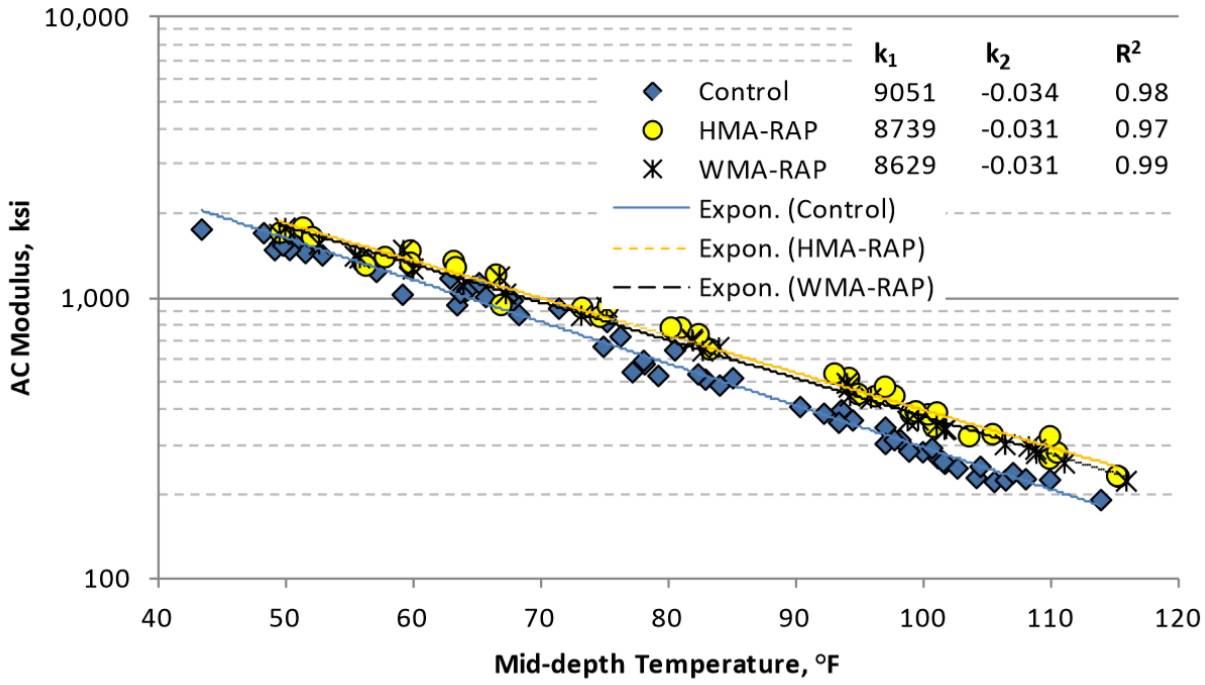

FIGURE 2.15 NCAT FWD Backcalculated AC Modulus Graphical Trends (West et al., 2012).

All strategies including the ASGs, the EPCs, the temperature probes, the weekly field testing, and the biweekly FWD testing were proven to be useful during the structural characterization of past test track sections.

SUMMARY

This literature review briefly discussed the reasons and benefits for researching thick lift paving as well as the past studies and implementation of thick lift paving. Examples of a few thick lift studies include the SCDOT two 4.5-inch lift pavement, the German base course study, and the NYDOT base course study. Also, this synthesis deliberated the major concerns of thick lift paving including compaction, mat cooling, and long-term performance and past studies that incorporate conventional and unconventional pavement test sections regarding three significant issues. However, none of the case studies regarding the three major concerns researched a one thick lift pavement that combined the wearing and base course into a single layer. Lastly, the importance of pavement response analysis and field characterization was discussed to predict pavement performance and potential distressing. Based on the literature review, research into this method is still need and a full-scale analysis of a thick lift pavement is necessary to verify the practicality of implementing thick lift paving.

CHAPTER 3

CONSTRUCTION

INTRODUCTION

Although there has been substantial research, including practical applications, relating to the construction of two to three lift AC pavements, investigation of the constructability of a single thick lift pavement is still necessary. Section S9 was used to answer questions that surround single thick lift pavements such as structural integrity, pavement performance, and the overall quality control during construction. Pavement instrumentation including ASGs, EPCs, and temperature probes were embedded within S9 to enable structural integrity characterization over time under accelerated trafficking. A trial section was constructed the day before the construction of S9 for last minute checks and adjustments, as necessary, of the construction process and mix design. Figure 3.1 illustrates the as-built cross-section of Section S9 including the depths of embedded instrumentation.

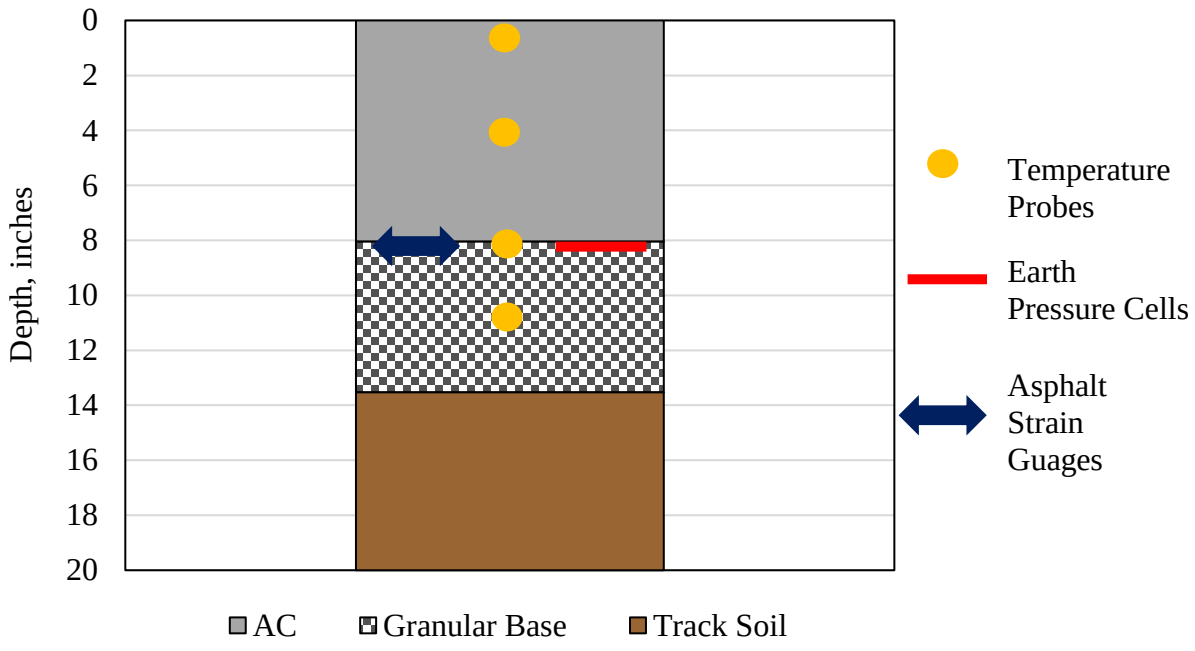

FIGURE 3.1 Section S9 As-Built Cross-Section.

This chapter will discuss the instrumentation used within Section S9, the calibration procedure for the ASGs and the EPCs, how the instrumentation was installed, and the overall construction of Section S9.

PAVEMENT INSTRUMENTATION

The ASGs, EPCs, and temperature probes were used within S9 to measure the pavement response to applied traffic and varying environmental conditions. The instrumentation process was consistent with past NCAT Test Track construction cycles and was implemented into the 2018 research cycle with a few modifications (Timm et al., 2009). The adjustments for the 2018 Test Track cycle included adding local calibration for the ASGs and modifying the arrangement and orientation of gauges.

Twelve ASGs and two EPCs were placed on top of the GB and at the bottom of the AC layer to measure the structural response of the pavement. A bundle of thermistor probes was assembled to measure temperatures at the top, middle, and bottom of the AC as well as 3 inches into the GB layer. This was done to capture the temperature gradient through the depth of the pavement. The ASGs were Geocomp's 4"x6" 2013 Model with 30-foot leads. The EPCs were Geokon's model 3500-2-250KPA semiconductor with 30-foot leads. Lastly, the thermistors were Campbell-Scientific's 108-U-L30-PT model with permanent temperature measurement and type J thermocouples. Figure 3.2 a, b, and c depict the ASGs, thermistors and EPCs used in S9, respectively.

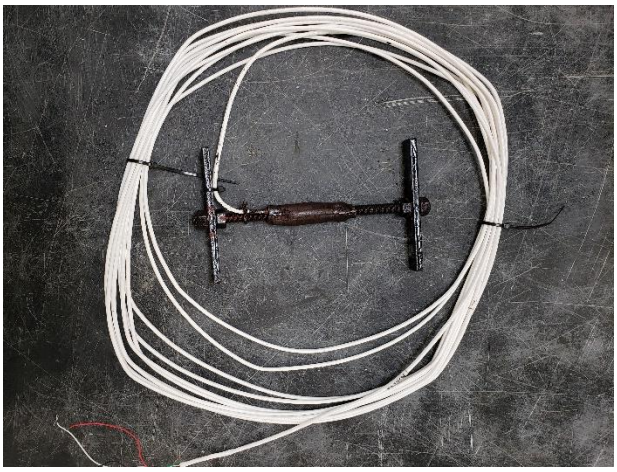

a) Geocomp ASG

b) CSI Temperature Probe Bundle

c) Geokon EPC

FIGURE 3.2 Pavement Instruments.

Figure 3.3 illustrates the instrumentation plan view. The ASGs were assigned to channels 1 through 12 within the instrumentation layout in Figure 3.3 and the EPCs were assigned to channels 13 and 14. The gauges were centered over the outside wheel path to ensure capturing peak responses of multiple truck passes while taking natural wheel wander into account. The gauge array pictured in Figure 3.3 had gauges centered at 2 foot spacing with the exception of gauge 14 which was centered at 4 feet from the nearest ASG to provide sufficient spacing for the pressure cell transducer. Also, based on past Test Track measurements illustrating that the maximum tensile strain came from responses in the direction of traffic (i.e.,

longitudinal strain), the ASGs were setup to only measure in this direction for this test section (Timm and Priest, 2008). This change was one of the two variations from past NCAT test track structural study research cycles.

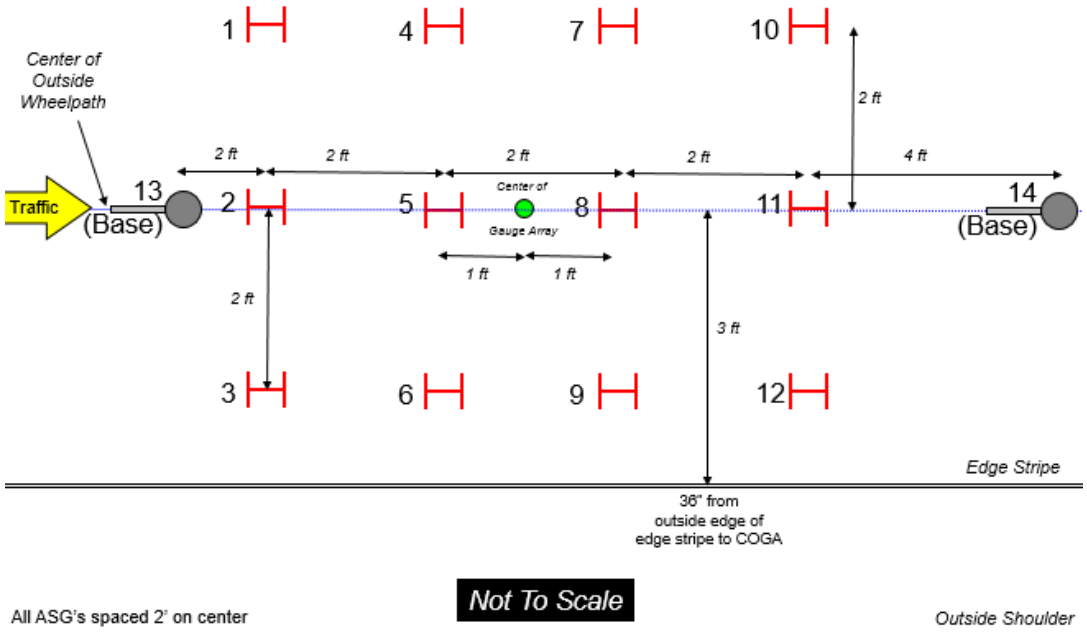

FIGURE 3.3 Section S9 Gauge Array.

Calibration Procedure

As stated above in the pavement instrumentation section, the ASG local calibration procedure was newly added to Test Track instrumentation preparation protocols. The procedure began with ensuring gauge functionality. The strain gauges were wired into the data acquisition system (DATAQ) to record their baseline voltages. While connected to the DATAQ, the gauges were pushed into compression and pulled into tension by hand to ensure the gauges responded with the proper sign (push = negative or compression; pull = positive or tension). Once basic functionality was established, each ASG was mounted into the calibration jig as shown in Figure 3.4a and Figure 3.4b. Pre-strain was then applied to remove any slack from the ASG and

mounting brackets. Next, a digital caliper (Figure 3.4c) was used to measure the inside-to-inside lengths of both sides of the gauge. After the measurements were taken, a potentiometer was attached and used to adjust the baseline of the ASG while mounted in the calibration jig back to the original baseline voltage found when the ASG was wired into the DATAQ but not under any external strain. Once back to the baseline, the crank on the calibration jig was used to put the ASG into tension by a displacement of approximately 0.02 mm increments in tension until the ASG read a voltage near +5V. The applied displacements were recorded from the digital readout on the calibration jig as pictured in Figure 3.4d. The ASG was then unloaded by approximately 0.02 mm increments until the displacement decreased to 0 mm. The displacement measurements from 0 mm were then used to calculate strain. The process of loading and unloading was repeated as a reliability check. Figure 3.4e illustrate the ASG calibration set up.

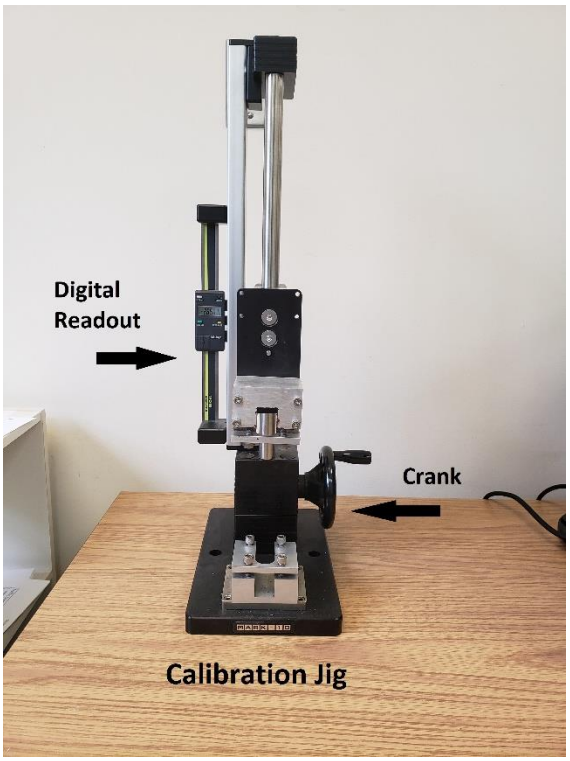

a) ASG Calibration Jig

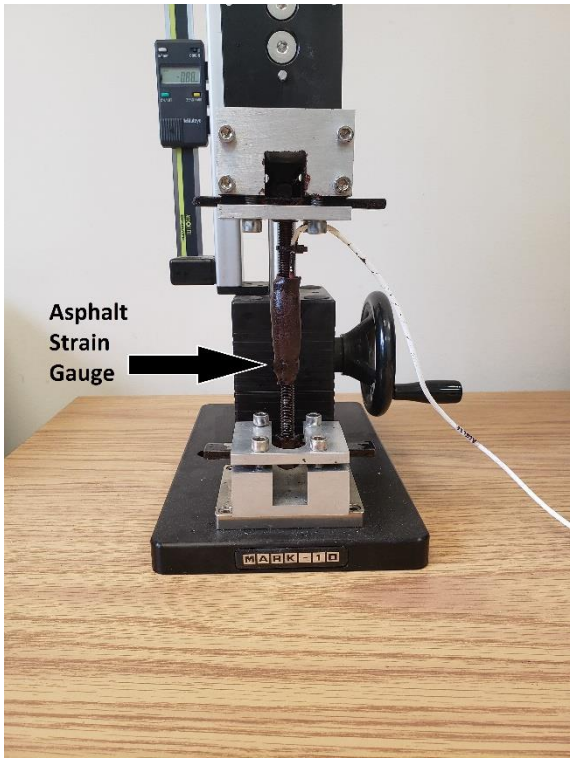

b) Calibration Jig with Strain Gauge

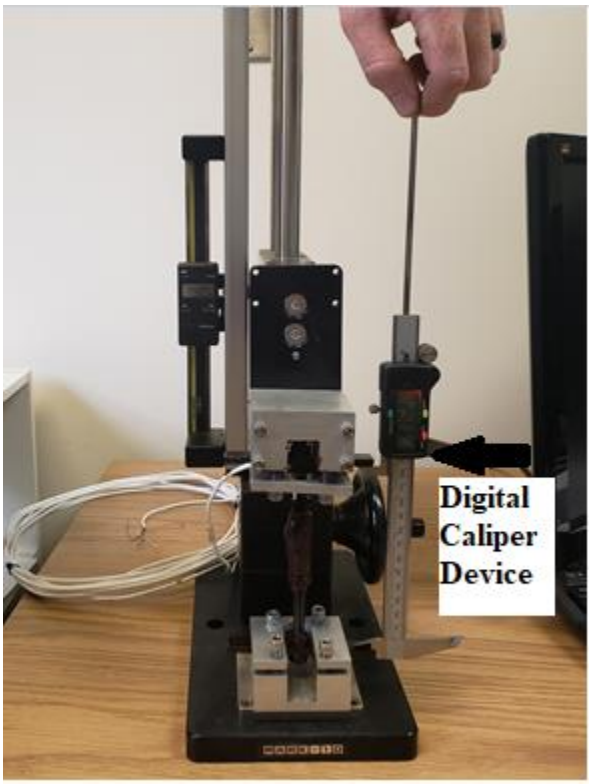

c) Utilizing Digital Caliper Device

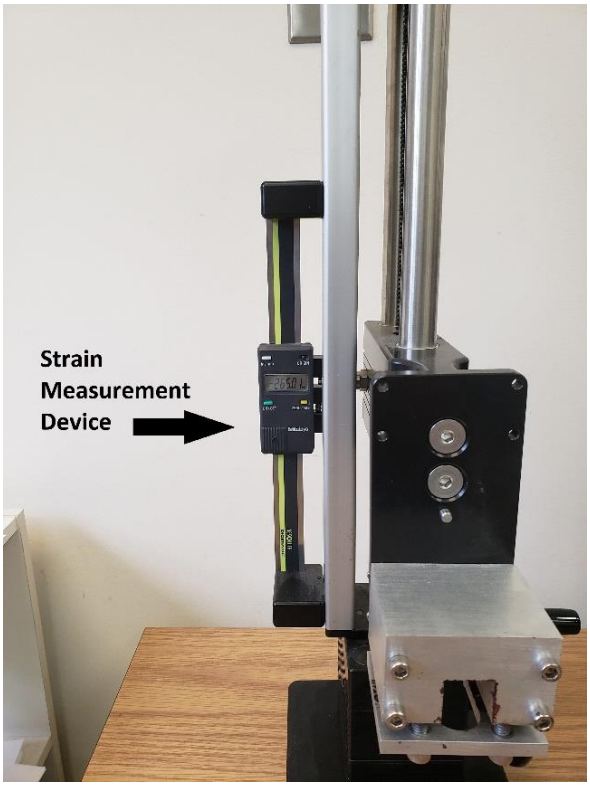

d) Strain Measurement Device

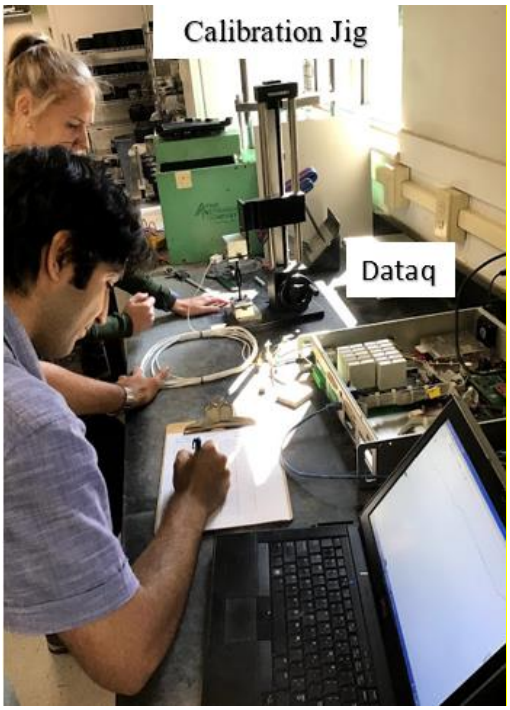

e) ASG Calibration Set-Up

FIGURE 3.4 ASG Calibration.

The average gauge length measured in the jig with the digital caliper before loading (*Avg. Length*) and the total applied displacement at each strain increment, δ, was used to calculate the applied microstrain according to:

$$\mu\varepsilon = \frac{\delta}{Avg.\ Length} * 10^{-6} \qquad \text{(Equation 3.1)}$$

The gauge calibration factor was found by plotting the measured voltage against the calculated microstrain with a linear trendline (see example in Figure 3.5 for ASG 1). The slope of the trendline converts voltage change into microstrain. The results of each gauge calibration factor for Section S9 can be viewed in Table 3.1. The detailed calibration data for each gauge in Section S9 can be seen in Appendix A.

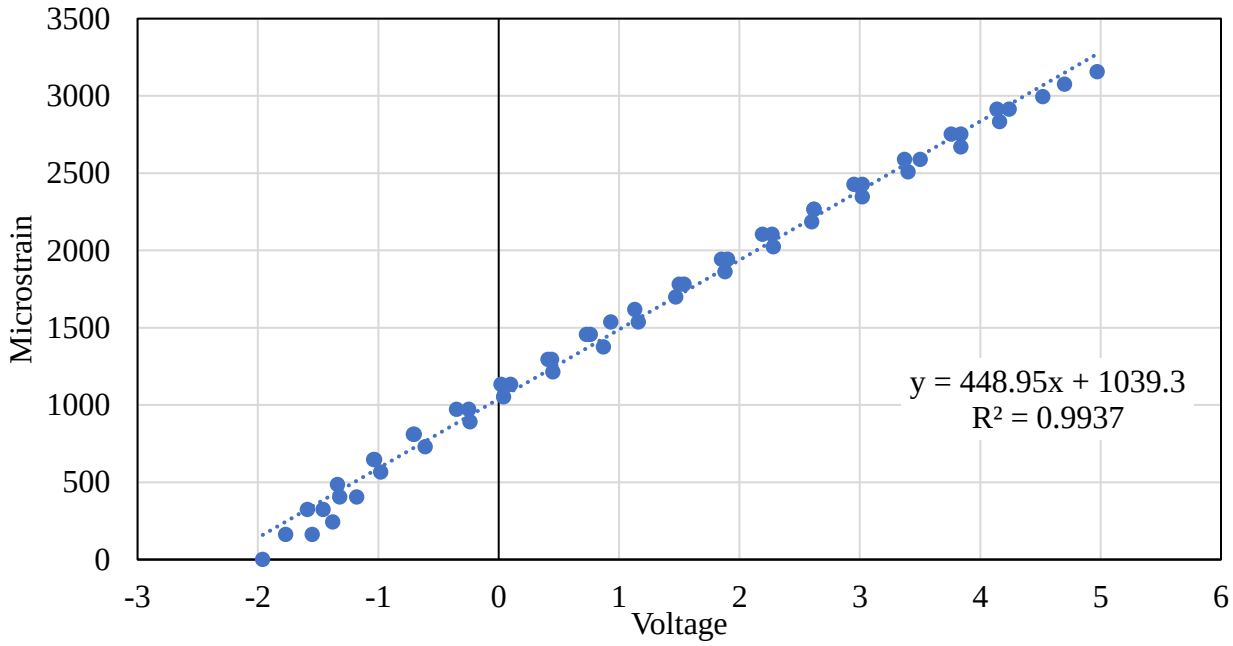

FIGURE 3.5 ASG Calibration Graph.

TABLE 3.1 S9 Gauge Assignments and Gauge Factors

Channel	GeoCompID	BaselineVoltage	GaugeFactor (microstrain/Volt)
1	10	-1.97	448.95
2	12	2.16	416.97
3	30	-1.33	434.71
4	8	1.54	450.76
5	28	0.05	496.19
6	36	1.24	430.84
7	2	0.11	445.00
8	25	0.97	402.2
9	29	0.14	398.14
10	14	0.83	454.04
11	9	0.34	480.95
12	27	0.41	425.65

The EPC calibration process mirrored the procedure from past Test Track cycles. First, EPCs were placed into the calibration chamber (Figure 3.6a). The EPC cables were then fed out of the chamber and connected to the DATAQ. The EPC's wires were taped where they passed through the chamber wall to ensure that the chamber would be air and watertight. The chamber was then filled with water. The voltage for each EPC within the water-filled chamber without the lid attached was measured using the DATAQ when no additional pressure was added. The lid was then placed and bolted onto the top of the chamber as seen in Figure 3.6b and the voltage was measured using an Omega gauge as shown in Figure 3.6c. Then, an adjustable pressure regulator was attached to the chamber and was subjected to pressure increases at increments of approximately 5 psi until reaching roughly 25 psi (well below the maximum gauge rating of 35 psi). The voltage was recorded at each 5-psi increment. Once 25 psi was attained, the pressure was decreased in increments of 5 psi each until the 0 point was again reached. This process was conducted twice to ensure reliability of the voltage readings. Figure 3.6d depicts the EPC calibration process set up.

a) EPC in Calibration Chamber

b) Calibration Chamber Lid Application

c) Omega Pressure Measurement Device

d) EPC Calibration Set-Up

FIGURE 3.6 EPC Calibration.

The voltage results and the corresponding pressure were plotted to determine the calibration factor for each EPC (Figure 3.7). Like the ASGs, the EPC gauge factors were the slope of the linear trendlines. The gauge response was found to be highly linear with good repeatability. The gauge assignments and calibration factors are listed in Table 3.2.

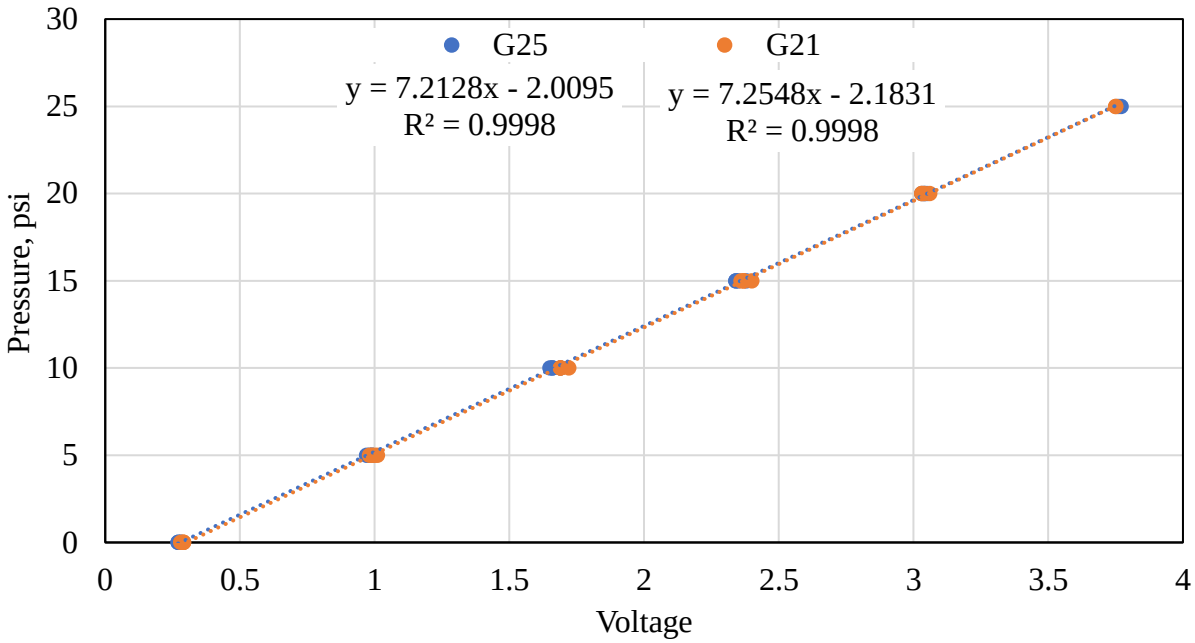

FIGURE 3.7 EPC Calibration Results.

TABLE 3.2 EPC Assignments and Calibration Results

Gauge	Geocomp Gauge ID	Track Calibration (psi/Volt)
13	G21	7.25
14	G25	7.21

Instrumentation Pre-Installation

There were three instrument installation stages in Section S9. The first phase was calibration of the ASGs and EPCs described in the previous section. The next stage was the pre-installation of the ASGs and EPCs within Section S9 which was similar to past test cycles except for the gauge arrangement and orientation as discussed previously. The installment of the gauges and pressure cells occurred on top of the GB. Section S9's GB is shown in Figure 3.8.

FIGURE 3.8 Section S9 Before Gauge Installation – Granular Base.

The pre installation began by threading the ASG and EPC wires into flexible conduit as seen in Figure 3.9a. The flexible conduit helped ensure that the wires would not get pinched or cut by aggregate during the construction process. Next, the gauges were arranged on the GB to match the alignment and spacing found in Figure 3.3 from the previous section. Figure 3.9b depicts the spray-painted grid on the GB to aid in gauge placement. The blue dots in the figure indicate the center of each gauge once fully installed. The gauges and cables were placed so the conduit covered wires led into the roadside data collection system. Shallow trenches were cut so that the cables were buried just beneath the surface of the GB as seen in Figure 3.9c. Once all the flexible conduits were placed within the trenches, the trenches were refilled and compacted with the same GB within the section to create a flush surface illustrated in Figure 3.9d.

The EPC pre-installation varied slightly from the ASGs pre-installation. Trenches were dug for each EPC for their cables. However, each EPC was placed in shallow holes. Next, aggregate base was sieved through a #8 and a #16 sieve for placement underneath the EPCs to make them level with the aggregate base surface and provide a layer of protection from larger stones. The -#8 material was placed first followed by a thin layer of finer -#16 material. Figure 3.9e illustrates a leveled EPC from Section S9. Once leveled, each EPC was covered with more -

#16 followed by -#8 material as shown in Figure 3.9f. The last phase of gauge installation occurred during the paving of Section S9, described below.

a) Threading Wires in Conduit

b) Painted Grid for Gauge Placement

c) Digging Shallow Trenches

d) Conduit Buried in Granular Base

e) Leveled EPC

f) EPC's Flush with Surface and Covered

FIGURE 3.9 Instrumentation Pre-Installation Procedure.

CONSTRUCTION OF SECTION S9

Section S9 was paved on August 24, 2018 beginning at 10:00 AM. On the day of construction, the high temperature was 85°F and the low temperature was 67°F. The AC plant used for the 2018 Test Track cycle was the East Alabama Paving Company plant located in Opelika, AL 6 miles from the Test Track.

The AC was a dense graded mix with a PG 64-22 binder and a NMAS of 12.5mm. The AC layer was designed as a single 8" lift on top of the existing GB. However, the as-built thickness was 8.36". The materials in the mix were considered local to the Test Track but matched closely to the gradation and volumetrics of South Carolina's Asphalt Intermediate Course Type B mixture. This mixture is primarily used for SCDOT rehabilitation repairs, interstates, and high-volume primary roads. Section S9 was produced as a WMA, which was a

required by the SCDOT standards based on the mix type used (Intermediate Course B mixture). This particular mix type's standards can be view in Appendix C. Although it was required, WMA also has social, ecological, and financial benefits such as lower temperatures for the construction crew, lower energy required, and lower costs with the associated lower energy. The plant configuration settings and mix design are listed in Table 3.3.

TABLE 3.3 S9 Plant Configuration

Material	% Setting
Binder Content	5.5
Shorter Sand	14
78 Granite	25
89 Granite	36
EAP -1/2 RAP	25
Evotherm M1	0.5

The plant configuration for this mix design adds up to 106% because East Alabama Paving Company operates their plant based on aggregate weight and not based on the total mixture weight. This results in 100% for total aggregate as shown in Table 3.3. Furthermore, the Evotherm M1 additive is based on the weight of the binder content and not based on the weight of mixture or aggregate.

Before the mix was placed, a PG 64-22 binder was used to tack the vertical edges in addition to the entrance and exit portion of the milled section as seen in Figure 3.10. The tack was used to increase bonding between the new pavement material and the existing pavement.

FIGURE 3.10 Tack Application in Transition Zone.

Section S9 was placed and compacted using conventional equipment used in the construction of past research cycle sections. Section S9 was delivered by 7 truckloads at an average temperature of 248ºF. The mix was transferred from trucks into a material transfer vehicle, then loaded into the Roadtec paver pictured in Figure 3.11.

FIGURE 3.11 Paver in Use During S9 Construction.

The last phase of the gauge installation began as the WMA was being placed. Again, this process was the same procedure used in past Test Track cycles (Timm and Priest, 2008). The ASGs were first tacked to the GB using asphalt binder mixed with sand. Then, mix was taken from the paver and sieved through a #4 screen to remove the large particles. The -#4 material was used to cover the EPCs and ASG gauges to ensure the paver and compactors would not pull out the conduit and gauges or affect the survivability of the gauges. Figure 3.12 shows the covered instrumentation.

FIGURE 3.12 Section S9 AC Covered Instrumentation.

Following paving, only ASG Gauge 5 was found inoperable. Section S9 had a 93% gauge survivability rate with thirteen out of the fourteen gauges surviving the construction process. Figure 3.13 shows Section S9 after paving.

FIGURE 3.13 Section S9 after Paving.

The mix design was compared to the as-built AC to quality control the materials used. Table 3.4 and Figure 3.14 show the mix design target gradation, the as-built gradation, and the required standard gradation. The slight deviations were considered within the acceptable tolerance of normal construction practice and were deemed acceptable by SCDOT as seen below in Table 3.4.

TABLE 3.4 S9 Gradation Target versus In-Place

Sieve Size, mm	Percent Passing, %		SCDOT Gradation Requirements
	Target	As-Built	
25	100	100	100
19	99	100	98-100
12.5	95	98	90-100
9.5	83	92	72-90
4.75	54	67	44-90
2.36	35	37	23-43
1.18	26	29	
0.6	18	21	1-25
0.3	13	12	
0.15	8	7	4-12
0.075	4	4.5	2-8

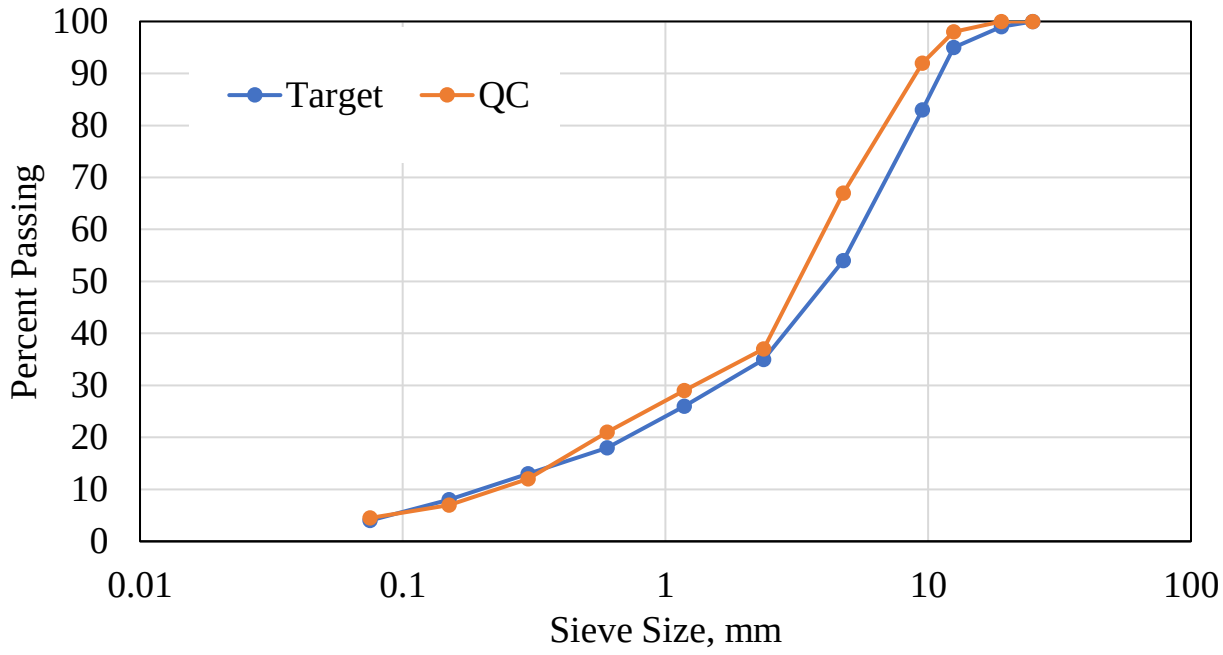

FIGURE 3.14 S9 Gradation of Target vs. In-Place.

The volumetrics for the as-built section were checked against the mix design and the mixture's standards as shown in Table 3.5. The slight deviations of the as-built mix properties from the mix design were considered acceptable by SCDOT as seen below in Table 3.5.

TABLE 3.5 S9 Volumetric Target versus In-Place

Volumetrics	Mix Design Target	As-Built	SCDOT Requirement
Rice Gravity (Gmm)	2.426	2.461	
Bulk Gravity (Gmb)	2.364	2.402	
Air Voids (Va), %	2.5	2.4	2.5-3.0
Aggregate Gravity (Gse)	2.642	2.678	
VMA, %	15.7	15.2	>14.5
VFA, %	84	84	70-85

Achieving adequate density was a major concern for the thick lift pavement section. The pavement was compacted with the same rollers and using similar rolling patterns as previous test track cycles. The rollers used include a breakdown roller, a rubber tire roller, and a steel finishing roller as seen below in Figure 3.15 a, b, and c respectively.

a) Breakdown Roller

b) Rubber Tire Roller

c) Finish Steel Wheel Roller

FIGURE 3.15 Rollers Used on Section S9 for Compaction

Two methods were used including taking cores and using the nuclear gauge to determine if the thick lift section adequately achieved compaction. Three full depth cores were taken from the section to analyze the density throughout the pavement. The cores were cut into thirds to analyze the differences of density throughout the depth of the thick lift pavement. Eight total locations were tested using the nuclear gauge including four locations on the inside wheel path and four locations on the outside wheel path. The nuclear gauge was tested four times at each of the eight locations at 90-degree offsets. Overall density was determined to not be an issue for this section with an average section compaction of 95%.

The second major concern with the single thick lift constructability was controlling smoothness across the pavement. Based on past experience with this issue, the SCDOT recommends diamond grinding to achieve adequate smoothness. Table 3.6 displays the IRI from both the right and left wheel paths and the mean IRI after paving and after the diamond grinding.

TABLE 3.6 S9 IRI Before and After Diamond Grinding

All in/mile	L, IRI	R, IRI	Mean, IRI
Pre Grind	457.3	335.5	396.4
Post Grind	79.3	122.5	100.9

Considering 170 in/mile IRI is failure based on performance monitoring and management requirements from the Federal Highway Administration (FHWA), the pavement before diamond grinding fell into the failing category with an IRI of 396.4 in/mi. However, after the diamond grinding on the pavement, the mean IRI was under the 170 in/mile failure point and was within the normal range. The SCDOT does not require a certain IRI for new pavements; however, the SCDOT does provide incentives for smoother riding surfaces which can be viewed in Appendix D. Typically, the SCDOT incentives for contractors begin if the newly constructed pavement smoothness was less than 80 in/mile. Section S9 illustrated that thick AC layer did have

smoothness problems but was successfully addressed with diamond grinding. Figure 3.16 shows Section S9 after the diamond grinding, before opening to traffic.

FIGURE 3.16 S9 Post Diamond Grinding.

Lastly, a temperature probe was installed within Section S9 after the paving and diamond grinding occurred. Based on past Test Track cycles, the temperature probe was found useful to the structural integrity research because of the high correlation among AC mid-depth temperature, AC strain levels, and AC elastic modulus determined from backcalculation (Timm and Priest, 2008). The temperature probe was installed near the edge of the pavement. The process began by saw cutting horizontally approximately a foot from the pavement edge and cutting vertically roughly 1 inch down into the pavement as seen in Figure 3.17a. This created a shallow slot for the temperature probe wires. Next, as shown in Figure 3.17b and Figure 3.17c, a vertical hole was drilled into the pavement deep enough so that the temperature probe can fit and have the top of the probe flush with the surface. The probe and the connecting wires were test fit into the hole and trench to determine if more saw cutting or drilling was necessary as depicted in Figure 3.17d. Lastly, the temperature probe confined into the hole using roofing cement illustrated in Figure 3.17e. The installed temperature probe within Section S9 acquires hourly average temperatures throughout the depth of the pavement and 3 inches into the aggregate base

layer. Also, the pictures in Figure 3.17 are representative of the process followed in S9 but were taken during an earlier Test Track reconstruction cycle.

a) Saw Cutting Probe Trench

b) Drilling Probe Hole

c) Hole and Trench

d) Probe in Hole and Trench

e) Roofing Cement Process

FIGURE 3.17 Temperature Probe Installation Process (not from section S9).

SUMMARY

A major concern of thick lift paving is the construction and long-term performance of the pavement specifically looking at density, smoothness, and structural integrity of the section. To structurally analyze the pavement, 12 ASGs and 2 EPCs were placed within the pavement. Each gauge and pressure plate was subjected to local calibration procedures. Every gauge but one

survived the construction process. After construction, it was determined that the pavement did achieve adequate density but had issues in regards to smoothness. Diamond grinding was used to remedy the roughness issue and produced a pavement that had an adequate IRI (100 in/mile) measurement for the “new” pavements category. Lastly, a temperature probe was placed within the pavement to record mid-depth pavement temperatures to help analyze and characterize the pavement throughout the experiment cycle.

CHAPTER 4

COOLING ANALYSIS

INTRODUCTION

While there are many benefits to using thick lift paving such as the less energy, time, and materials used to build the pavement, the technique is not without associated concerns, the most notable pertaining to the construction and cooling of the mat. Mat cooling is important because the pavement should not be trafficked until the entire depth has cooled to 175°F to prevent premature rutting under traffic. With this in mind, there are two significant issues when considering the cooling of a thick lift pavement. The first concern is whether conventional means of measuring temperature are appropriate for thick lift paving. Specifically, will the use of an infrared temperature sensor (i.e., "thermal gun") provide adequate information to determine when the pavement can be opened to traffic? The second question relates to the ability of simulation software to accurately predict the cooling rate for planning and management purposes. One such program, MultiCool, predicts cooling curves of AC mats based on heat transfer theory (Chadbourn et al., 1998; Timm et al., 2001). The software uses many factors including construction location, date and time, ambient conditions, existing surface conditions, and mix specifications. MultiCool has been validated for pavements with a thickness of less than 3 inches under a wide range of conditions (Vargas-Nordcbeck et al., 2009). However, MultiCool has not undergone field validation with pavements using a single thick lift of 6 inches or more. Although these questions have been answered for thinner pavement layers, the increased thickness of S9 presents a host of issues requiring validation.

This chapter discusses and compares the measured cooling rates, evaluates the measured cooling rates against predicted cooling rates provided by MultiCool, and evaluates the in situ cooling rates against measured surface monitoring temperatures for three sections constructed as thick lift pavements.

METHODOLOGY

Test Sections

This part of the investigation utilized data from three sections constructed in August 2018 at the Test Track. The first two were placed as trials leading up to the placement of S9. All three sections were placed on top of a GB, had a design thickness of 8 inches, and were placed in a single lift. The three sections include: S9 Trial, N11, and S9. Each section was constructed at different times of the day: S9 was constructed mid-morning; S9 Trial was placed mid-afternoon; and N11 was constructed at sunset. While N11 and S9 were placed directly on the track at a length of 200 ft, S9 trial was placed near the Test Track at length of 40 ft and was constructed to work out last minute plant production and placement issues for the thick lift section.

Construction Data Collection

One thermocouple probe, shown in Figure 4.1a, was embedded into each of the three sections during construction. The thermocouple probes had the same height as the depth of the lift. The temperature data was recorded at an interval of ten seconds, and the average per minute was tabulated. Each probe had eight Type J thermocouple wires measuring the temperature gradient throughout the lift at an interval of every 1 inch. For each section, the thermocouple probe location was near the middle of the section and about 1 ft from the shoulder. A hand-held

weather monitoring device (Figure 4.1b) and Seek© Thermal Compact Pro Image Viewer thermal camera (Figure 4.1c) were used during the construction of each section. The thermal imaging camera was utilized to evaluate the surface temperature of the mix during construction. The camera was used in lieu of a thermal gun to determine the surface temperature and visualize the thermal signature of the mixture. The hand-held weather device was used to collect the wind speed while the weather application on a cell phone was used to record the ambient air temperature.

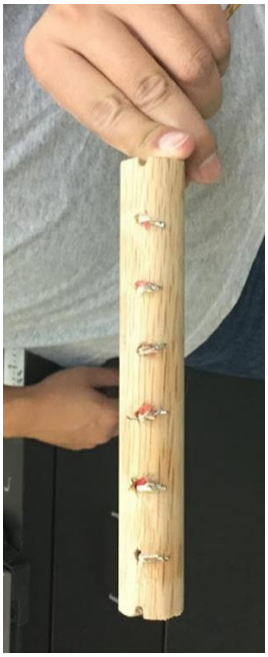

a) Wooden Dowel **b) Hand-Held Weather Station** **c) Thermal Imaging Camera**

FIGURE 4.1 Cooling Curve Measurement Tools and Set-Up.

Once the paver placed the mix, the thermocouples probes were immediately inserted and pushed vertically into the full depth of the lift at the selected locations. This process began by creating a pilot hole into the mat with a steel rod as shown in Figure 4.2a to create space for the thermocouple probe. Next the temperature probe was pushed into the mix at an approximate 30

degree angle from vertical into the direction of the first roller approach so that the first roller pass would push the probe into a vertical orientation. Next the wires from the temperature probe were pushed into the mix to protect them from the roller passes (Figure 4.2b, 4.2c and 4.2d). The thermocouple probes relayed temperatures throughout the depth of the mat in real time.

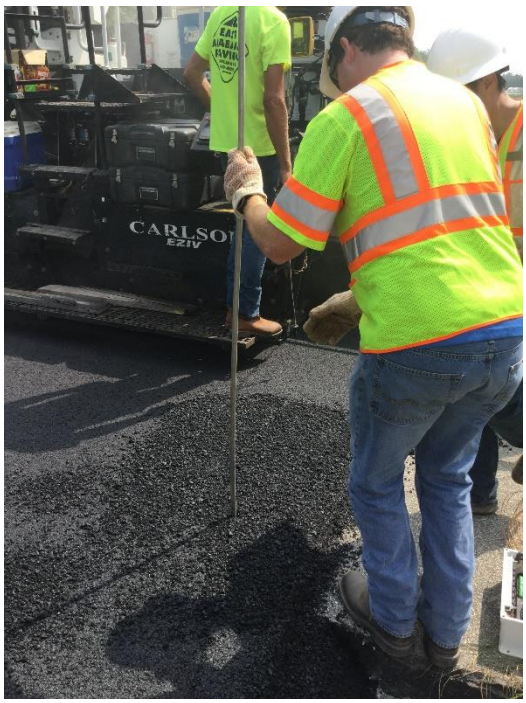

a) Creating Pilot Hole

b) Pushing the Dowel into the Mat

c) Pushing Wires into Mat

d) Covering Mat over Wires and Dowel

FIGURE 4.2 Temperature Probe Placement Procedure.

Every three minutes, from immediately before the paver placed mix until compaction was completed, a thermal image of the pavement section was taken and ambient conditions, such as wind speed, ambient air temperature, and cloud coverage, were recorded. All data was collected at the same location near the embedded thermocouple probe. The thermal imaging camera captured a photo of the same section of pavement. An example of a thermal image taken is shown in Figure 4.3a. The thermal images were used as a substitute for a conventional construction temperature gun to determine the pavement surface temperature. The same point of the pavement surface was used in every photo to represent the pavement's overall temperature. This point is represented by the crosshair as seen on Figure 4.3a. The camera was placed on a tripod facing the pavement at a constant angle (Figure 4.3b). An iPad was used to display the thermal images taken by the Seek camera. After the picture was taken, the wind speed, cloud

coverage, and ambient air temperature were determined using the hand-held weather station and publicly available weather information at the test location. The hand-held weather station was placed on a tripod located next to the thermal imaging camera which provided a constant location for the wind speed reading as shown in Figure 4.3c. This recorded data was then used in MultiCool to execute the cooling simulation. The simulations were compared against data obtained from the embedded thermocouple probes. The probes were left overnight to collect the cooling temperatures after construction.

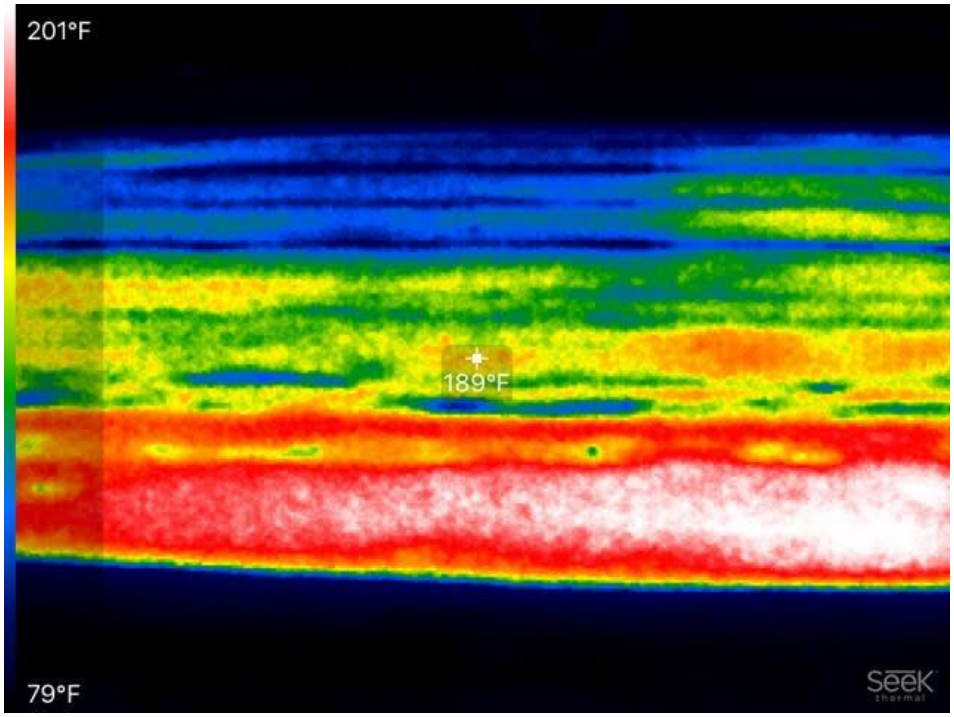

a) Thermal Image – Section S9

b)Wind Speed Detector

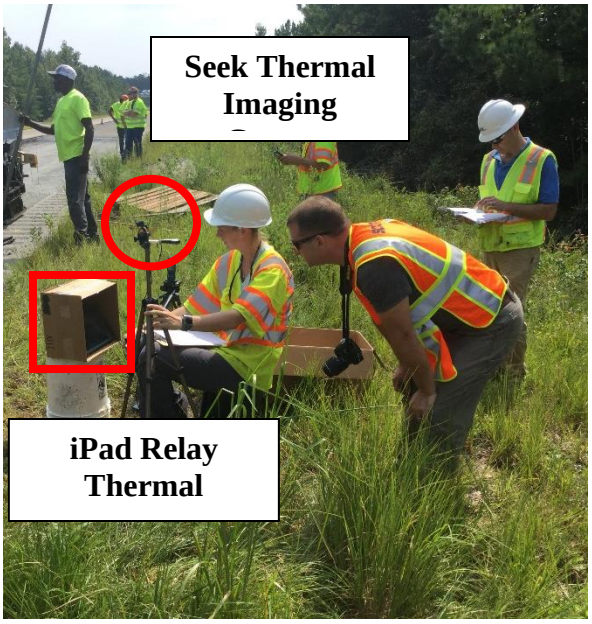

c) Thermal Imaging Measurement Set-Up

FIGURE 4.3 Section S9 Construction Ambient Conditions Recording Set-Up.

MultiCool Software Simulations

MultiCool uses heat transfer theory to predict cooling curves of an AC mat during construction. The software has four main categories including start time, environmental conditions, mix specifications, and existing surfaces. Figure 4.4 illustrates the input screen of the MultiCool software.

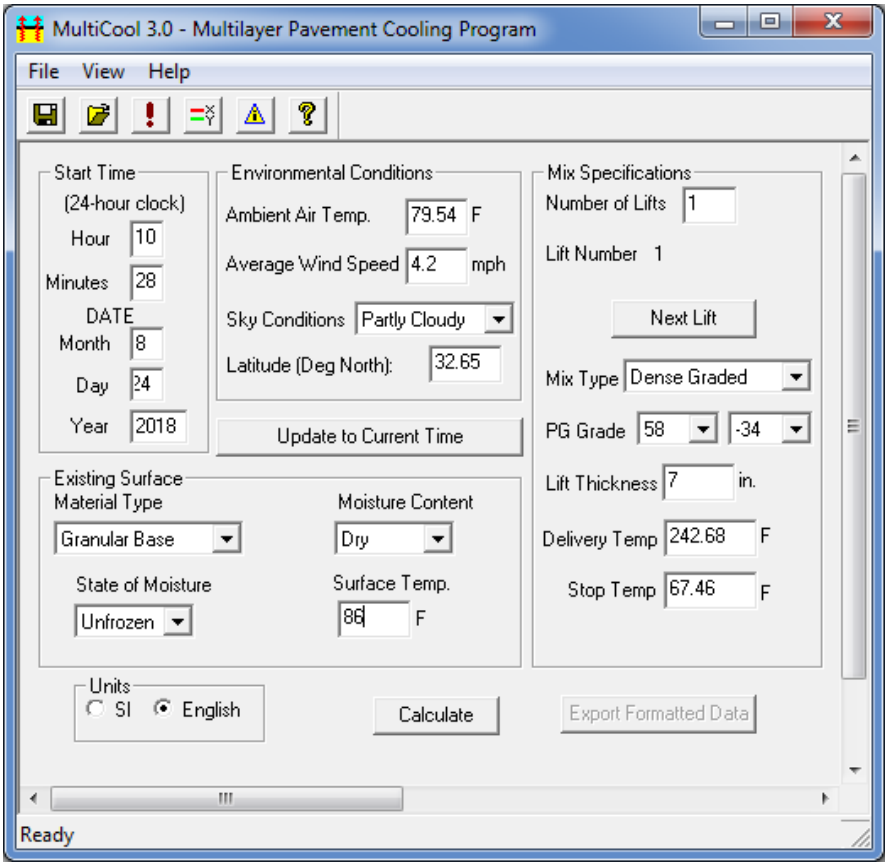

FIGURE 4.4 MultiCool Software Inputs Screen.

The start time category includes time of day and time of year. The environmental conditions includes the ambient air temperature, the average wind speed, the sky conditions, and the latitude of the construction site. The mix specifications category includes the number of lifts, mix type, PG grade, lift thickness, delivery temperature of mix, and the stop temperature of mix. The set of inputs included the existing surface material type, moisture content, state of moisture, and surface temperature. Each of the sections had one lift, a design lift thickness of 8 inches, was a dense graded mixture, and had a compaction cessation temperature of 175°F. The as-built thicknesses of the sections are shown in Table 4.1.

TABLE 4.1 As-Built Thicknesses of Test Sections

Section	As-Built Thicknesses, inches
S9 Trial	6.08
N11	8.15
S9	8.36

The thicknesses in Table 4.1 were used in the MultiCool simulation for each section, respectively. The base material type for each section was a GB, the moisture content was dry, and the state of moisture was unfrozen. The surface temperature was determined using the thermal imaging camera immediately before paving began. Table 4.2 lists all MultiCool inputs used for each section.

TABLE 4.2 MultiCool Software Inputs

		Sections		
		S9 Trial	**N11**	**S9**
Start Time	**Time**	3:02 PM	6:01 PM	10:28 AM
	Date	8/22/2018	8/23/2018	8/24/2018
Environmental Conditions	**Ambient Air Temperature**	86°F	80°F	86°F
	Average Wind Speed	4.28 mph	0 mph	4.20 mph
	Sky Conditions	Partly Cloudy	Overcast	Partly cloudily
	Latitude	32.65°	32.65°	32.65°
Existing Surface	**Material Type**	Granular Base	Granular Base	Granular Base
	Moisture Content	Unfrozen	Unfrozen	Unfrozen
	State of Moisture	Dry	Dry	Dry
	Surface Temperature	100°F	90°F	100°F
Mix Specifications	**Number of Lifts**	1	1	1
	Mix Type	Dense-Graded	Dense-Graded	Dense-Graded
	PG-Grade	64-22	64-22	64-22
	Lift Thickness	6.09 in	8.15 in	8.36 in
	Delivery Temperature	223°F	230°F	243°F
	Stop Temperature	175°F	175°F	175°F

RESULTS AND DISCUSSION

Measured Cooling Rates

Each section's measured cooling data from the wooden dowel, the predicted curve from MultiCool, and the thermal imaging data for surface monitoring were all compared. Figures 4.5, 4.6, and 4.7 depict the S9 trial, N11, and S9 measured cooling curves, respectively. T1 is the surface temperature, T5 is mid-depth and T8 is the bottom of the AC.

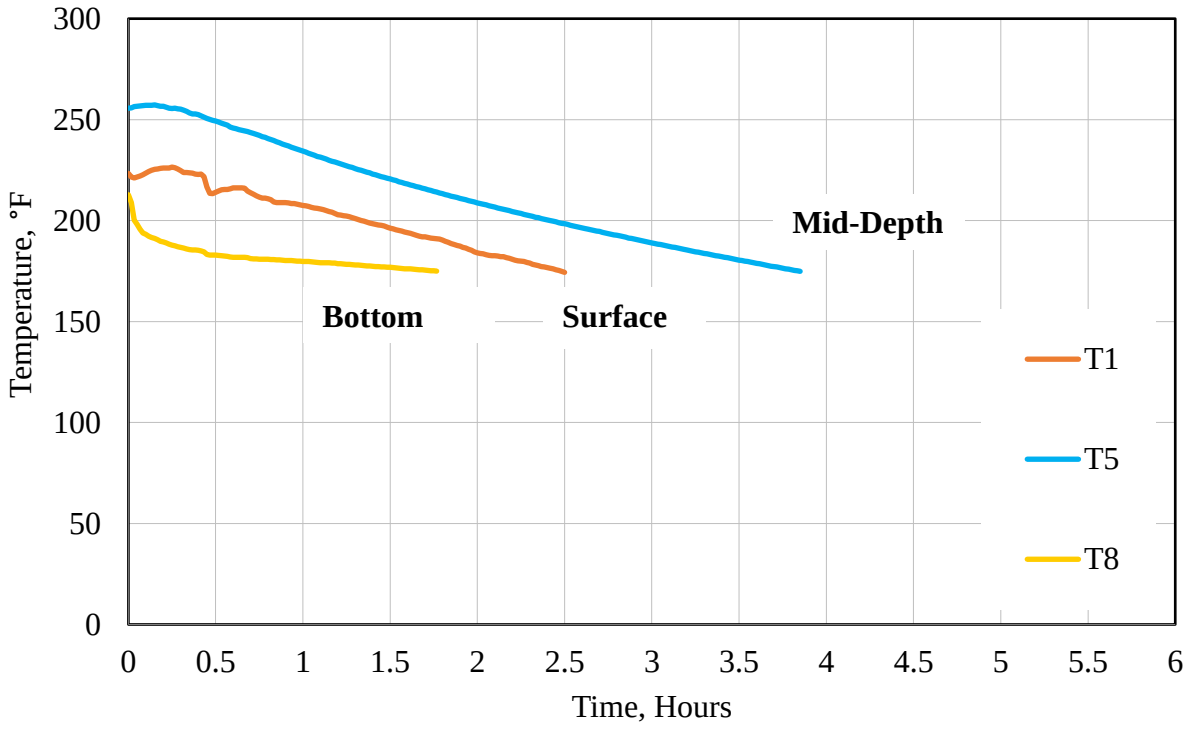

FIGURE 4.5 Measured Cooling Curves – S9 Trial.

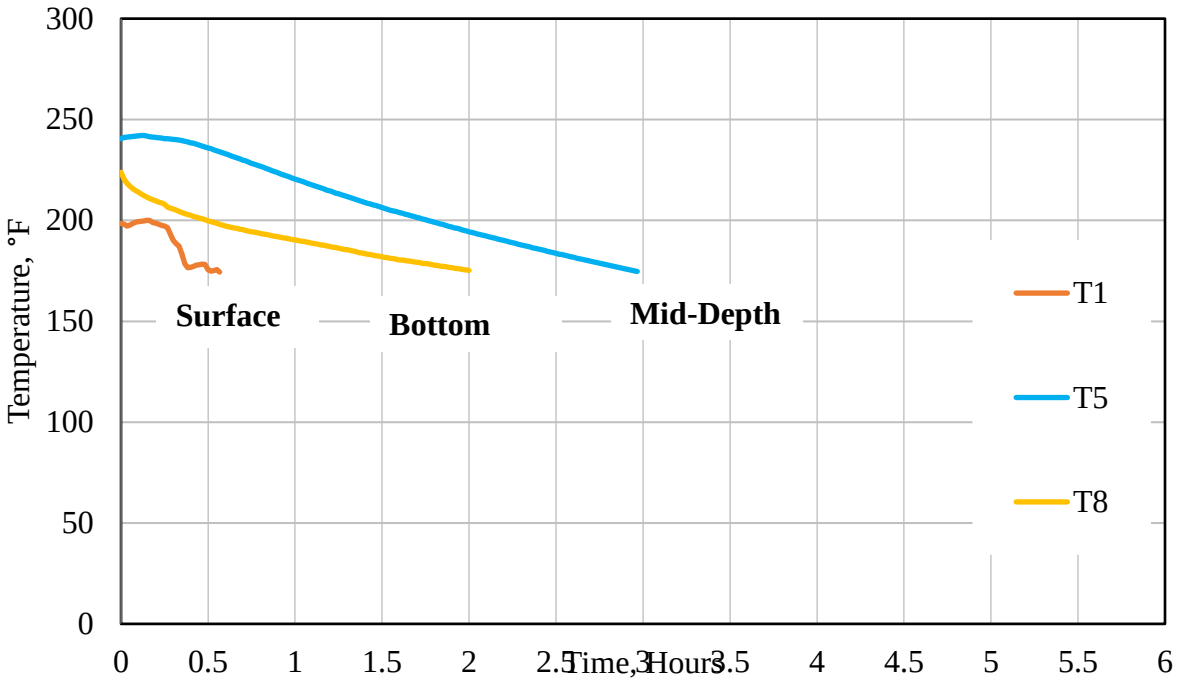

FIGURE 4.6 Measured Cooling Curves – N11.

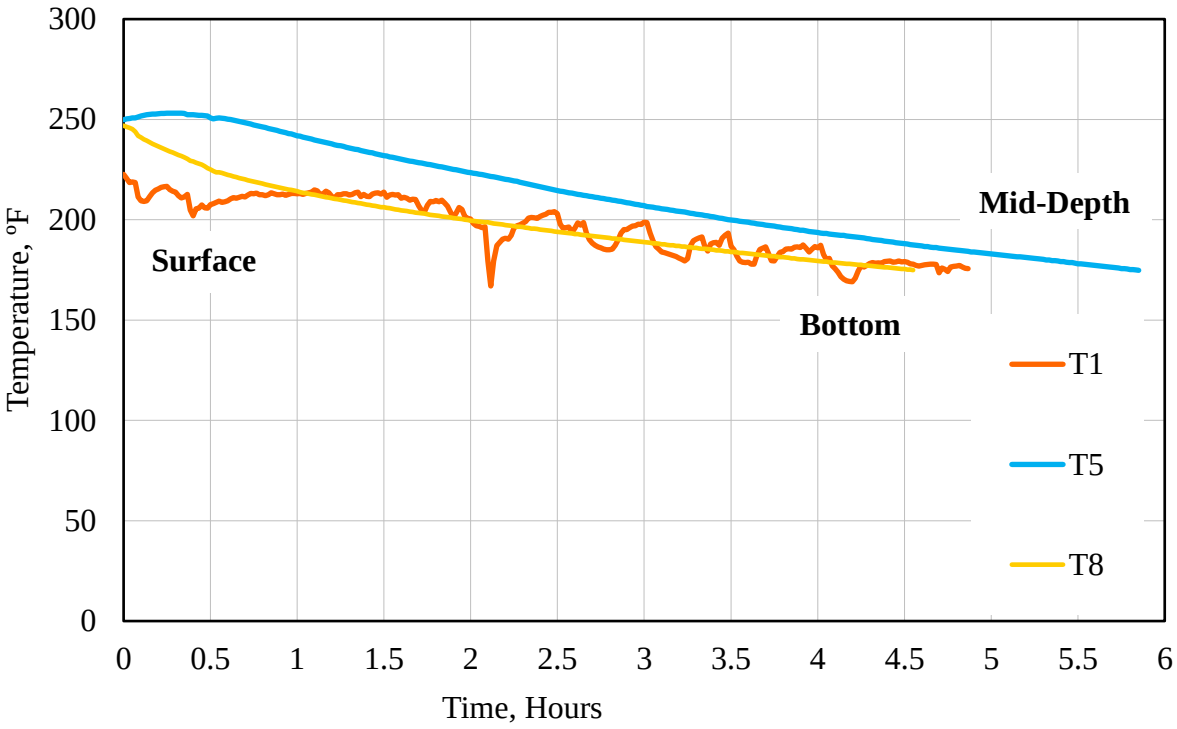

FIGURE 4.7 Measured Cooling Curves – S9.

As seen in Figure 4.5, 4,6, and 4.7, Sections S9 Trial and S9 cooled fastest at the bottom of the AC layer, followed by the surface, and lastly the middle. Section N11 cooled fastest at the surface of the mix, followed by the bottom of the AC layer, and lastly the middle. This data shows how influential time of day is to the cooling time throughout the pavement. Since S9 construction began mid-morning, the rising ambient air temperature and rising sun, slowed down the cooling of the surface and increased the overall pavement cooling time. This is informative of why the bottom cooled faster than the surface layer. A similar trend was seen for the S9 Trial cooling times and temperature depth locations, T1, T5, and T8, because of the mid-afternoon time of construction. The ambient air temperature was at a peak and maintaining high temperatures for the next few hours of the day, which illustrates why the bottom of the AC layer cooled faster than the top. However, section N11, which was paved at sunset with decreasing ambient air temperature and limited solar input, had the fastest surface cooling rate. It also had the fastest cooling time throughout the entire pavement cross-section compared to the other two sections. Table 4.3 catalogs the cooling times to reach 175°F for all three sections. The "Taverage" row in Table 4.3 represents all 8 probes averaged over each one minute time increment.

TABLE 4.3 Time to Cool to 175°F for Each Section

Cooling Curve	S9 Trial	N11	S9
Time of Day	**Mid-Afternoon**	**Sunset**	**Mid-Morning**
MultiCool	2 Hour 18 Minutes	2 Hours 34 Minutes	3 Hours 57 Minutes
T1	2 Hours 30 Minutes	34 Minutes	4 Hours 52 Minutes
T5	3 Hours and 50 Minutes	2 Hours 58 Minutes	5 Hours 50 Minutes
T8	1 Hour 46 Minutes	2 Hours 1 Minute	4 Hours 32 Minutes
Taverage	3 Hours 18 Minutes	2 Hours 23 Minutes	5 Hours 12 Minutes

As seen in Table 4.3, based on the goal of turning newly constructed pavements over to traffic as soon as possible and the cooling times collected during these three sections, it is recommended that thick lift pavements be paved after sunset during the summer season. Based on T5 data from the thermocouple probes, Section N11 which was considered nighttime paving, finished cooling to 175°F within 2 hours and 58 minutes. However, S9 Trial which was paved during the mid-afternoon, reached 175°F in 3 hours and 50 minutes. Lastly, S9, which was paved mid-morning, took 5 hours and 50 minutes to reach 175°F. Based upon the data collected for the three sections, paving after sunset significantly reduces the cooling time. Another advantage of starting at sunset is to hopefully avoid peak traffic hours.

MultiCool Reliability in Thick Lift Paving

Although MultiCool has been validated for lifts less than 3 inches (Chadbourn et al., 1998), a comparison of the MultiCool-predicted curves and the Taverage cooling curves for each section was performed to determine predictive capability for thicker lifts. The comparison was based on the measured Taverage data since MultiCool outputs a cooling curve averaged through the depth. Figures 4.8, 4.9, and 4.10 illustrate the S9 Trial, N11, and S9 comparisons, respectively. Table 4.4 catalogs the cooling times of the MultiCool simulation and the Taverage from the thermocouple probes.

Based on Figures 4.8, 4.9, and 4.10 and Table 4.4, S9 and S9 Trial both have a significant differences between the measured and simulated curves. It appears that longer cooling times results in less accurate simulations. As the time of cooling increases, the ambient temperature, wind speed, and cloud coverage can change more, all of which have significant impacts on the cooling rate. In MultiCool, these are only set as initial conditions and used as constants for the

duration of the simulation. In contrast, the cooling time for N11, which was paved after sunset, decreased because of the lower ambient temperature, yet the variables such as cloud coverage remained constant which yielded a more accurate prediction. These results suggest that improvement should be made to the MultiCool software to account for changing environmental conditions for thicker lift pavements resulting in longer cooling times.

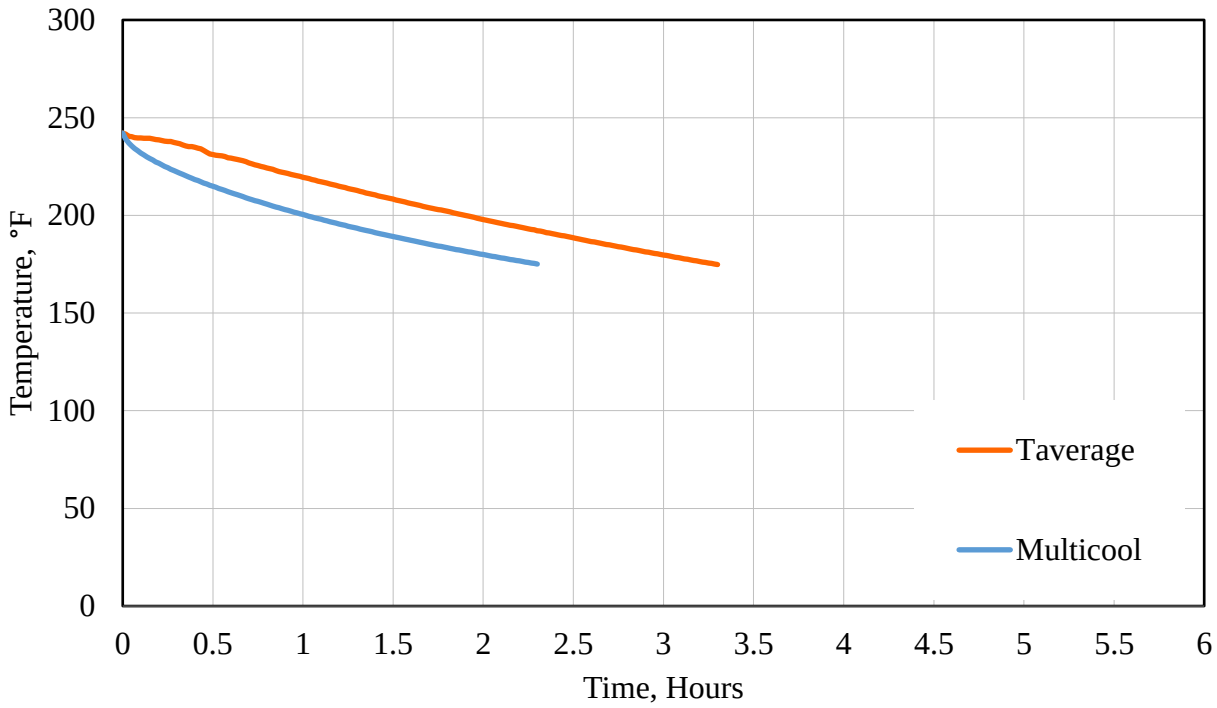

FIGURE 4.8 Measured versus Simulated Cooling Curves – S9 Trial.

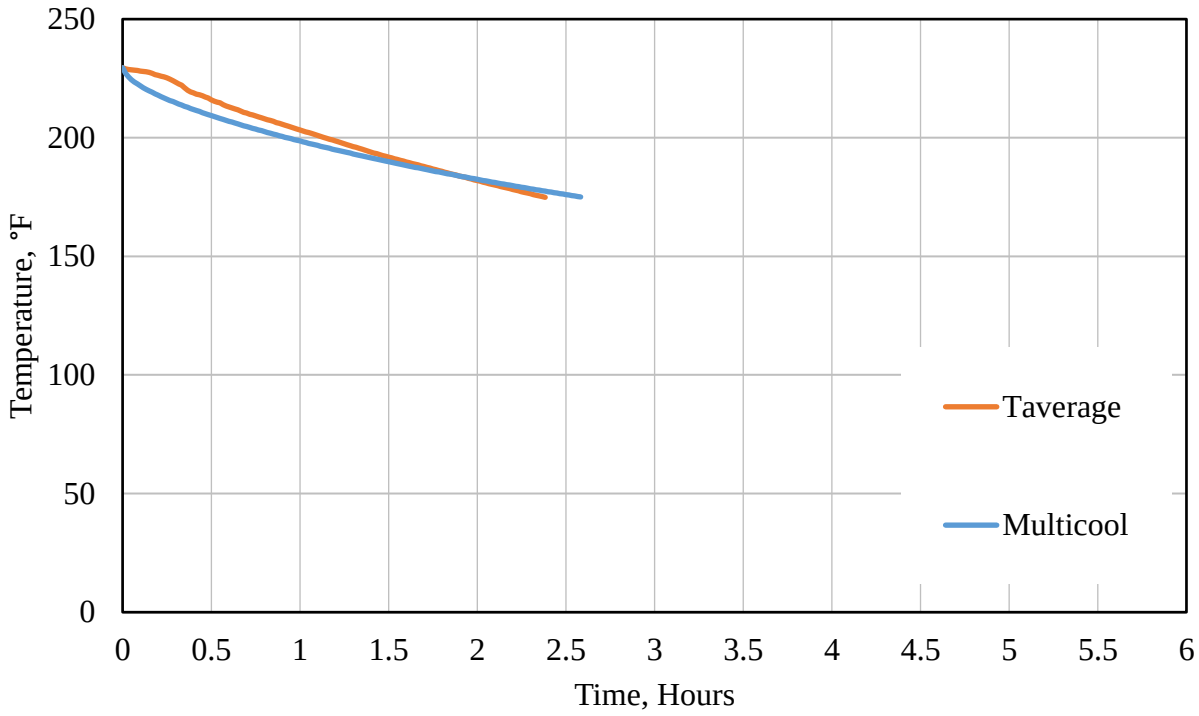

FIGURE 4.9 Measured versus Simulated Cooling Curves – N11.

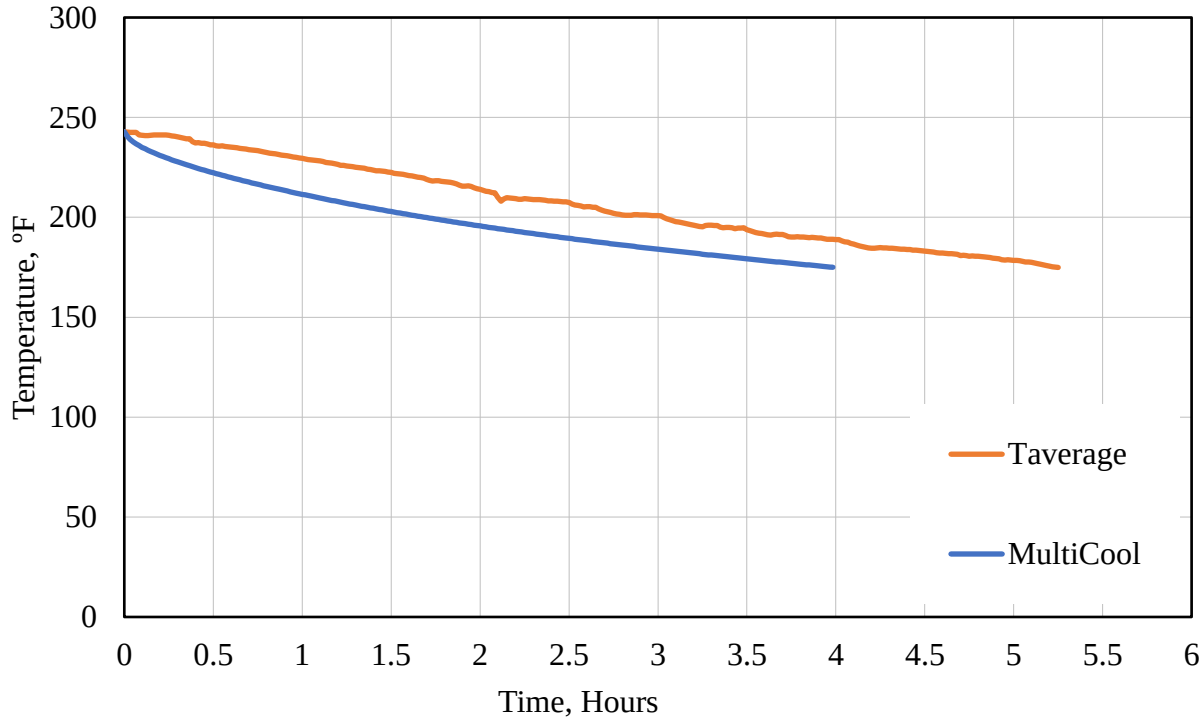

FIGURE 4.10 Measured versus Simulated Cooling Curves – S9.

TABLE 4.4 Cooling Times – Taverage versus MultiCool

Cooling Curve	S9 Trial	N11	S9
Time of Day	**Mid-Afternoon**	**Sunset**	**Mid-Morning**
MultiCool	1 Hour 59 Minutes	2 Hours 13 Minutes	2 Hours 49 Minutes
$T_{average}$	3 Hours 18 Minutes	2 Hours 23 Minutes	5 Hours 12 Minutes
Difference ($T_{average}$ – MultiCool)	***1 Hour 19 Minutes***	***10 Minutes***	***2 Hours 23 Minutes***

Thick Lift Paving Opening to Traffic

Placing traffic on the pavement too early, when it has not fully cooled, could cause unintentional densification in the wheelpaths (i.e., rutting). To avoid unintended rutting, the entire pavement cross section needs to be cooled down to 175°F. With regard to thick lift pavements, the primary concerns about opening the pavement to traffic are the reliability of surface infrared sensors (thermal imaging cameras or temperature guns) and using the surface temperature to best estimate when to open the pavement to traffic. While the thermal gun can be accurate for conventional lift thicknesses, having an 8 inch lift may have significantly different cooling rates from the surface to the mid-depth. This fact may impact when traffic is allowed onto the pavement. Figures 4.11, 4.12, and 4.13 depict the thermal imaging data, embedded thermocouple probe at the surface (T1) and mid-depth (T5) for each section S9 Trial, N11, and S9 respectively.

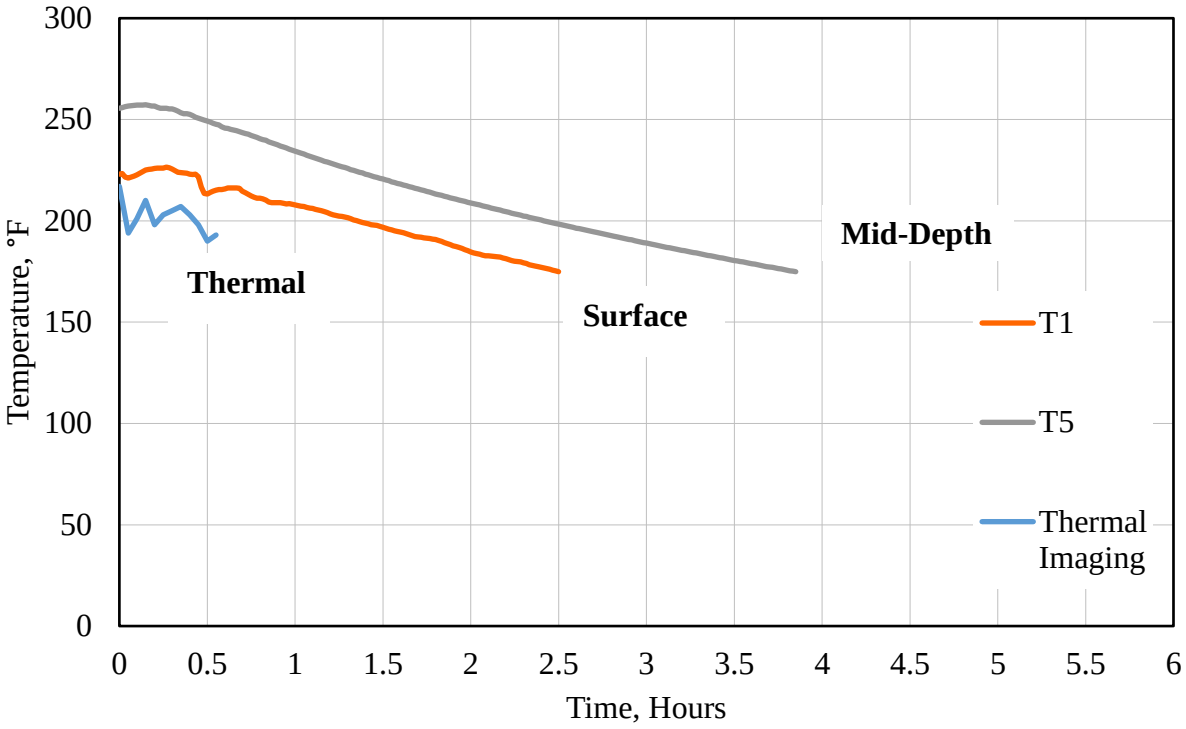

FIGURE 4.11: In Situ and Surface Monitored Cooling Curves –S9 Trial.

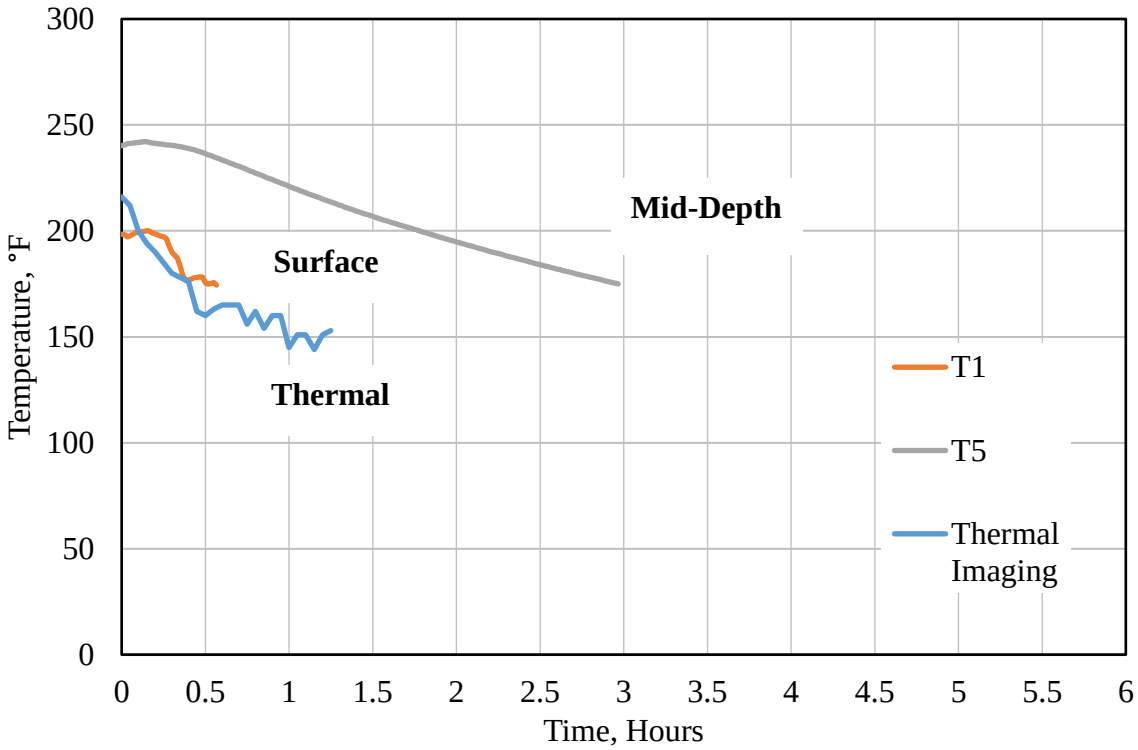

FIGURE 4.12: In Situ and Surface Monitored Cooling Curves – N11.

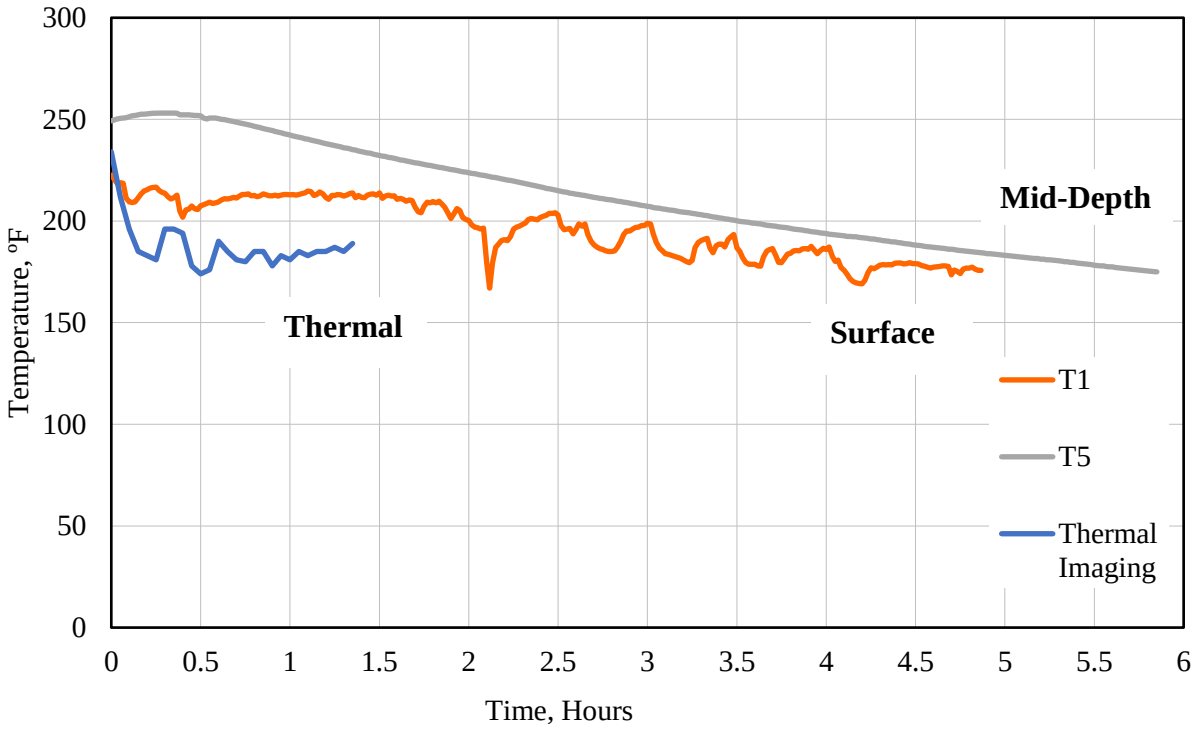

FIGURE 4.13: In Situ and Surface Monitored Cooling Curves – S9.

Each section's graph illustrates that the thermal imaging camera does correlate somewhat to T1, but with some deviation. For S9 trial, the thermal imaging is an average of 10% lower in temperature over time and a maximum of 29°F lower than the measured surface temperature from the temperature dowel. Section S9 had an average of 12% difference between the measured surface and the thermal imaging with a maximum difference of 36°F. While, Section N11 had the most correlation between the thermal camera and the measured surface temperature with an average difference of 7% and a maximum temperature difference of 17°F. However, when comparing the thermal imaging temperature at the surface to the mid-depth temperature, significant variations are noted. S9 trial had an average of 23% temperature difference with a maximum temperature difference of 66°F. Section S9 had an average 27% higher in mid-depth temperature than the thermal imaging camera with a maximum of 78°F difference. Lastly, Section N11 had an average temperature difference of 31% and a maximum difference of 76°F.

Relying only on a surface temperature could falsely indicate the pavement is sufficiently cool and yield premature rutting if opened to traffic too soon. A simple solution would be to fashion an inexpensive probe, much like that shown in Figure 4.1a, but with only one sensor to measure the mid-depth temperature during construction. To create a probe similar to the one used in this experiment, a thermal imaging reader, thermocouple wires, and wooden dowel would be needed. The thermocouple reader would cost approximately $75, the 10-foot Type J Thermocouple would cost about $30, and a 1-inch wooden dowel would cost approximately $6. The total cost would be $110. All dollar prices for materials were found in 2018. However, the thermocouple reader can be used again in many projects, but the wooden dowel and the Thermocouple would have to be purchased for each project. In comparison, a typical infrared gun costs about $20. The accuracy of the thermocouple probe over the typical thermal gun would be worth the $35-$90 per project extra cost specifically for thick lift paving.

SUMMARY

Three sections were constructed to a design thickness of 8 inches in a single lift. Thermocouple probes, MultiCool software, and a thermal imaging camera were used to compare measured in-situ cooling rates, predicted cooling rates, and surface temperatures. Based on the results of this study, time of day has a strong influence on cooling rates and should be considered when constructing very thick lifts. Also, MultiCool is most accurate over shorter durations when the ambient conditions are less subject to change. Although MultiCool has been shown to be a successful predictor of cooling curves for pavements with a thickness of less than 3 inches, the software needs some enhancements for use with thicker lift pavements that are being constructed during the day resulting in longer cooling times. Lastly, a different thermal measurement

technology, such as an embedded thermocouple probe, is recommended in place of an infrared sensor measuring surface temperatures to determine an accurate representation of when the thick lift has achieved the target temperature to be opened to traffic.

CHAPTER 5

EARLY PERFORMANCE AND STRUCTURAL CHARACTERIZATION

INTRODUCTION

Although thick lift paving offers various construction benefits, they are meaningless unless the method yields comparable pavement performance to traditional paving methods. Therefore, using the instrumentation described in Chapter 3 and field performance measures, Section S9 was subjected to an early performance and structural characterization. This chapter first describes the data collection procedure and traffic loading. Next, the field performance of the pavement including the cracking, rutting, and roughness is presented. Third, the structural characterization and results from the instrumentation and FWD data through August 2019 of the traffic cycle is documented. Lastly, the pavement is compared to another older, but similar, section which was also instrumented.

DATA COLLECTION PROCEDURE AND TRAFFICKING

The NCAT Test Track operates on three year research cycles. The first year is utilized for planning and construction of new research sections. The second and third years are used for trafficking and forensic analysis of the research sections. The trucks run five days a week for nearly 16 hours a day to apply the 10 million ESALs during the two year period. The trucks lap the track roughly 200 times a day at approximately 45 mph. The Test Track uses tractor, triple-trailer combination trucks as shown in Figure 5.1.

FIGURE 5.1 Truck Configuration.

The tractor and trailer combinations were interchanged as needed to maximize the trafficking productivity. The tractors consist of a steer axle and a drive tandem axle while the trailers consist of five single axles. The weight range per each axle is detailed below in Table 5.1.

TABLE 5.1 Truck Per-Axle Weight Ranges

Steer, lbs.	Tandem, lbs./axle	Single, lbs.
9,900 – 13,500	19,750 – 22,050	17,600 – 22,450

As stated previously in Chapter 3, S9 contained 14 gauges (12 strain gauges and 2 pressure plates). As the truck passed over the section during the collection time, each working ASG and EPC would experience a strain or stress and the computer would record each truck and truck axle's influence on the section. Next, the truck recordings from the collection time period were loaded into DADiSP, a visual spreadsheet program designed for handling time-series data. Customized algorithms within DADiSP then extracted the peak responses from the stress and strain sensors as seen in Figure 5.2.

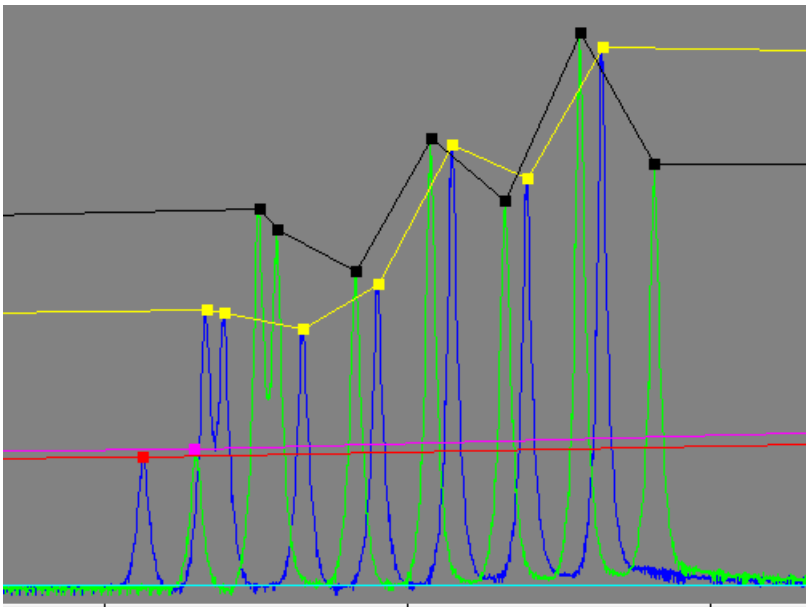

FIGURE 5.2 DADiSP Peak Responses on Earth Pressure Cells.

The axles were then grouped together by axle type (steer, tandem, or single) and the 95th percentile response for both the strain gauges and the pressure plates was determined. It should be noted that the strain and stress data used in this analysis was from the five rear single axles which represents the vast majority of loading events. Based on a prior research cycle at the Test Track, the 95th percentile of the highest hit from each day's collection period was the best data to use in the structural characterization analysis (West et al., 2009).

The temperature probe, discussed in Chapter 2, determined the mid-depth temperature, T2, of the pavement during each collection period. The current testing describes only the early performance of the pavement using the traffic data collected from November 26, 2018 up to August 31, 2019. The data were collected on a rotating schedule including mornings (8 am) and afternoons (2 pm) to ensure the responses included varying ambient and mid-depth AC temperatures. This data pool includes 3.815 million ESALs on the pavement which less than half of the full data collection cycle.

FIELD PERFORMANCE MEASUREMENTS

Three field performance measurements including cracking, rutting, and roughness were taken every two weeks to monitor the pavement over time and under accelerated traffic. Cracking was determined using visual inspection. Rutting and IRI were determined using the Dynatest Mark IV profiler bar mounted on a van manufactured by Pathways.

From the beginning of traffic application, November 26, 2018, through October 21, 2019, Section S9 had no cracking. Figure 5.3 shows the section as of October 21, 2019.

FIGURE 5.3 Section S9 on October 21, 2019.

Section S9 did experience some rutting as seen in Figure 5.4 increasing with time and traffic with a rutting depth at the end of August 2019 of approximately 0.17 inches, but not approaching the commonly used failure point of 0.5 inches. It is common for a pavement to increase rutting as temperatures start to increase. However, this analysis only includes early performance and will need to continue throughout the winter months to determine the impact of

colder temperatures on rutting progression. Rutting should be less of a concern in the winter months because of the asphalt's viscoelastic properties and the stiffening of the asphalt modulus.

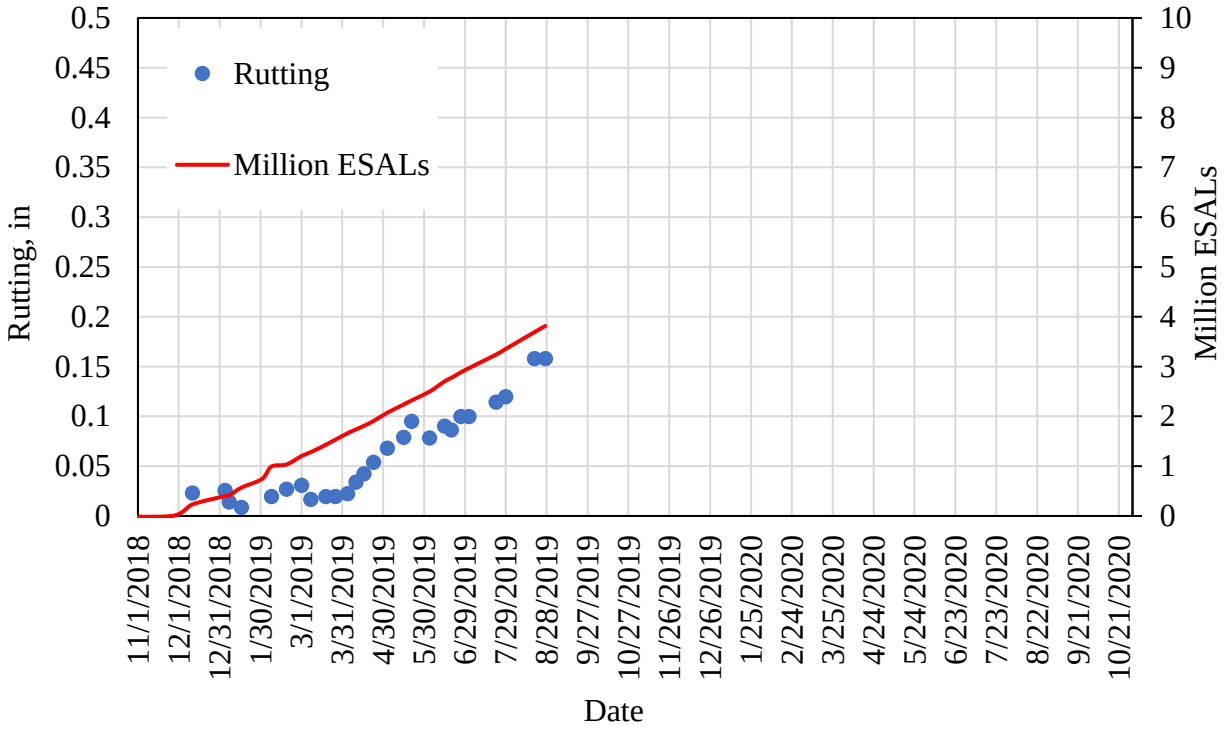

FIGURE 5.4 Section S9 Rutting.

Section S9 was subjected to a weekly roughness assessment as seen in Figure 5.5. The starting roughness of the pavement before diamond grinding was approximately 410 in/mi and is not shown in Figure 5.5. After diamond grinding the IRI reduced to approximately 100 in/mi. Figure 5.5 illustrates Section S9's IRI slightly decreased over time based on the negative linear trendline equation. However, with such a minimal decrease of approximately 10 in/miles over the first third of the cycle, it is determined that the decrease is within the normal range of deviation over time for pavements. Therefore, the smoothness is remaining relatively steady and shows no signs of distress.

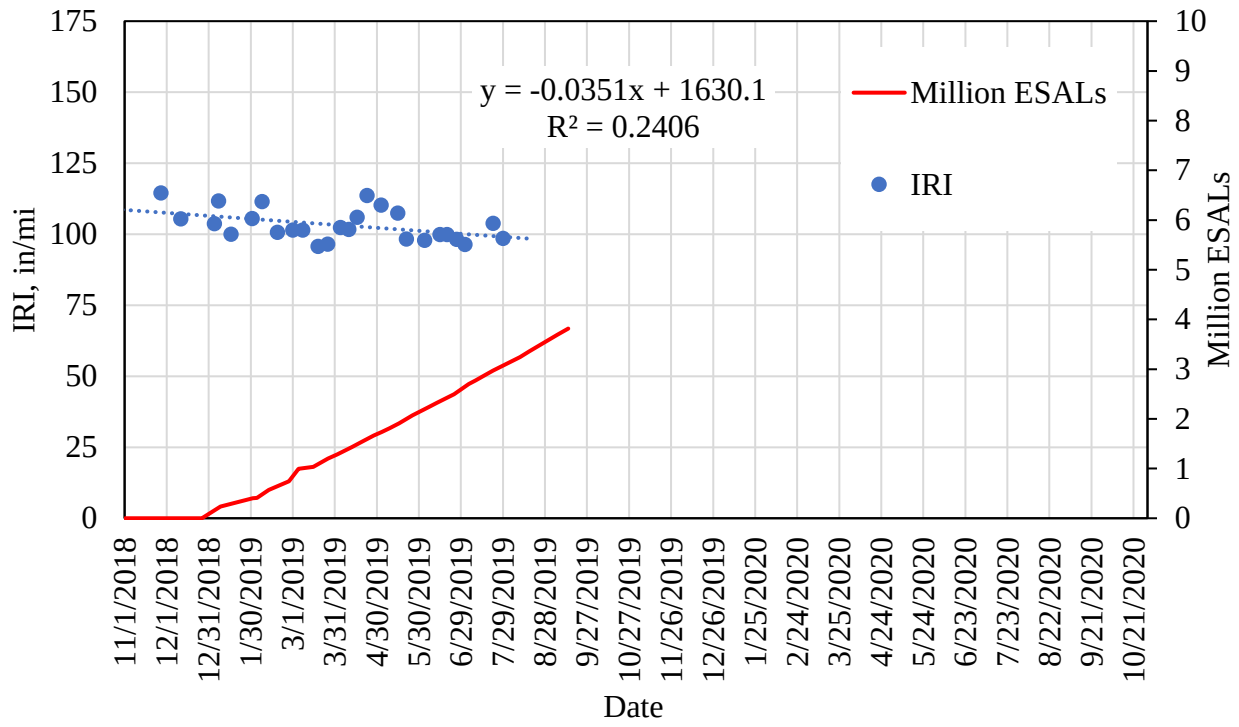

FIGURE 5.5 Section S9 IRI.

EARLY STRUCTURAL CHARACTERIZATION

14 instruments, including two EPCs and 12 ASGs, are embedded within Section S9 and were utilized to help measure the structural health of the pavement section. The ASG instruments were installed to measure bending tensile strain at the bottom of the AC layer and help understand or predict cracking if and when it develops. The EPCs were used to look at the compressive stresses at the top of the GB as an indication of rutting distress.

Figure 5.6 compares the tensile microstrain data from the ASGs and measured temperatures at the time of testing to the testing date. The strain responses appeared to track well with the changes in temperatures. For example, as the temperature increased the microstrain increased and vice versa for temperature decrease. The series in Figure 5.6 were replotted in Figure 5.7 to confirm microstrain temperature dependency. As seen in Figure 5.7, the microstrain is exponentially dependent on temperature.

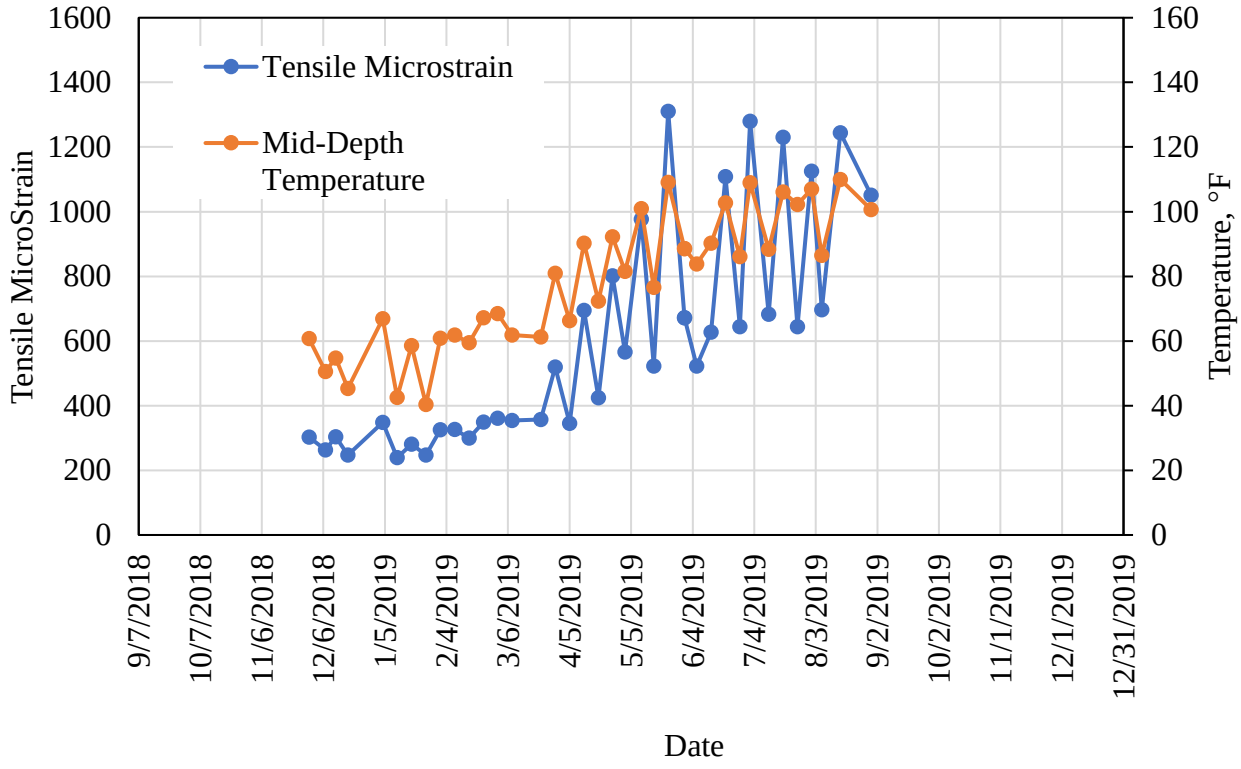

FIGURE 5.6 Tensile Microstrain versus Temperature and Date.

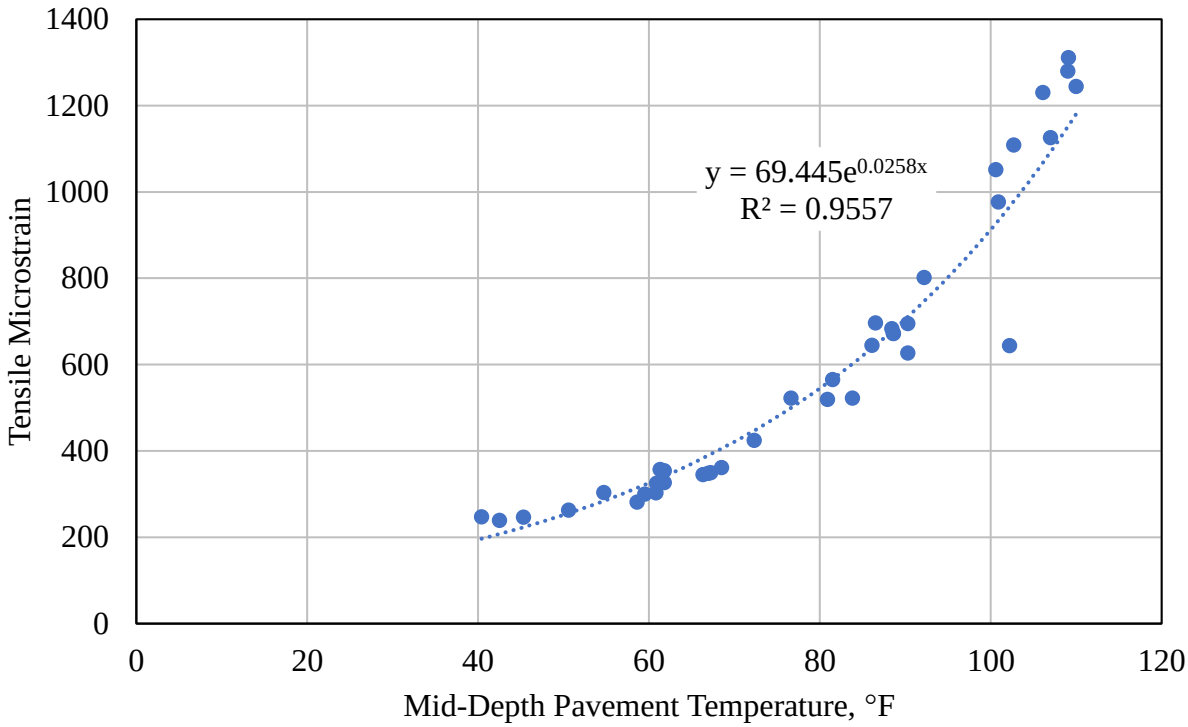

FIGURE 5.7 Tensile Microstrain versus Temperature.

As discussed in Chapter 2, the strain versus temperature data in Figure 5.7 was fitted with an exponential regression equation:

$$\varepsilon_T = k_1 e^{k_2 T} \quad \text{(Equation 5.1)}$$

Where,
ε_T = measured tensile microstrain
k_1,k_2 = regression coefficients (see values in Figure 5.7)
T = mid-depth pavement temperature, ^{o}F

The regression equation was utilized to temperature-correct the microstrain data based upon the calculation described in Equation 5.2 to 68°F per American Association of State Highway and Transportation Officials (AASHTO).

$$\frac{\varepsilon_{68°\mathrm{F}}}{\varepsilon_T} = \frac{k_1 e^{k_2 68°\mathrm{F}}}{k_1 e^{k_2 T}} \quad \text{(Equation 5.2)}$$

Where,
$\varepsilon_{68°\mathrm{F}}$ = temperature-corrected microstrain at 68^{o}F
ε_T = measured microstrain at temperature, T
k_1, k_2 = defined above with equation 5.1
T = defined above with Equation 5.1

Equation 5.2 was simplified algebraically into Equation 5.3. This equation essentially takes the measured strain (ε_T) at the measured mid-depth temperature (T) and multiplies it by a correction factor derived from the regression equation, reference temperature (68^{o}F) and the measured temperature.

$$\varepsilon_{68°F} = \varepsilon_T e^{k_2(68°F - T)} \quad \text{(Equation 5.3)}$$

Where,
$\varepsilon_{68°F}$ = temperature-corrected microstrain at 68°F
ε_T = measured microstrain at temperature, T
k_2 = defined above with Equation 5.1
T = defined above with Equation 5.1

Figure 5.8 illustrates the temperature-corrected data along with the uncorrected data to depict the influence temperature has on the tensile strain response. As in Figure 5.8, the data was corrected to 68°F, had an average of 402 $\mu\varepsilon$, a standard deviation of 43 $\mu\varepsilon$, and a coefficient of variation of 10.7%.

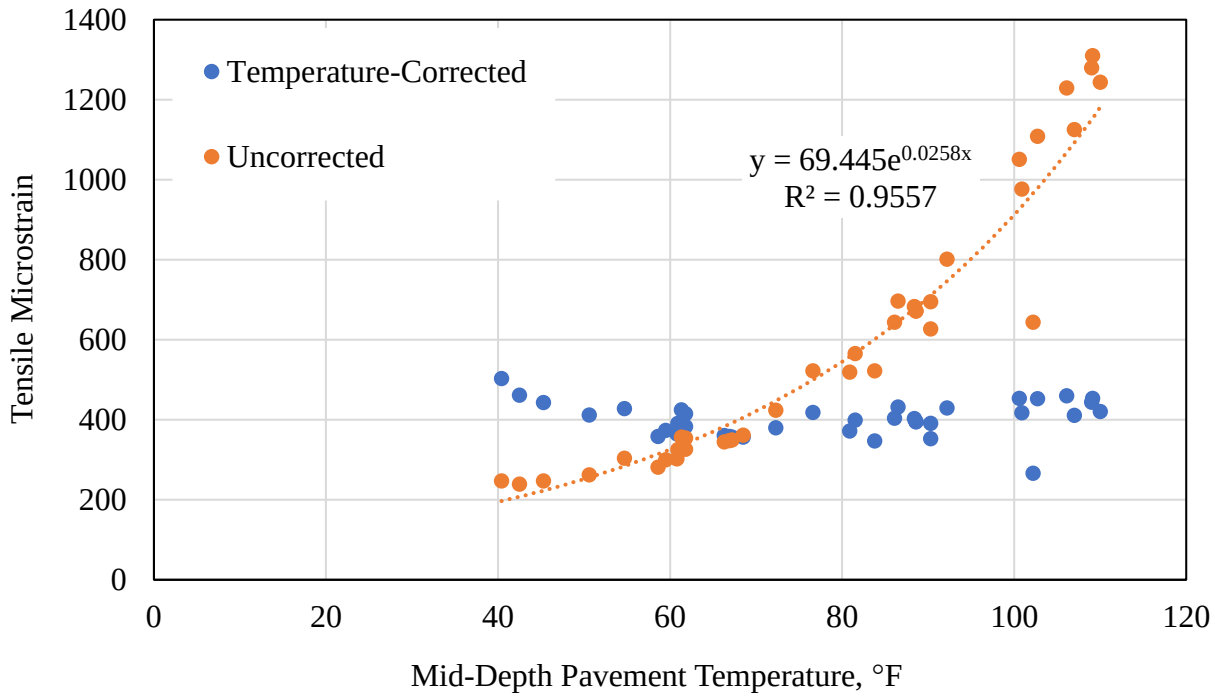

FIGURE 5.8 Tensile Microstrain (Corrected and UnCorrected) versus Temperature.

The temperature-corrected tensile microstrain was then graphed against date (Figure 5.9) to determine if there was any indication of distresses on the pavement over time. As seen below,

the microstrain remains fairly steady with a R^2 close to 0 suggesting that the pavement is not changing over time, a sign of good structural health.

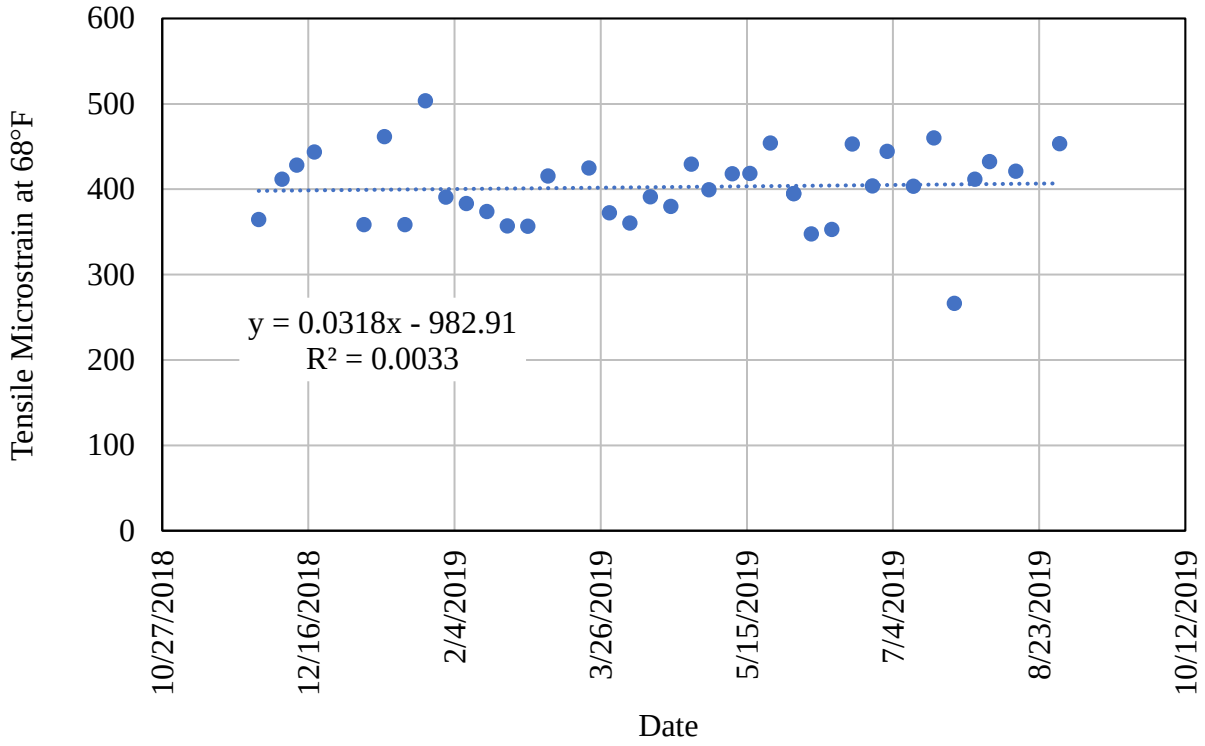

FIGURE 5.9 Temperature-Corrected Tensile Microstrain Versus Time.

The EPCs stress data was analyzed to consider the early performance of the compressive stresses on the GB. Two EPCs, EPC_1 and EPC_2, were placed within Section S9 approximately twelve feet apart as stated in Chapter 3. When a truck drove over the gauges the data were recorded for each axle. The two EPCs were compared to determine if the EPCs were recording similar readings during each truck pass. Figure 5.10 documents that comparison.

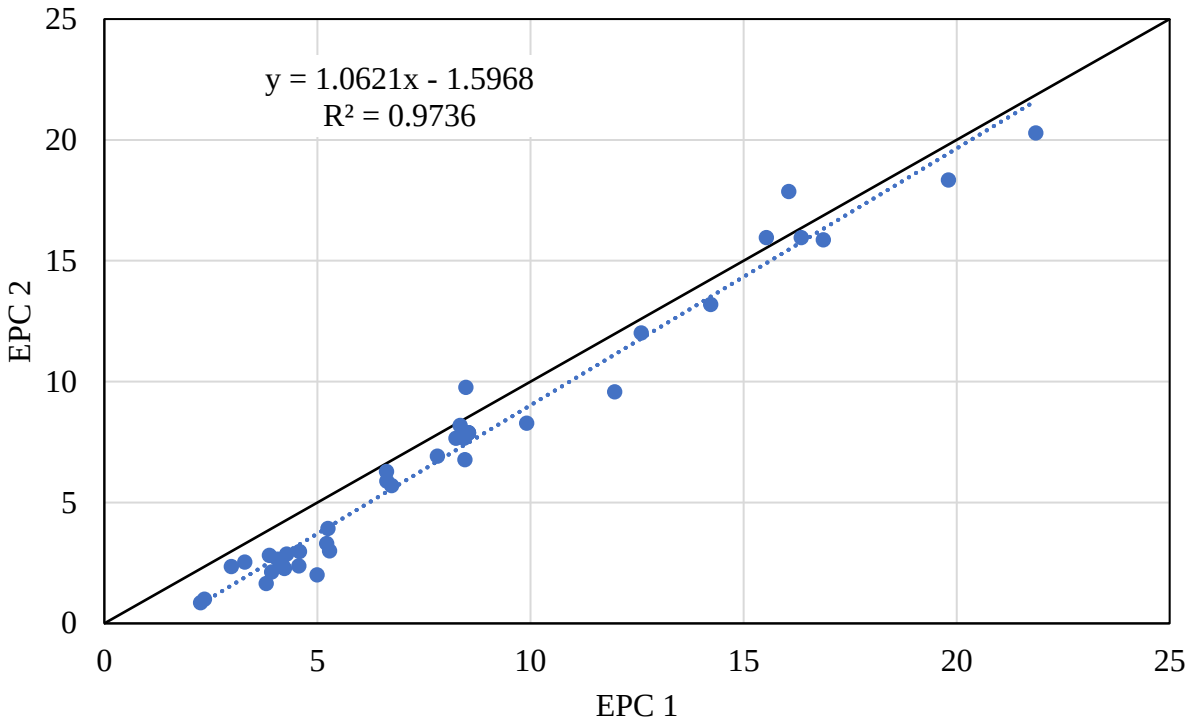

FIGURE 5.10 EPC_1 versus EPC_2.

Figure 5.10 confirms that the data recorded during the collection process were very similar to each other. The R^2 is very high and the points all surround the line of equality with a skew towards EPC_1. With the intercept of the trendline set to zero, it appears that EPC_1 stresses are approximately 8% larger than EPC_2. Upon further review of surveyed thicknesses over the gauges, it was determined that EPC_2 had 0.57 inches more of AC covering the gauge than EPC1 as shown in Table 5.2. The lower readings the EPC_2 data appears to be attributable to larger amount of AC covering EPC_2.

TABLE 5.2 AC Thickness Over EPCs

Gauge	Thickness, in
EPC1	8.01
EPC2	8.58

Since there were two stress measurements to choose from for a given day's testing, it was decided to use the maximum GB pressure (EPCMAX), measured between EPC_1 and EPC_2. First, the GB pressure and temperature were plotted versus time (Figure 5.11) to determine whether the compressive stress recorded on Section S9 would illustrate patterns similar to conventional AC pavements.

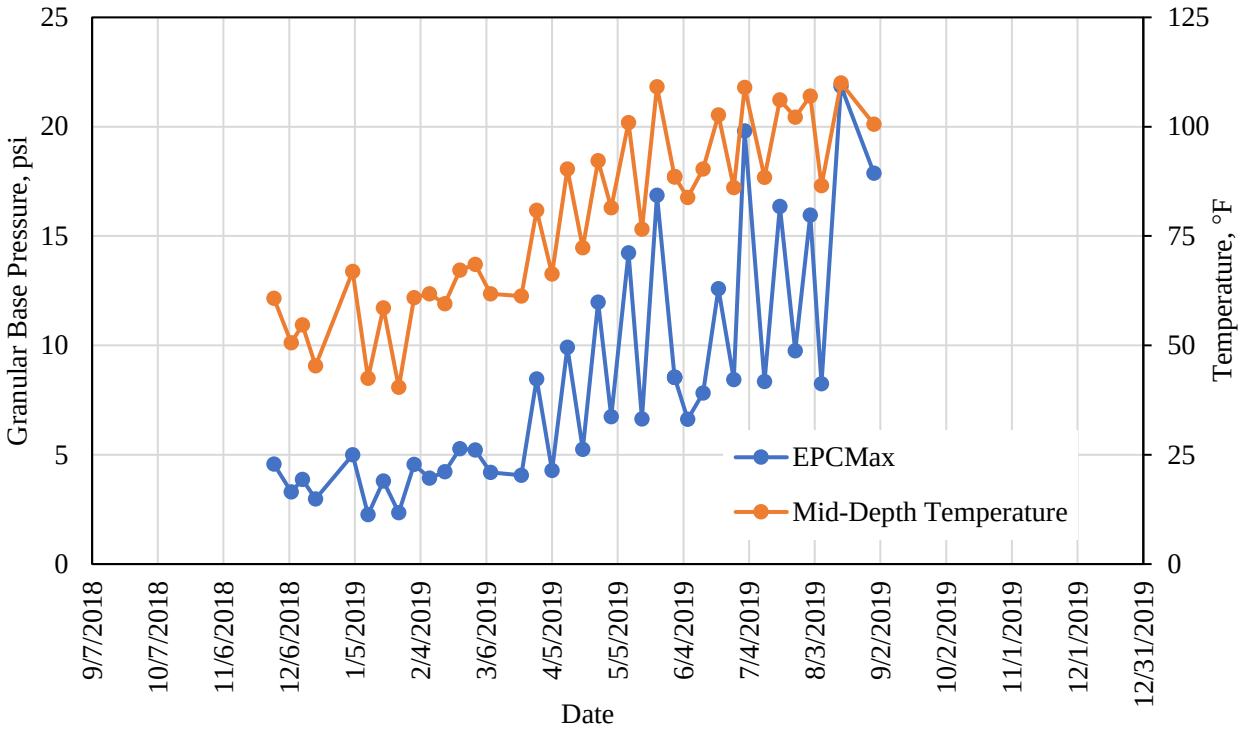

FIGURE 5.11 Granular Base Pressure, Temperature, versus Date.

As seen in Figure 5.11, the GB pressure increases as the temperature increased indicating that the GB might be temperature dependent as depicted by the short-term seasonal trends over this six-month period. As stated previously, the full two-year cycle should be finished before the long-term trends can be fully analyzed. However, with the preliminary indication of temperature dependency from Figure 5.11, Figure 5.12 plots GB pressure versus temperature.

Similar to the microstrain analysis, Figure 5.12 confirms that the GB pressure has an exponential relationship with temperature. The R^2 demonstrates that 95.67% of the GB pressure variability can be explained by the change in temperature.

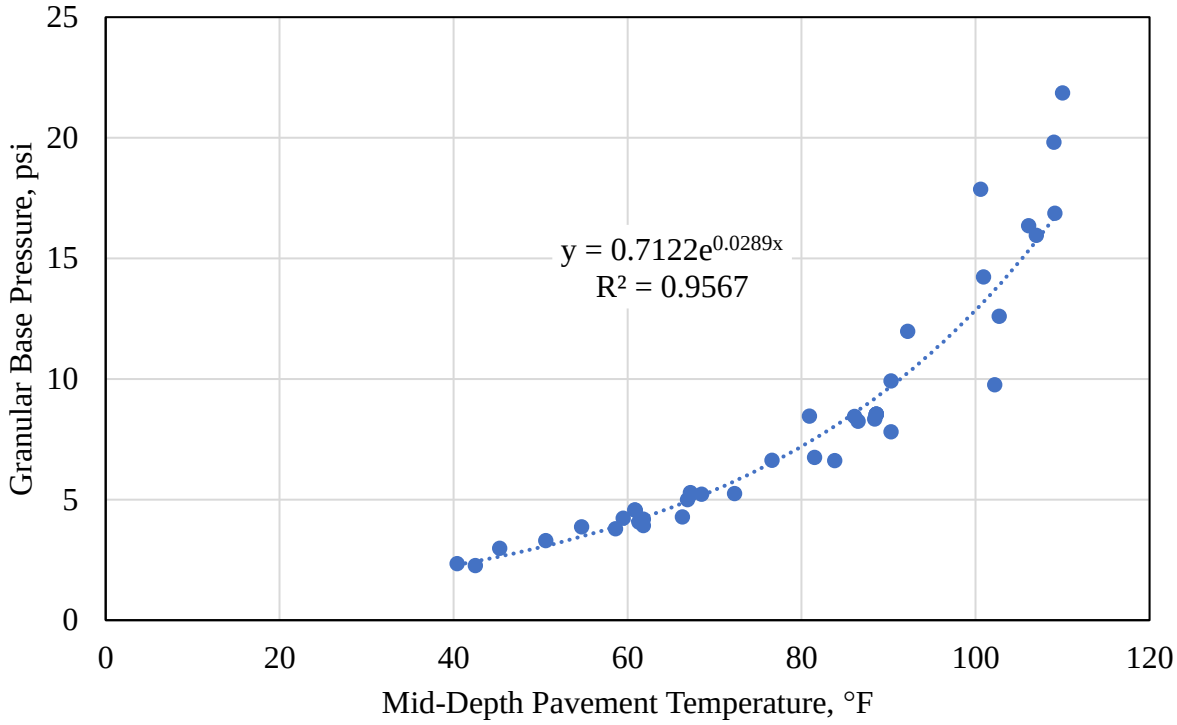

FIGURE 5.12 Granular Base Pressure versus Temperature.

The exponential trendline in Figure 5.12 was used to temperature-correct the GB pressure using Equation 5.4 per AASHTO recommendations. This equation followed the same methodology as the microstrain temperature-correction procedure.

$$\sigma_{68°F} = \sigma_T e^{k_2(68°F - T)} \qquad \text{(Equation 5.4)}$$

Where,
$\varepsilon_{68°F}$ = temperature-corrected stress at 68°F
ε_T = measured stress at temperature, T
k_1, k_2 = defined with Equation 5.1
T = defined with Equation 5.1

Figure 5.13 illustrates the comparison of the uncorrected GB pressure and the temperature-corrected GB pressure. As seen below and similar to the microstrain anaysis, the GB pressure is temperature dependent. The average temperature-corrected stress was 5.13 psi with a standard deviation of 0.62 psi and coefficent of variation of 12.2%.

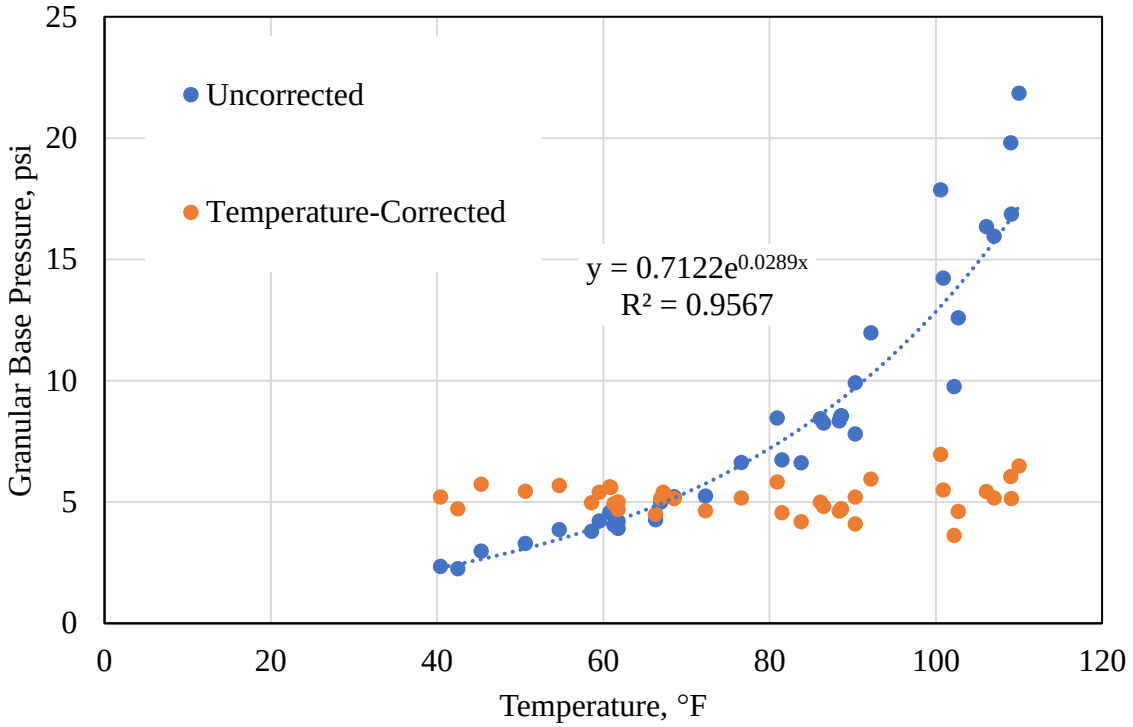

FIGURE 5.13 Granular Base Pressures (Corrected and UnCorrected) versus Temperature.

Looking at the temperature-corrected data over time helped determine if the compressive stress was showing any indication of pavement damage. Figure 5.14 depicts the temperaure corrected GB pressure versus date. As seen below, the GB pressure remained relatively constant, or even slightly declining, indicating that the pavement is performing well over the first third of the test cycle.

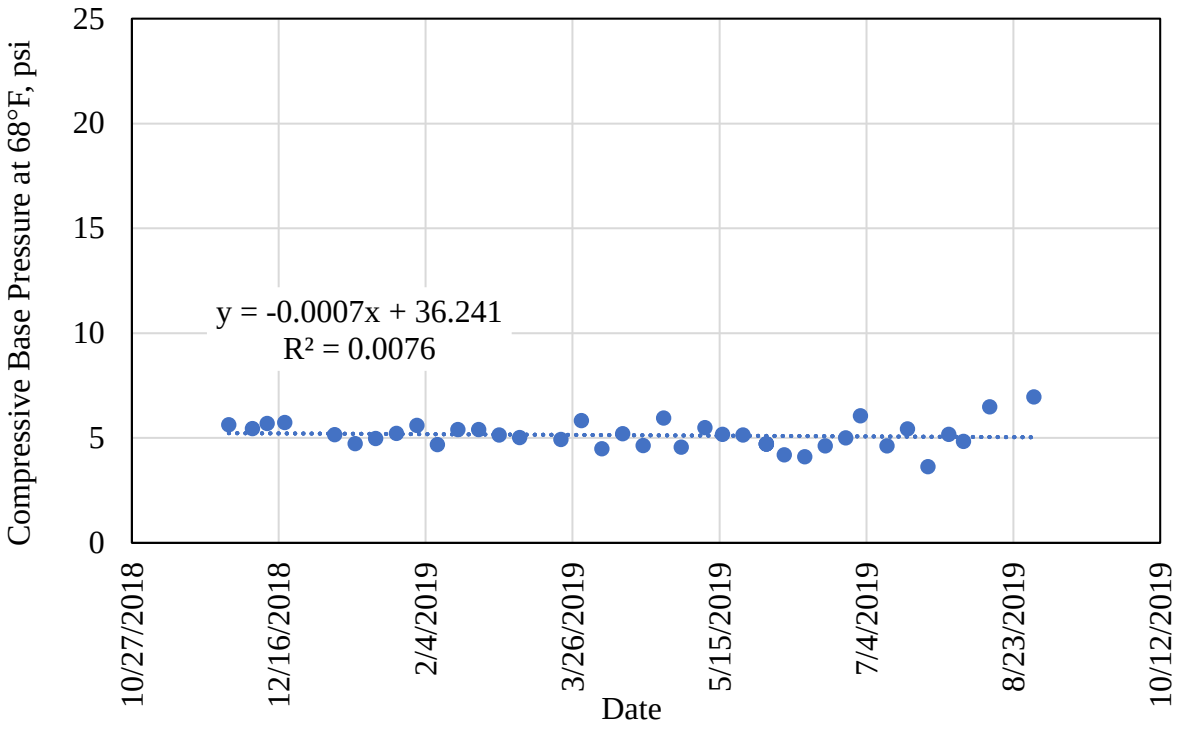

FIGURE 5.14 Temperature-Corrected Granular Base Pressure versus Date.

Another key component of the structural analysis was the evaluation of Section S9 moduli over time, traffic, and temperature. The AC layer, GB layer, and the subgrade moduli were determined multiple times per month using an FWD. Within the 200 ft. section, 4 random locations within three different wheelpaths (inside, outside, and between) were chosen as test locations. Also, it should be noted that one of the four random locations was in the gauge array. Each FWD test had three drops at each location using three different load levels (6,000 lb., 9,000 lb., and 12,000 lb.). For this analysis, only the 9,000-load level was utilized. The analysis only used data points that had a root mean square error (RMSE) of less than 3% to ensure valid backcalculation results would be analyzed. EVERCALC 5.0 was used to backcalculate the layer properties using a trial-and-error method that minimized the RMSE for each measured versus predicted deflection basin.

Based on past research at the Test Track, to facilitate optimum backcalculation across the entire pavement cross-section, a backcalculation pseudo-base layer of 16 inches added to the original as-built GB thickness was needed (Timm and Tutu, 2017). Therefore, the backcalculation cross-section shown in Figure 5.15 was used within EVERCALC 5.0.

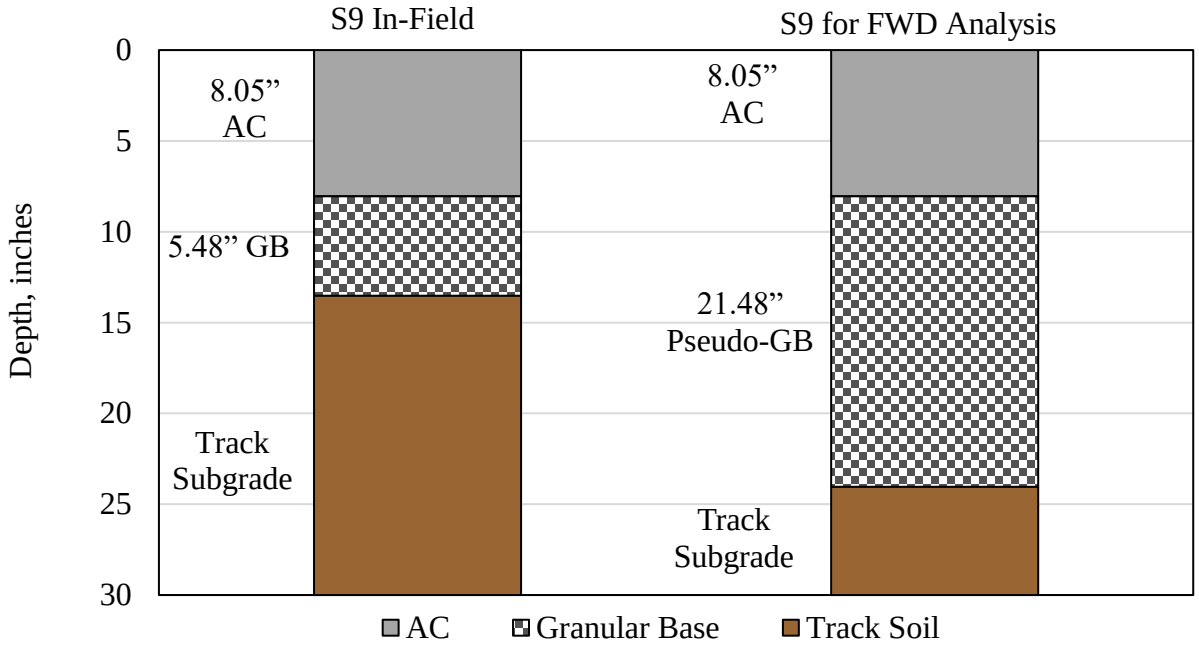

FIGURE 5.15 Cross-Section Comparison Used for FWD Backcalculation.

The AC modulus was plotted over time to visually portray the short-term seasonal trends as shown in Figure 5.16. As seen below, as the seasons change from summer to winter, the AC modulus stiffness decreases illustrating seasonal and temperature dependency. Figure 5.16 illustrates that there is vertical scatter on particular testing days. This scatter is due to the time each wheelpath and location was tested on the particular day. Some locations were tested in the morning during colder temperatures, while some locations were tested in the middle of the afternoon with warmer temperatures. Another cause of vertical scatter is the construction variability.

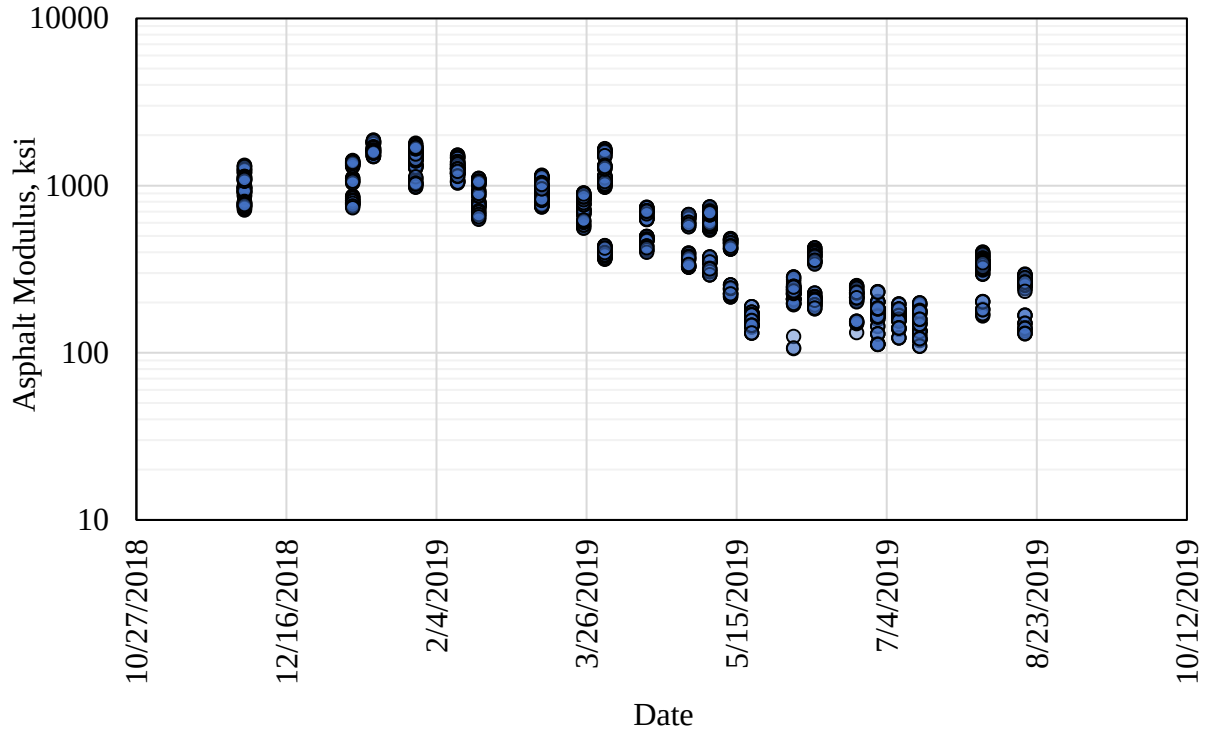

FIGURE 5.16 Asphalt Modulus versus Date.

The modulus from Figure 5.16 was plotted against temperature, Figure 5.17, to verify the AC modulus temperature dependency. Figure 5.17 illustrates that AC modulus has a strong correlation to temperature with the R^2 of 0.951. The strain, pressure, and modulus have all proved to be temperature dependent. However, contrary to the strain and pressure results discussed previously, the AC modulus has a negative exponential trendline. As the temperature increases, the AC modulus decreased. Conversely, as the temperature decreased, the AC stiffened. As the AC modulus decreases with rising temperatures, more bending strain and pressure reach the base layer which results in higher strain and compressive stress results.

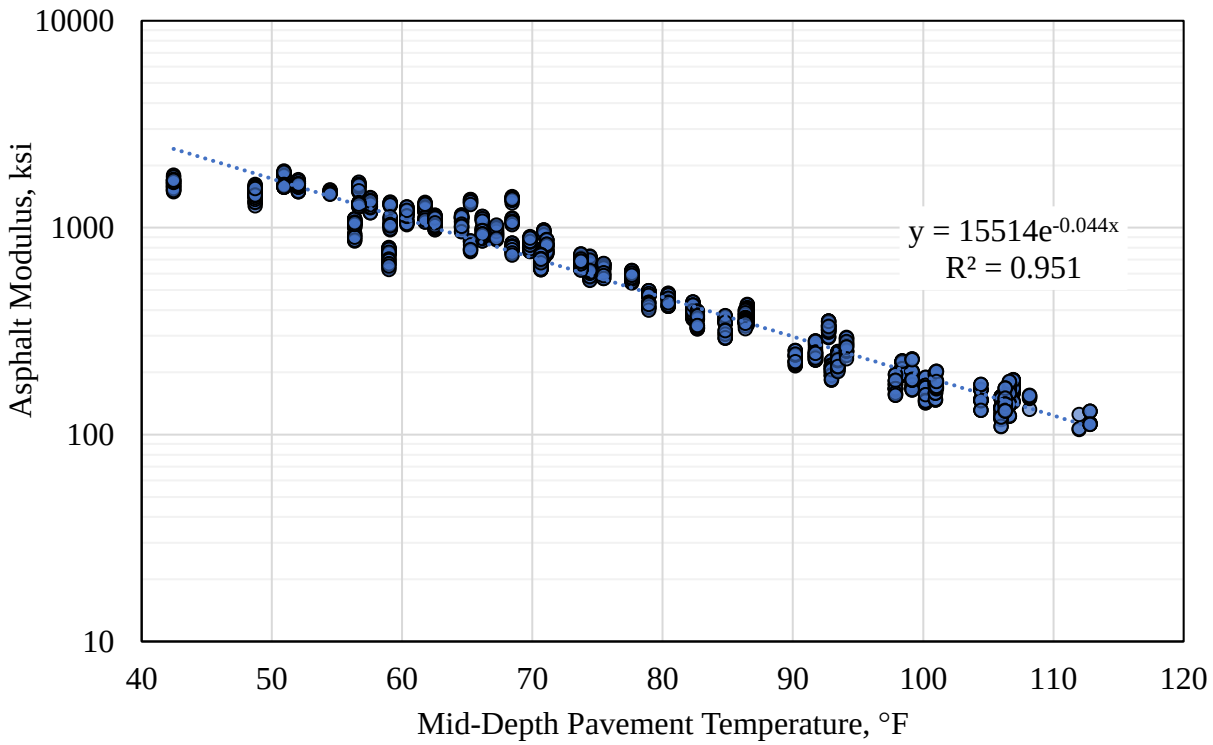

FIGURE 5.17 Asphalt Modulus versus Temperature.

With the confirmation that the AC modulus is temperature dependent. Figure 5.17 was fitted to an exponential trendline. The trendline was used to temperature-correct the AC modulus data using the formula shown in Equation 5.5. The AC modulus was corrected to 68°F to be consistent with the strain and pressure corrections presented earlier in this chapter. This equation followed the same methodology as the microstrain and the compressive stress temperature-correction.

$$E_{68°F} = E_T e^{k_2(68°F - T)} \qquad \text{(Equation 5.5)}$$

Where,
$\varepsilon_{68°F}$ = temperature-corrected AC modulus at 68°F
ε_T = measured AC modulus at temperature, T
k_1, k_2 = defined above with Equation 5.1
T = defined above with Equation 5.1

Figure 5.18, the uncorrected AC modulus compared to the temperature-corrected modulus, depicts the influence temperature has on the AC modulus. Contrary to the microstrain and the GB pressure, as the temperature increased the AC modulus decreased. This was expected because the AC material softens with warmer temperatures and stiffens in colder temperatures. The pavement experiences a strain and pressure due to the AC being a softer material. However, as the material stiffens, the pavement strain and pressure are reduced. The average temperature-corrected modulus was 795 ksi with a standard deviation of 139 ksi and a coefficient of variation of 17.4%.

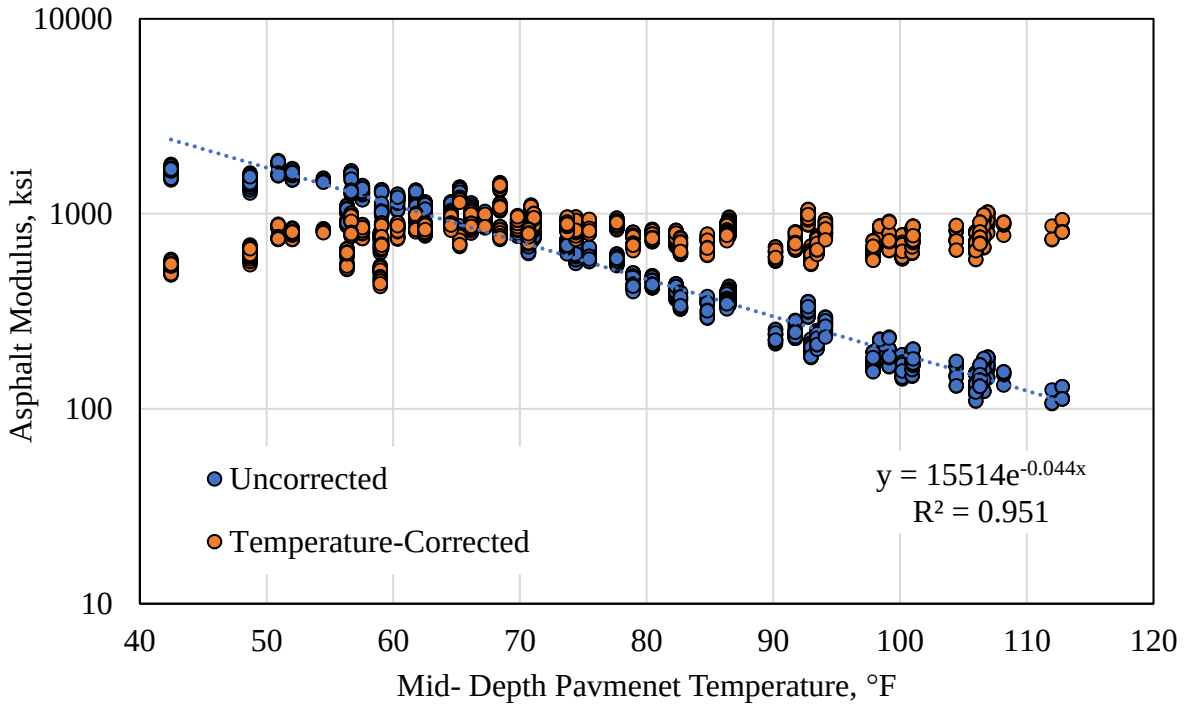

FIGURE 5.18 Asphalt Modulus (Corrected and UnCorrected) versus Temperature.

Figure 5.19 depicts the temperature-corrected AC modulus and date to visualize if the AC stiffness changes with time and without the impact of temperature. As shown below, AC modulus remained steady over the first part of the traffic cycle indicating that the AC layer is performing well over time and there is no indication of pavement distresses. However, there are

still slight vertical variations on each days' data due to the construction variation of each testing location.

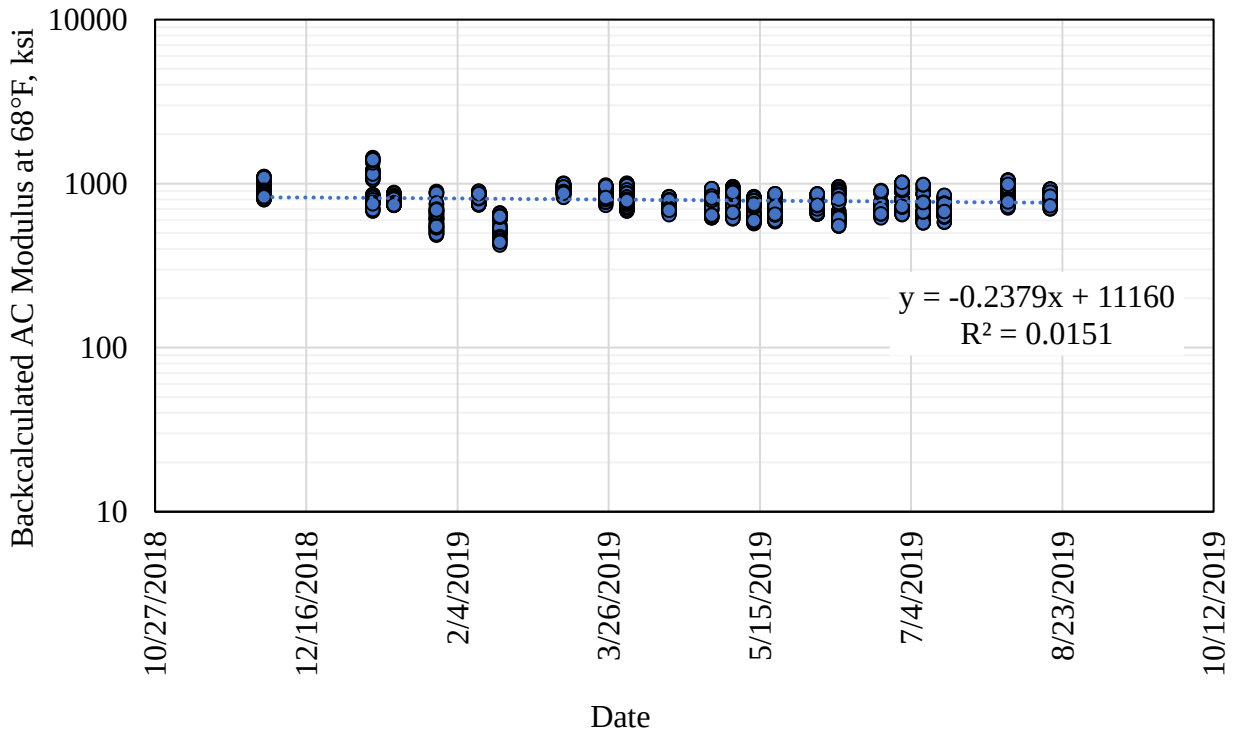

FIGURE 5.19 Temperature-Corrected Asphalt Modulus versus Date.

The FWD backcalculated AC modulus data was also analyzed by wheelpath. Figure 5.20 depicts AC modulus based on wheelpath and date. As seen below, the wheelpaths all look similar indicating that the wheelpath has no impact on the AC modulus. This is significant because the plot indicates that the traffic over time and varying AC temperatures had little impact on the stiffness of the AC. Typically, when a pavement begins to fail, in rutting or cracking, the location of the failure will begin in one of the wheelpaths.

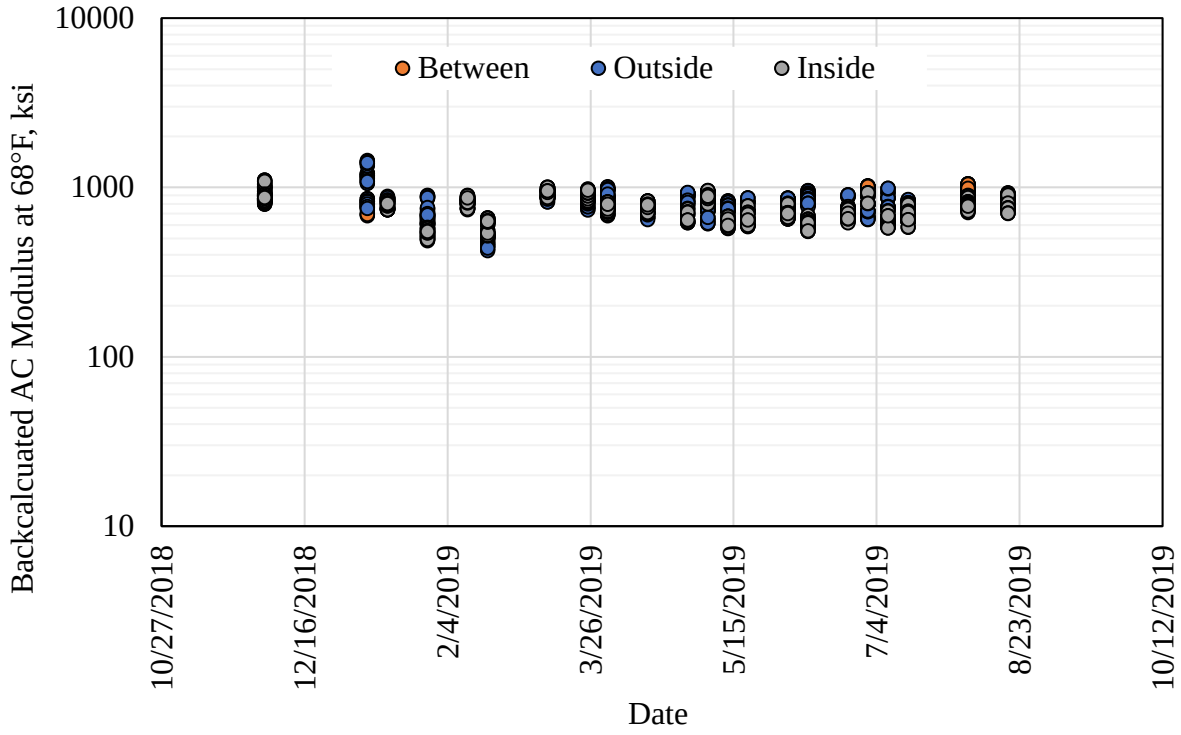

FIGURE 5.20 Wheelpath Asphalt Modulus Comparison.

Table 5.3 lists a few statistics including the count of data points, the average, the standard deviation, and the coefficient of variation to facilitate a more detailed analysis of each wheelpath. As seen demonstrated in Table 5.3, the between wheelpath had the softest average AC layer, whereas the inside wheelpath showed a stiffer average AC layer.

Table 5.3 Wheelpath Statistics

Wheelpath	*Count*	*Average, ksi*	*Standard Deviation, ksi*	*Coefficient of Variation*
Inside	663	745.30	124.20	16.7%
Outside	509	817.47	143.75	17.5%
Between	327	861.09	119.98	13.9%

To determine whether the backcalculated FWD modulus data of each wheelpath differed significantly from the others, the three wheelpaths were subjected to an analysis of variance (ANOVA) test. Table 5.4 summarizes the results of the ANOVA tests performed on all three

wheelpaths, including inside versus outside, inside versus between, and outside versus between with full results shown in Appendix B. The null hypothesis for this analysis was that there were no resulting statistical differences in AC modulus results between the three wheelpaths. This hypothesis is consistent with the observations made regarding Figure 5.20. However, as seen in Table 5.4, each of the four ANOVA tests produced significantly small p-value determining that each wheelpath was significantly different from the other. Although the analysis did determine there was a significant statistical difference, the limited sample size and the magnitude variation illustrated the difference between wheelpaths were not practicaly different.

Table 5.4 ANOVA Wheelpath Analysis

Test	***P-value***	***Accept/Reject***
All 3	1.38E-40	Reject
Inside vs. Outside	1.65E-19	Reject
Inside vs. Between	1.95E-40	Reject
Outside vs. Between	6.01E-06	Reject

The GB modulus and the subgrade were analyzed over time to identify seasonal and short-term trends. Figure 5.21 depicts the GB modulus over time. The average GB modulus was determined to be 4.73 ksi with a standard deviation of 1.10 ksi and a coefficient of variation of 23.2%. This graph illustrates that the GB material remained steady over time indicating the material was not stress dependent. Similar to the AC modulus data, the GB stiffness has vertical variations due to time of day of testing, the resulting testing temperatures, and the construction or spacing variation.

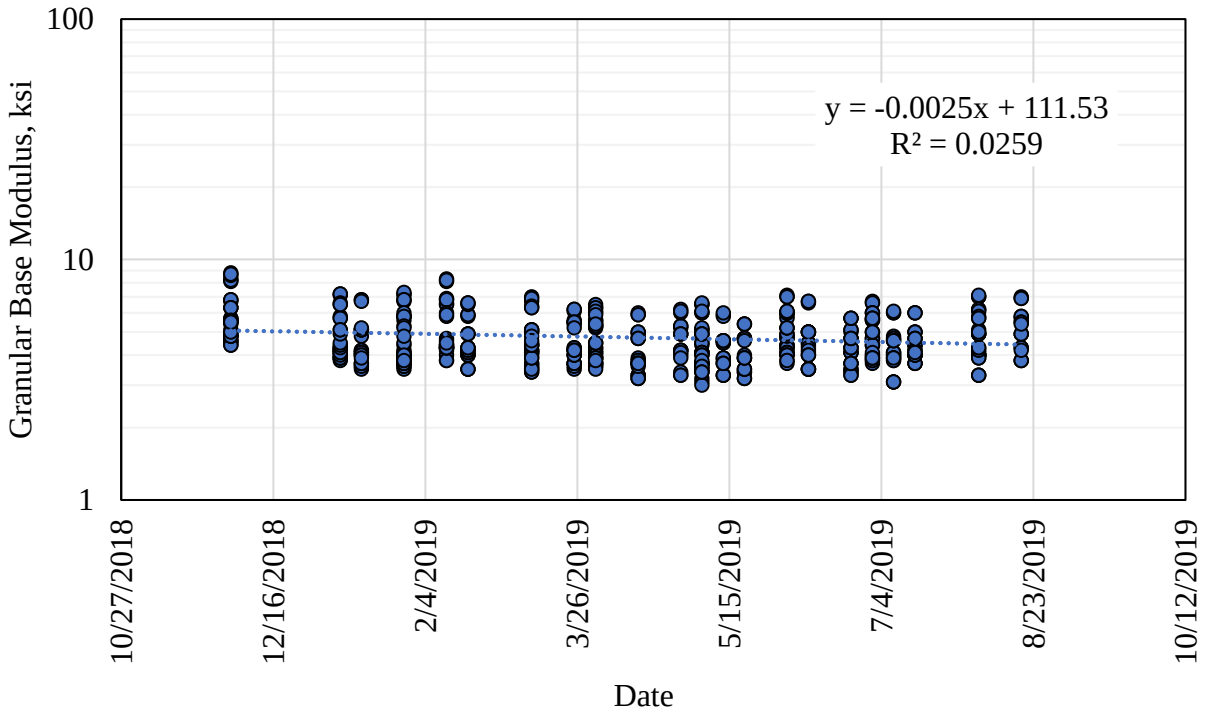

FIGURE 5.21 Granular Base Modulus versus Date.

To determine if the GB was stress dependent, FWD data from a particular day, wheelpath, and random location was chosen to graph against the FWD testing load. The chosen day was May 13, 2019 using the inside wheelpath and random location 2. Figure 5.22 illustrates the GB was not stress dependent with the minimal slope of $-5e^{-5}$ psi.

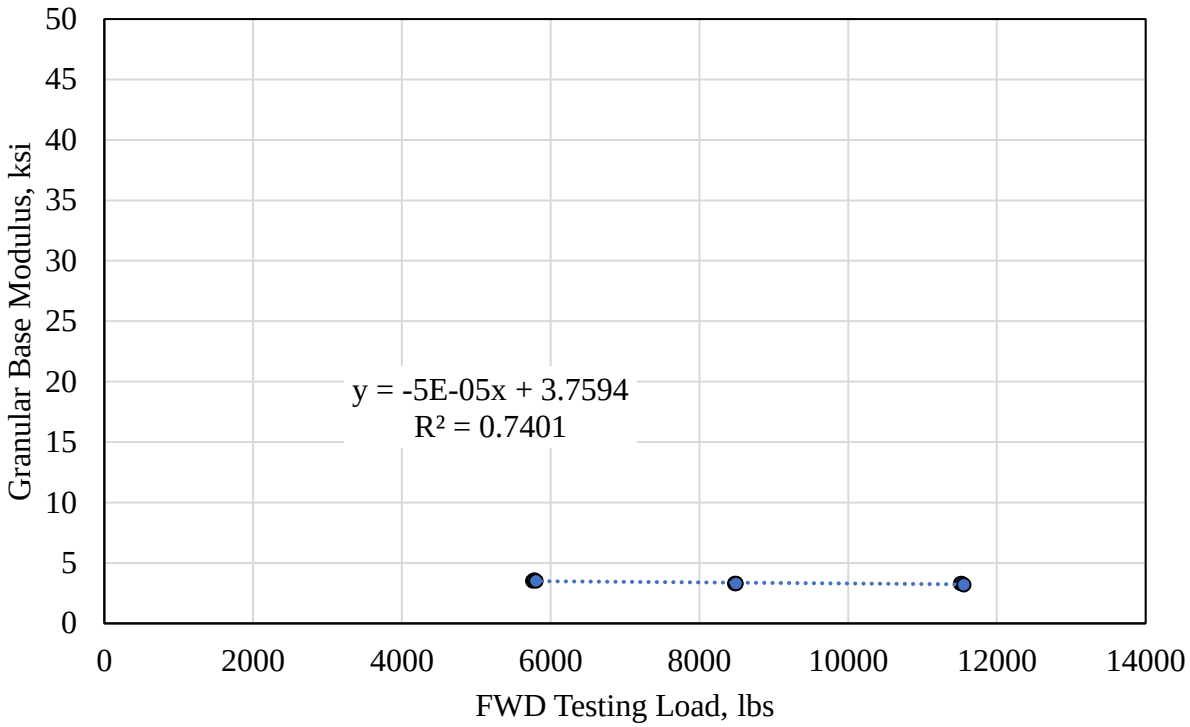

FIGURE 5.22 Granular Base Modulus versus Load.

Lastly, the subgrade soil modulus was analyzed over time as seen in Figure 5.23. As the temperature increased, the subgrade modulus decreased, indicating that the subgrade material might be stress softening soil. As the temperature increased, the AC layer's stiffness decreased, resulting in more stress on the subgrade layer. Similar to the AC and GB layers, as seen below, there is vertical variation due to testing time and temperature variation.

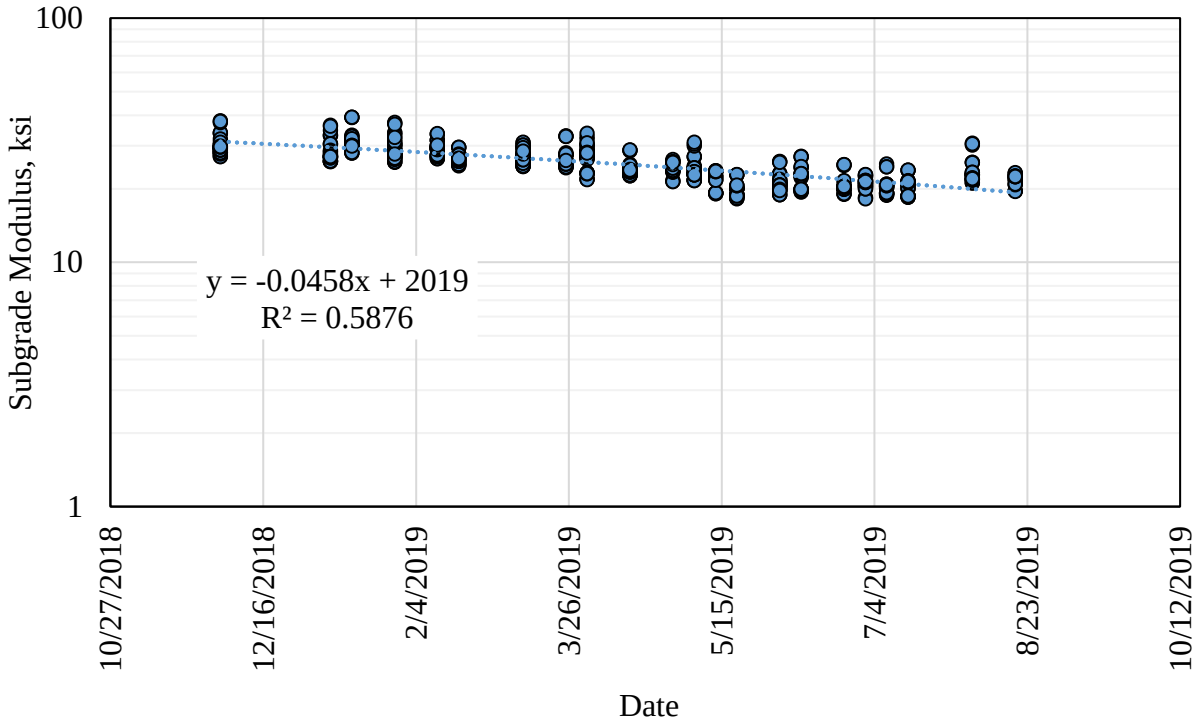

FIGURE 5.23 Subgrade Modulus versus Date.

Figure 5.24 depicts the subgrade modulus versus temperature to determine the soil temperature dependency. As shown below with the negative trendline, the soil's moduli decreased as the temperature increased.

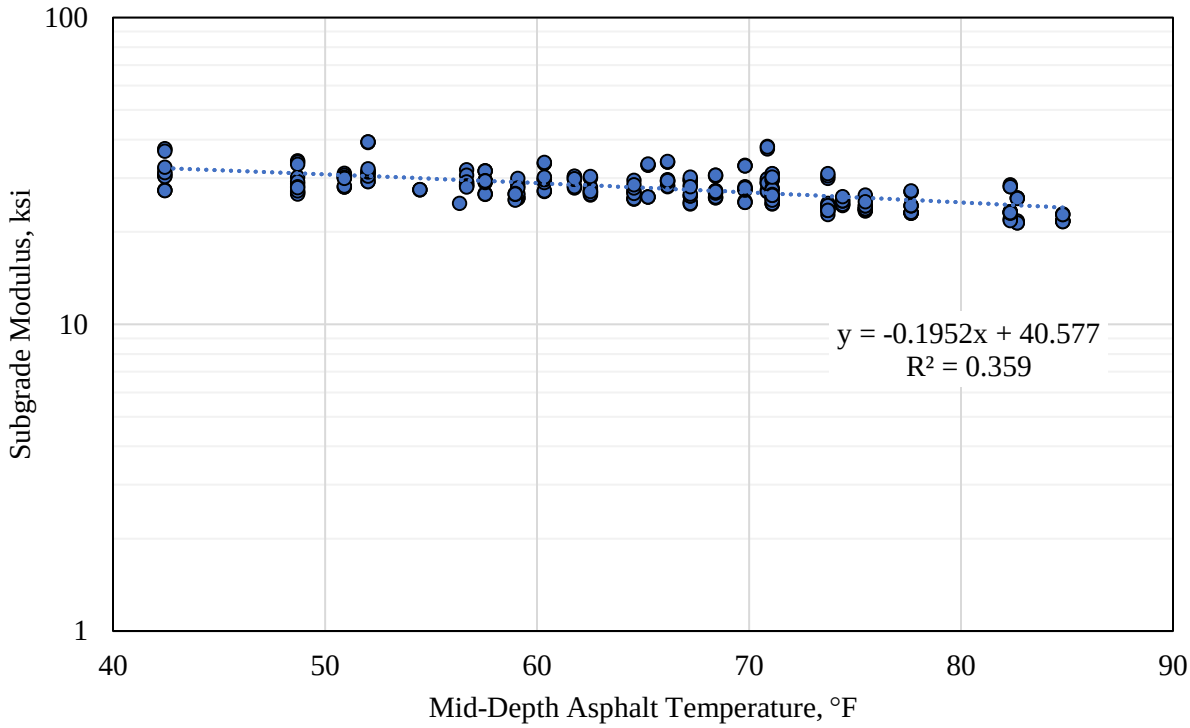

FIGURE 5.24 Soil Subgrade Modulus versus Mid-Depth Asphalt Temperature.

Along with the temperature, the subgrade modulus could be impacted by the load on the pavement. To verify if the subgrade material was stress-softening, the subgrade modulus was plotted against the FWD testing loads from a particular day, location, and wheelpath. Similar to the GB, the day was chosen to be May 13, 2019 in the inside wheelpath at random location 4. As shown below in Figure 5.25, the subgrade has a steeper slope, $-5e^{-4}$ psi/lb., than the GB. The three FWD testing loads created a difference of 300 psi in the soil subgrade. The larger difference between moduli and the negative slope indicates that the soil subgrade is a stress-softening material.

A regression analysis was performed on the slope of the trendlines from Figures 5.22 and 5.25 to determine if there is a true correlation between the FWD testing load and the granular base modulus or the soil subgrade modulus respectively. The results of the Excel regression analysis can be viewed in Appendix E. The null hypothesis of this test was that the true slope

was 0 proving there is no distinct or statistically significant correlation between the FWD load and the granular base or subgrade moduli. Based on the results, the null hypothesis was rejected with a granular base p-value of 0.017 and soil subgrade p-value of 2.52e-7 indicating there is a correlation between the FWD testing load and the layer's moduli. However, the different magnitudes of significance from the granular base and soil subgrade illustrate that the soil subgrade moduli's slope is more statistically significant. This proves that the correlation of the FWD testing load and the soil subgrade is stronger than the FWD testing load and the granular base modulus. Therefore, the conclusion that the soil subgrade modulus is stress-softening and the granular base is not stress-dependent was verified.

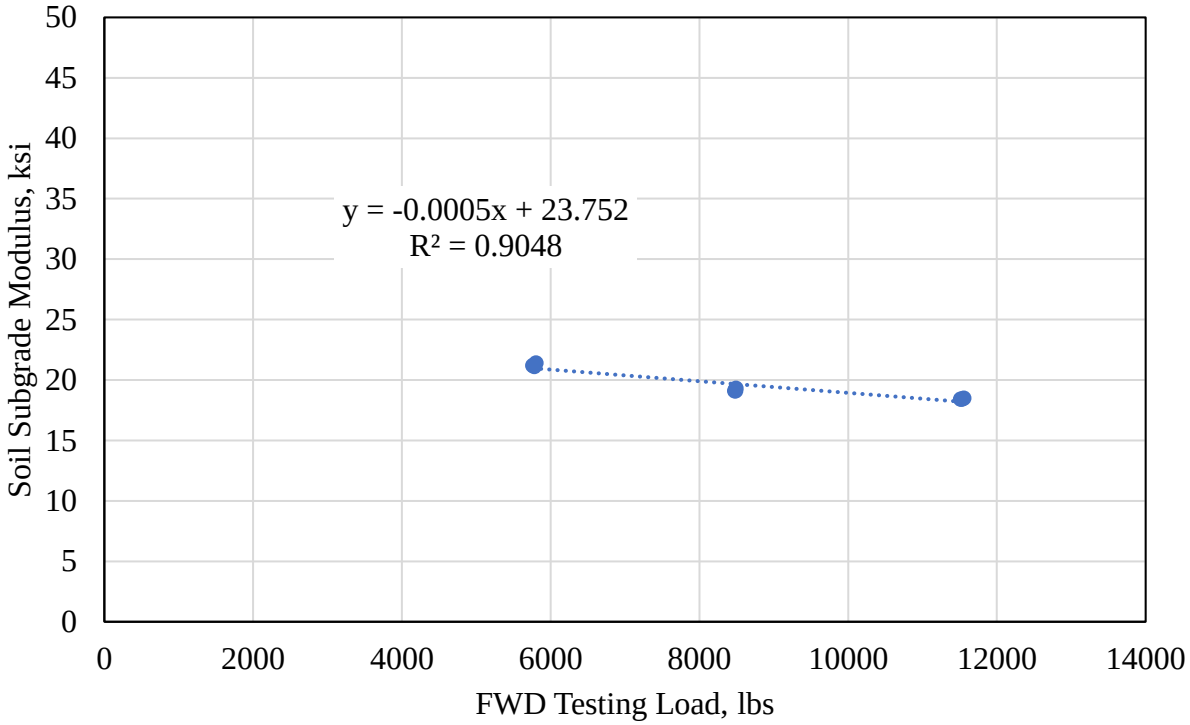

FIGURE 5.25 Soil Subgrade Modulus versus FWD loads.

The Excel correlation function was utilized to further determine the relationship between the AC modulus (E1), the GB modulus (E2), and the subgrade modulus (E3) as shown below in Table 5.5. A few observations were made from the table:

- The AC modulus had a low correlation with the granular base but a strong positive correlation of 0.83 with the soil subgrade.
- The granular base has no correlation with either of two layers.

The observations substantiate what was theorized about the three pavement layers. The soil subgrade modulus depends on the AC layer's stiffness. As the AC stiffness increases with colder temperatures, the soil subgrade modulus increased and vice versa when the AC modulus decreased. Also, the GB modulus acts independently from the AC layer and the soil subgrade modulus and remained steady over seasonal changes.

TABLE 5.5 Correlation Between E1, E2, and E3

	E1	E2	E3
E1	1		
E2	0.096	1	
E3	0.83571	-0.0889	1

COMPARISON OF THICK LIFT PAVEMENT AND CONVENTIONAL PAVEMENT

Without comparing the early performance results to a conventional pavement, it was hard to determine how well the pavement was truly performing. Therefore, S9 was compared to a previous section constructed in 2009 that was a part of the 2009-2012 test cycle. The test section, S9 Control, was placed at the same location and was the control section for another group experiment. The S9 control included three lifts of conventional dense-graded mix over a GB over the Test Track subgrade. The three lifts required a tack between layers, which was a key difference between the thick lift pavement and the older section. Since the thick lift pavement was constructed in one single lift, the possibility of slippage between layers was negated. S9

control contained embedded instrumentation and had similar weekly field performance measures taken.

Figure 5.26 compares cross-sections of the thick lift Section S9 and the 2009 Section S9 control. As observed below, the two test sections provided a very good comparison for two reasons. First, each section was placed on the same location of the Test Track using the same subgrade material. Secondly, the thicknesses of the AC layers and the GB layers were similar to each other. Some factors that may result in differences between the two sections are that each section had different mix designs, each section was paved at different times, the initial traffic was applied one month from each other, the truck configurations are always varying, and each section had slightly varying layer thicknesses. The 2012 Test Track cycle began traffic application on October 23, 2012. While, the 2018 Test Track began initial traffic application on November 26, 2018.

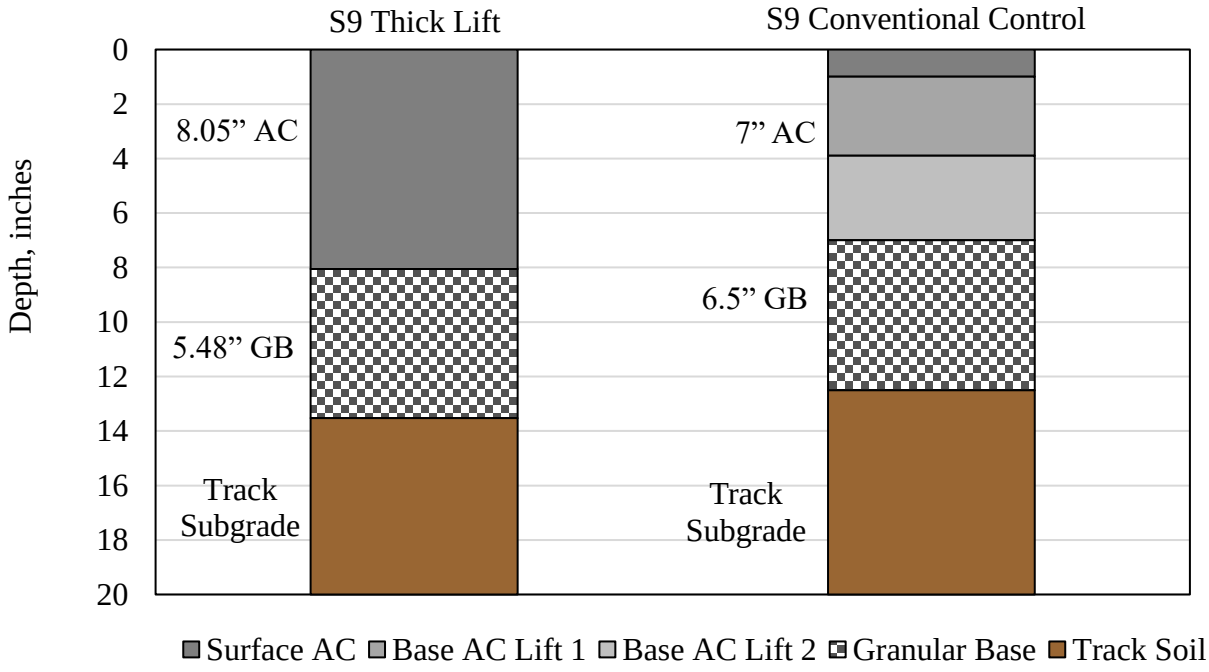

FIGURE 5.26 Thick Lift and Control Cross-Sections.

As noted previously, performance measurements were taken over time to determine the field performance of both sections. Shown below in Figure 5.27 is the rutting comparison of the thick lift S9 and the Control S9. The thick lift S9 had a rut depth of 0.158 inches by 3.815 million ESALs and the 2009 S9 control had a rut depth of approximately 0.170 inches after 3.700 million ESALs. The control did continue to rut slightly over the whole research cycle to a final rut depth of 0.225 inches at 10 million ESALs. With less than half of the traffic applied so far, it is too early to determine if the rutting will continue or if the colder temperatures will prevent further rutting. The thick lift pavement had less initial rutting in the first few million ESALs than the control section due to the pavement thickness. This is due to the fact the thick lift pavement's traffic application began one month later than the control section's traffic. The thick lift section's traffic began on November 26, 2018 while the S9 control's traffic began on October 23, 2012. The traffic for the thick lift pavement began during cooler temperatures, which results in a stiffer AC material and more resistance to initial rutting.

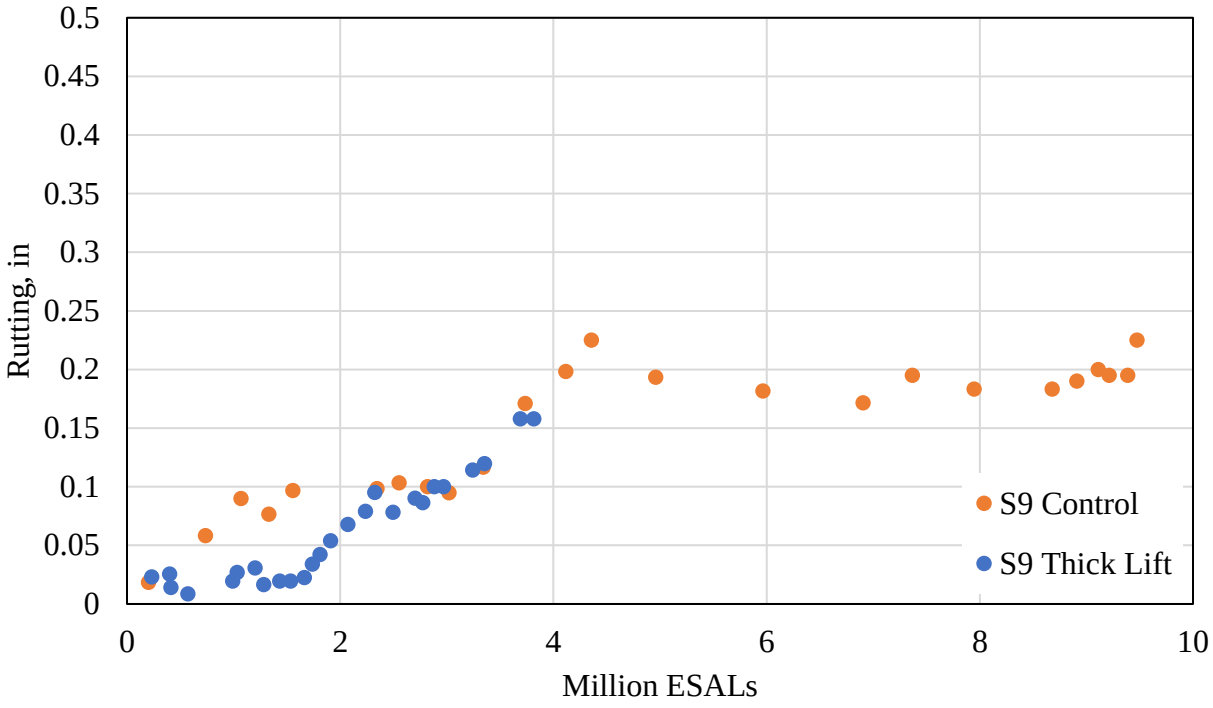

FIGURE 5.27 Section S9 Control versus S9 Thick Lift Rutting.

The tensile microstrain from the 2009 Section S9 was compared to the thick lift S9. With most potential mid-depth temperatures, T2, captured from November 2018 to August of 2019, the microstrain curve should be a good comparison on structural integrity and temperature dependency. Figure 5.27 depicts the impact of microstrain and temperature on each of the two test sections. The 2009 Section S9 control curve was taken from 2009 Test Track report (West et al., 2012). The S9 control curve was created from a previous exponential fitted curve on the control section's plot of microstrain versus temperature which can be viewed in Appendix C. The control S9's fitted equation had an R^2 of 0.89 substantiating that the line is a good fit and could be used in the comparison to Section S9 thick lift.

As shown below in Figure 5.28, each pavement produced very similar trendlines and patterns. The S9 thick lift had higher microstrain at warmer temperatures than the control. However, the magnitude of the difference is very miniscule indicating that the strain level at the

bottom of the AC layer was performing like a typical AC pavement. Traffic loading along with temperature plays a key role on the tensile microstrain of the AC layer. Since each experiment was performed on NCAT's controlled Test Track, the traffic pattern variation is minimal. However, the S9 control illustrates the tensile microstrain curve after all 10 million ESALs were applied to the pavement, while the S9 thick lift pavement on includes data up to 3.815 million ESALs.

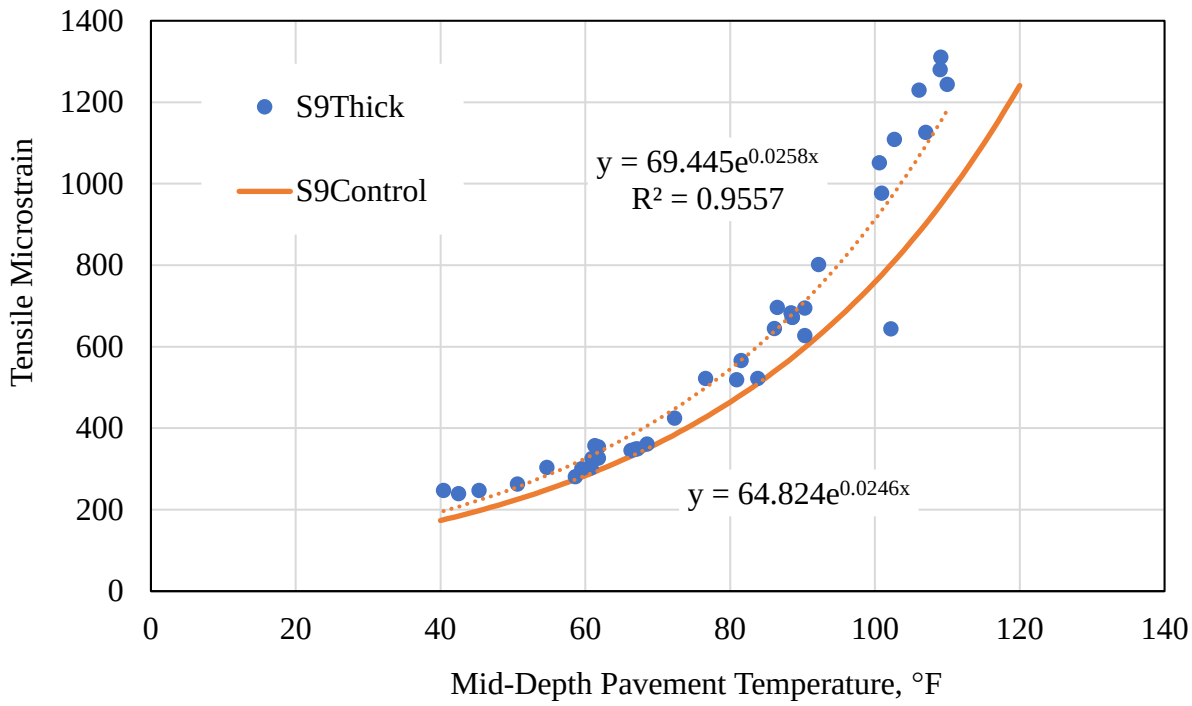

FIGURE 5.28 Tensile Microstrain Comparison of Thick Lift and Control.

The AC layer's modulus of the two sections were also compared as shown in Figure 5.29. The control section S9's data came from the same NCAT 12-10 technical report (West et al., 2012). The trendline taken from the plot, which can be viewed in Appendix C, had an R^2 of 0.96 demonstrating the data fit the trendline well and the trendline could be used in the comparison.

As seen in Figure 5.29, both section's AC modulus are very comparable to each other in pattern, temperature dependency, and magnitude. Like the microstrain response, the AC modulus

of the thick lift was similar to the control. However, the thick lift pavement had a steeper slope as the temperature rose compared to the control. The modulus did act comparable to the control indicating that this pavement would perform well and could be use in lieu of conventional pavement techniques. Again, it should be noted that Section S9 has only accumulated 3.815 million ESALs of traffic and still has more than half of the traffic yet to be applied.

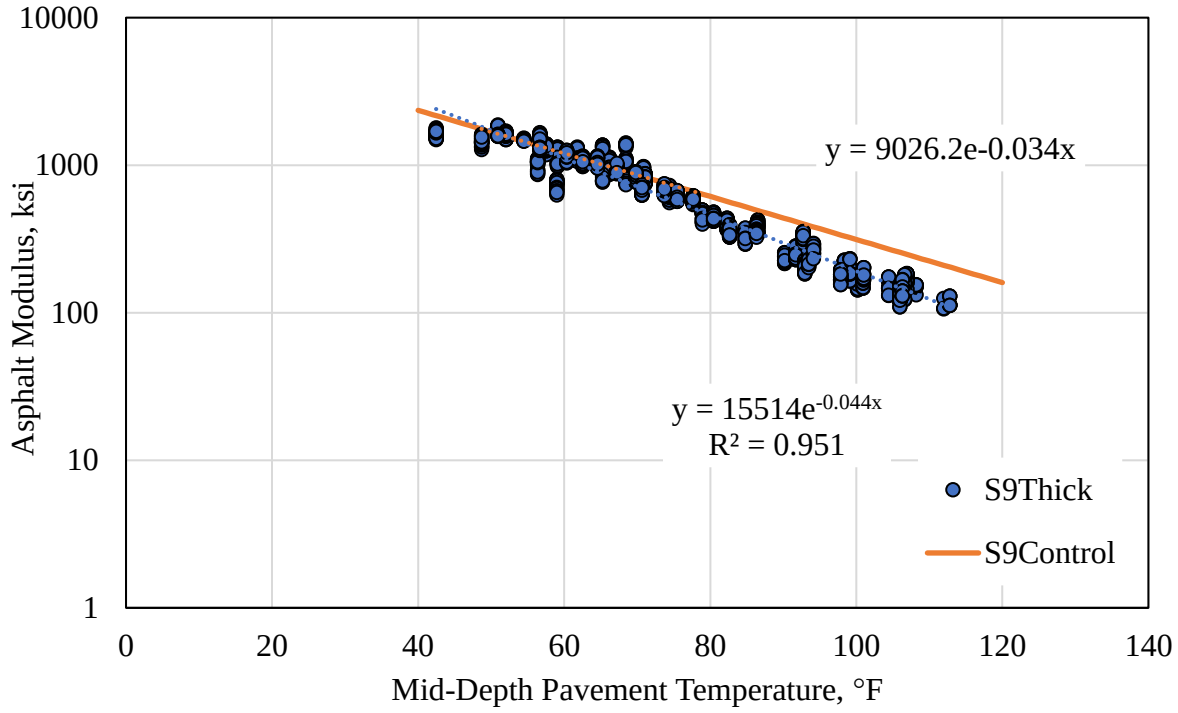

FIGURE 5.29 Asphalt Modulus Comparison of Thick Lift and Control.

SUMMARY

Section S9 thick lift pavement was subjected to an early field performance and structural characterization analysis. Strain and stress measurements at the bottom of the AC layer and the top of the GB layer were collected and recorded weekly. Every week field performance measurements were taken including IRI, rutting, and cracking. Lastly, every two weeks FWD testing was done on the section to look at the pavement's modulus over time and during different seasons.

It was determined that there was no cracking on the pavement as of 3.815 million ESALs. The pavement has incurred approximately 0.17 in of rutting and the IRI of 100 in/mi was in good condition for “new pavements” after diamond grinding occurred.

The AC modulus of the thick lift pavement was temperature dependent based on microstrain, GB pressure, and FWD backcalculated modulus measurements. As the temperature increased, the microstrain and the GB pressure increased exponentially.

However, as the temperature increased the modulus decreased exponentially and the AC softened. It was determined that the AC modulus was correlated to the subgrade modulus but not correlated to the GB modulus. The GB modulus had no significant indication of temperature or stress dependency. However, the subgrade modulus was determined to be a stress-softening material based on the relationship with the AC modulus. As the AC modulus stiffened, the soil subgrade modulus increased and vice versa for a softer AC modulus.

Section S9 thick lift was compared to an older control section that had similar materials, AC thicknesses, and GB thicknesses. The major difference between the two sections was that the control AC layer of approximately 7” was constructed in three lifts, while the thick lift Section S9 was constructed in one lift with an AC layer design thickness of 8”. It was determined through field performance measurements and instrumentation measurements that the two sections, as of August 2019, were performing in a similar fashion. Therefore, it can be concluded the thick lift pavement is performing well during the early stages of the research cycle and could be considered as a viable construction method that does not compromise short term performance.

CHAPTER 6

CONCLUSIONS AND RECOMMENDATIONS

SUMMARY

Thick lifts could be the key to speeding up the AC pavement construction process. A section at the NCAT Test Track was used to analyze if thick lift pavements could be constructed, have predictable cooling curves, and equal or better performance compared to conventional pavements. The pavement was subjected to a construction quality control analysis, cooling curve analysis, weekly field performance testing, and early structural characterization. The performance analysis did not include the entire two year, 10 million ESAL cycle, but rather focused on construction through approximately 3.815 million ESALs of accelerated traffic on the Test Track.

CONCLUSIONS

During construction, it was determined that the thick lift pavement achieved adequate density but did have issues controlling pavement smoothness. The smoothness problem was remedied through diamond grinding. The cooling analysis determined that the pavement would be best paved after sunset. Paving after sunset had the fastest cooling time, as well as the added benefit of not being during peak traffic hours. The results illustrated that nighttime paving had the closest comparison to cooling curve software MultiCool.

Based on weekly field performance testing, the thick lift pavement had no cracking, adequate IRI ratings (100 in/mi), and rut depths below 0.2 inches after 3.815 million ESALs. Section S9's field performance was compared to a conventional pavement. The conventional

pavement rut depth of 0.17 inches after 3.7 million ESALs was similar to the results from the thick lift section.

The thick lift section had embedded instrumentation, ASGs and EPCs, to structurally characterize the pavement. The tensile microstrain, the GB pressure, and the AC modulus were determined to all be temperature dependent. The tensile microstrain and the GB pressure increased exponentially as the temperature increased. Conversely, the AC modulus increased exponentially as the temperature decreased. The GB modulus was neither stress nor temperature dependent. Lastly, the subgrade modulus was determined to be stress-softening. It was determined that the AC modulus was correlated to the soil subgrade modulus and not correlated to the GB modulus. As the AC modulus stiffened, the subgrade modulus increased and vice versa as the AC modulus softened. However, the GB modulus remained constant over time.

The tensile microstrain, the GB pressure, and the AC modulus were used to determine if distresses were forming over time. The results from the field performance and instrumentation revealed no distresses as of August 31, 2019. Section S9's early performance was compared to a conventional pavement section. The comparison revealed that the thick lift pavement was demonstrating similar patterns of temperature dependency and magnitude of the strain at the bottom of the AC layer, the compressive stress at the top of the GB layer, and the AC modulus. Overall, the thick lift pavement performed very similarly to the traditional pavement. Based on all results, as of the first third of the research cycle, the thick lift pavement can be characterized as a successful alternative to conventional paving methods.

RECOMMENDATIONS

It is recommended that thick lift paving be utilized as an alternative to conventional pavements. This study determined that thick lift paving and the resulting benefits can be acquired. A few benefits include rapid construction and producing a homogenous structure that does not require tack to guard against layer slippage. However, a few concerns need to be addressed before implementing thick lift pavements into practice.

The smoothness of the pavement was hard to control and there needs to be a strategy to respond to this issue. For example, incorporating an extra step of diamond grinding into the paving process would be necessary. However, this additional phase can cause problems such as adding time until the pavement could be opened to traffic. Another recommendation is to use the thick lift technique to pave all base layers at once and then place a thin wearing course using traditional methods. This will still speed up the construction process while also correcting the smoothness concerns. Lastly, it is recommended that SCDOT and other agencies that want to implement thick lift paving into practice should introduce a specification that incorporates more realistic goals of IRI values for contractors to strive to achieve.

It is first recommended to complete the research cycle, including finishing the 10 million ESALs of traffic, the weekly field performance testing, the bi-weekly FWD testing, and conduct a final structural analysis. Lab testing such as Hamburg Wheel Test, the Illinois Flexibility Index Test (I-FIT), or the beam fatigue test should be included to correlate field performance of the section to the potential permeant deformation and intermediate cracking susceptibility in the mixture. Another suggestion is to perform a life cycle assessment (LCA) and a life cycle cost analysis (LCCA) on the section and compare the results to a conventional pavement's LCA and LCCA. Since this section includes different aspects of sustainability such as RAP and WMA,

looking at the LCA would provide a better understanding of the ecological impacts of this method of construction compared to conventional techniques. The LCCA would provide an economic analysis comparing the thick lift paving method to conventional paving methods to ensure thick lift paving is even practically feasible. Lastly, if the pavement was determined to be failing at the end of the research cycle and not to be kept in place for the next research cycle, it is recommended that destructive testing should be incorporated into the structural study. It is recommended to subject the section to destructive testing such as coring or even cutting a cross-section of the section to analyze the structural distresses (cracking and rutting). This will help identify where the distresses are beginning within the pavement structure. For example, if cracking is seen at the surface, taking a core on the crack will help determine if the cracking is top-down or if it is propagating from the bottom of the asphalt layer. Determining the extent of all distresses will help clarify which management or rehabilitation strategy would be best for thick lift paving. Lastly, repeating this experiment would be beneficial in analyzing this method further. One way to repeat this experiment would be to use a mix with a larger NMAS such as 19.5mm or 25mm to ensure the thick lift paving method can be used to pave more types of base layer mixtures. Another approach would be to repeat the experiment with two test sections. One test section would be the thick lift pavement and the second would be a conventional paved pavement. The sections should be produced using the same equipment, paved around the same time, and also use the same mixture. This would help better identify any issues with field and structural performance.

REFERENCES

Chadbourn, B.A., D. E. Newcomb, V. R.Voller, R. A. De Sombre, J.A. Lumoma, and D. H. Timm. *An Asphalt Paving Tool for Adverse Conditions.* Report MN/RC-1998-18. Minnesota Department of Transportation, Saint Paul, 1998.

"Fast Fix for Failing Freeway". *For Construction Pros*, 2016, https://www.forconstructionpros.com/asphalt/article/12253773/fast-fix-for-failing-freeway. Accessed 17 June 2018.

Vyce, John M. et al. *Thick-Lift Flexible Paving*. Engineering Research Publications, 1972.

Plati, Christina et al. "Use Of Infrared Thermography For Assessing HMA Paving And Compaction". *Transportation Research Part C: Emerging Technologies*, vol 46, 2014, pp. 192-208. *Elsevier BV*, doi:10.1016/j.trc.2014.05.013.

Tielmann, Moritz R.D., and Stefan Böhm. "Laying Of All Asphalt Courses In One Step". *Transportation Research Procedia*, vol 14, 2016, pp. 3562-3571. *Elsevier BV*, doi:10.1016/j.trpro.2016.05.330.

Timm, D.H., "Design, Construction, and Instrumentation of the 2006 Test Track Structural Study," Report No. 09-01, National Center for Asphalt Technology, Auburn University, 2009.

Timm, D.H. and A.L. Priest, "Flexible Pavement Fatigue Cracking and Measured Strain Response at the NCAT Test Track," Proceedings of the 87th Annual Transportation Research Board, Washington, D.C., 2008.

Timm, David H., and Angela L. Priest. *Material Properties Of The 2003 NCAT Test Track Structural Study*. Auburn, 2006, http://eng.auburn.edu/research/centers/ncat/files/technical-reports/rep06-01.pdf.

Timm, David et al. *PHASE II NCAT TEST TRACK RESULTS*. 2006, http://eng.auburn.edu/research/centers/ncat/files/technical-reports/rep06-05.pdf.

Timm, David, and Kenneth Tutu. "Determination Of An Optimum Backcalculation Cross Section For Unconventional Pavement Profiles". *Transportation Research Record: Journal Of The Transportation Research Board*, vol 2641, no. 1, 2017, pp. 48-57. *SAGE Publications*, doi:10.3141/2641-07.

Timm, D. H., V. R. Voller, E. Lee, ad J. Harvey. CalCool: A Multi-Layer Asphalt Pavement Cooling Tool for Temperature Prediction During Construction. *International Journal of Pavement Engineering*, Vol. 2, 2001, pp. 169-185

Vargas-Nordcbeck, A. and D.H. Timm. Validation of Cooling Curve Prediction Model for Nonconventional Asphalt Concrete Mixtures. *Transportation Research Record 2228*, Transportation Research Board, 2011, pp. 111-119.

West, Randy et al. *PHASE III NCAT TEST TRACK FINDINGS*. NCAT Report 09-08. Auburn, 2009, http://eng.auburn.edu/research/centers/ncat/files/technical-reports/rep09-08.pdf

West, Randy et al. *PHASE IV NCAT PAVEMENT TEST TRACK FINDINGS*. NCAT Report 12-10. Auburn, 2012, http://eng.auburn.edu/research/centers/ncat/files/technical-reports/rep12-10.pdf.

West, Randy et al. *PHASE V (2012-2014) NCAT TEST TRACK FINDINGS*. NCAT Report 16-04. Auburn, 2018, http://eng.auburn.edu/research/centers/ncat/files/technical-reports/rep16-04.pdf.

APPENDIX A

ASG AND EPC CALIBRATION GRAPHS

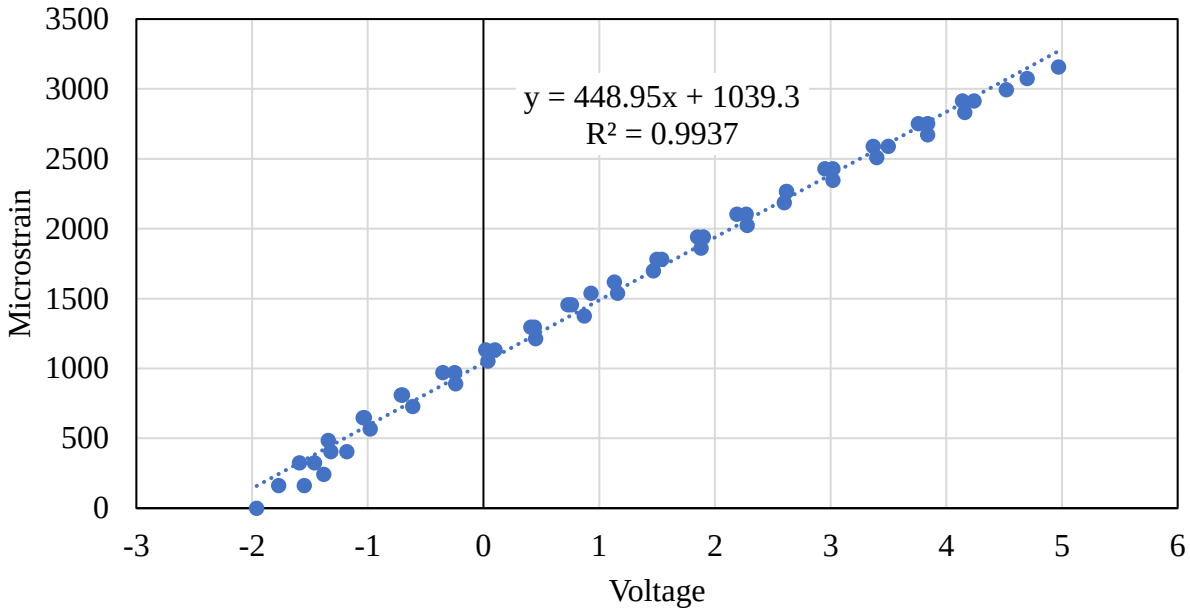

FIGURE A.1 ASG Channel 1 Calibration Graph.

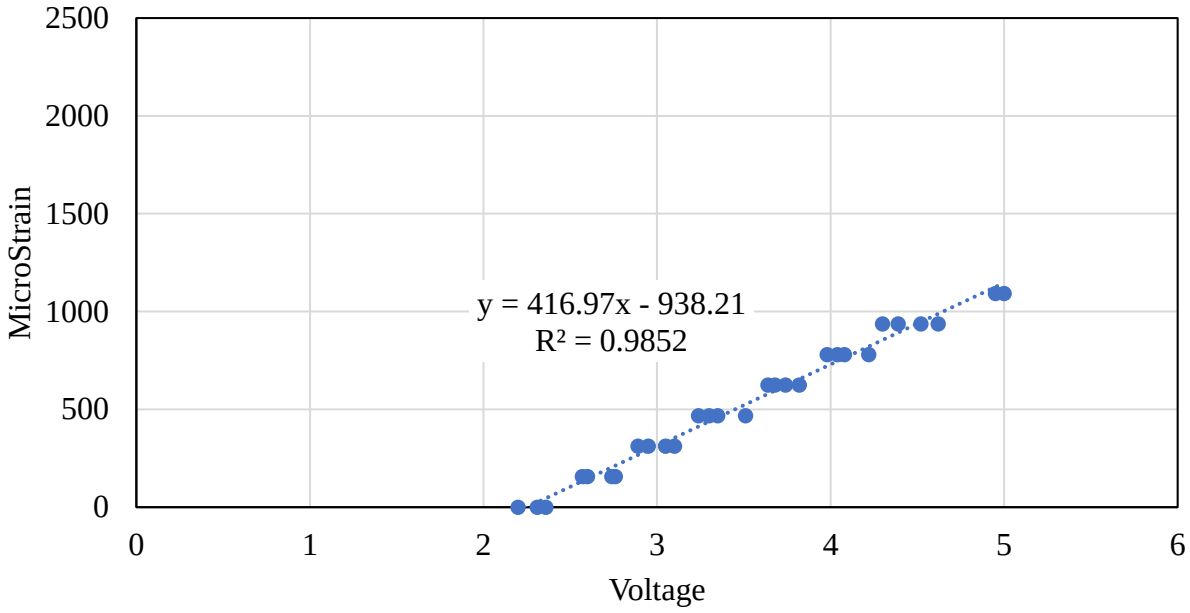

FIGURE A.2 ASG Channel 2 Calibration Graph.

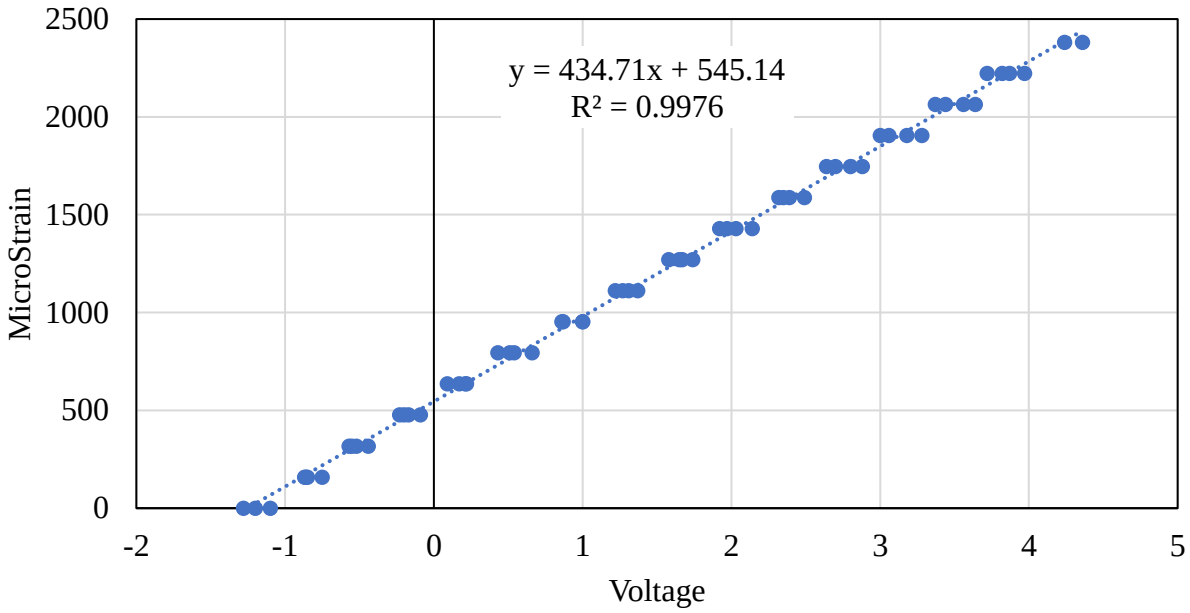

FIGURE A.3 ASG Channel 3 Calibration Graph.

FIGURE A.4 ASG Channel 4 Calibration Graph.

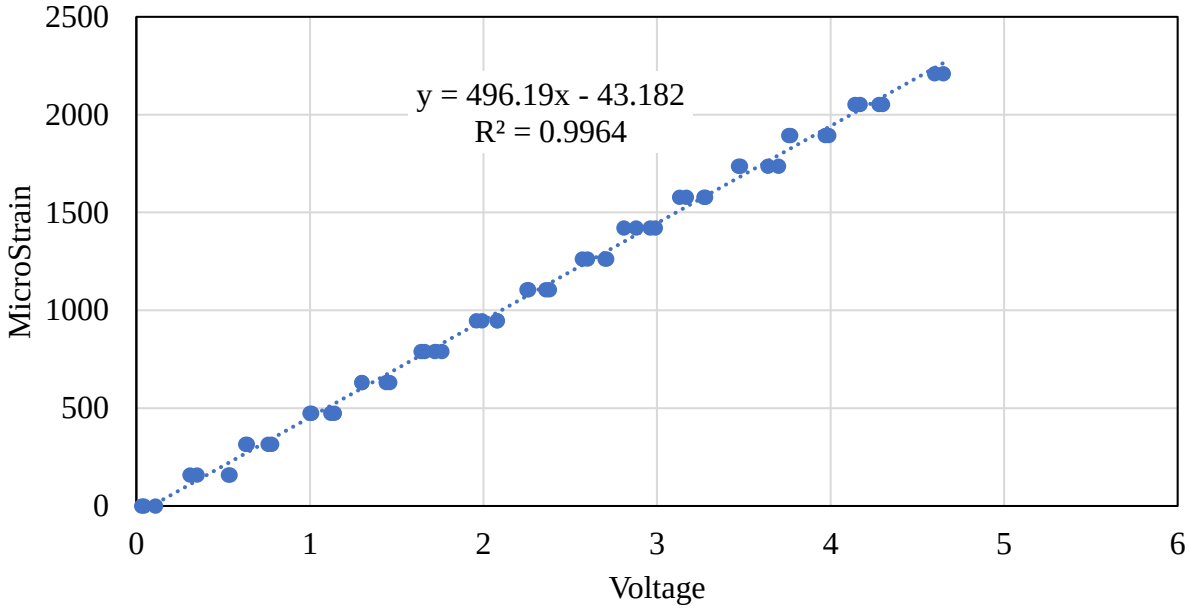

FIGURE A.5 ASG Channel 5 Calibration Graph.

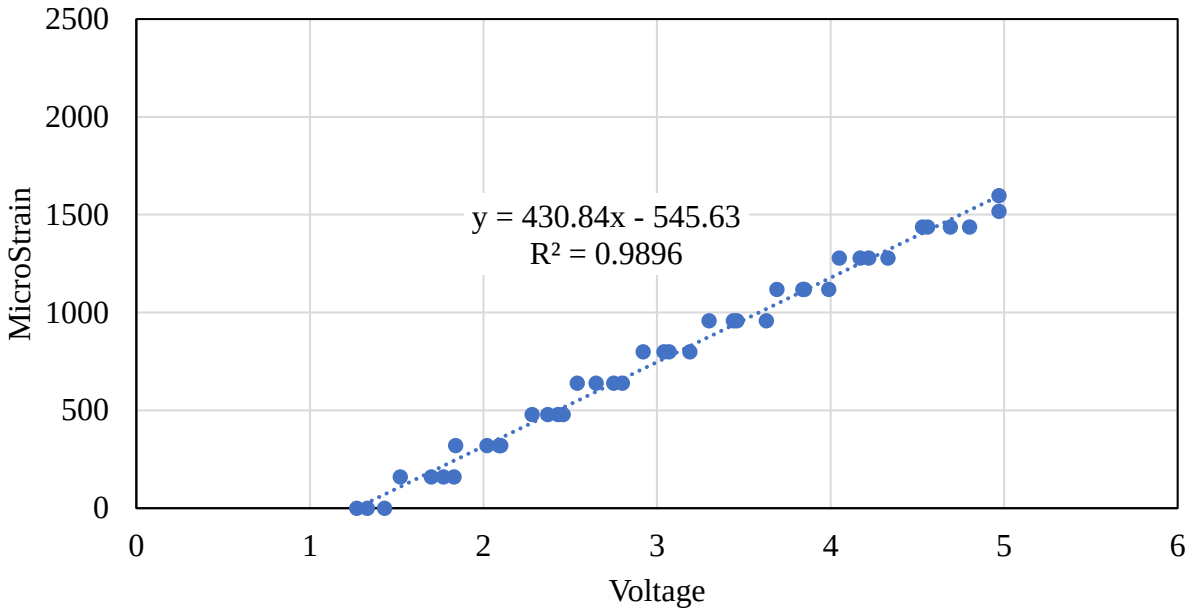

FIGURE A.6 ASG Channel 6 Calibration Graph.

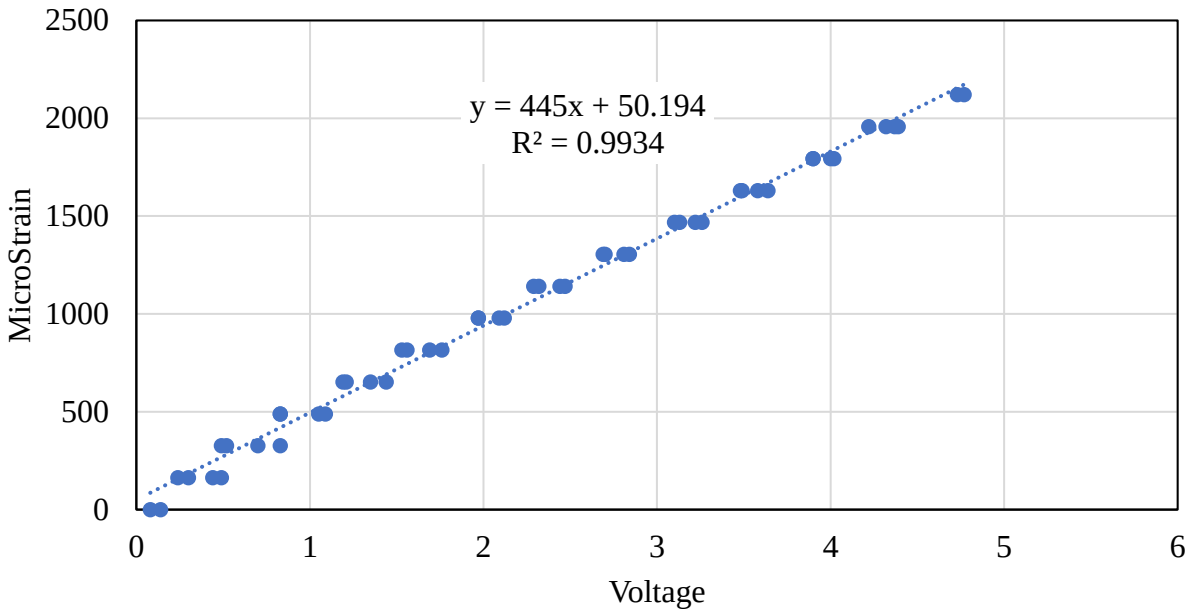

FIGURE A.7 ASG Channel 7 Calibration Graph.

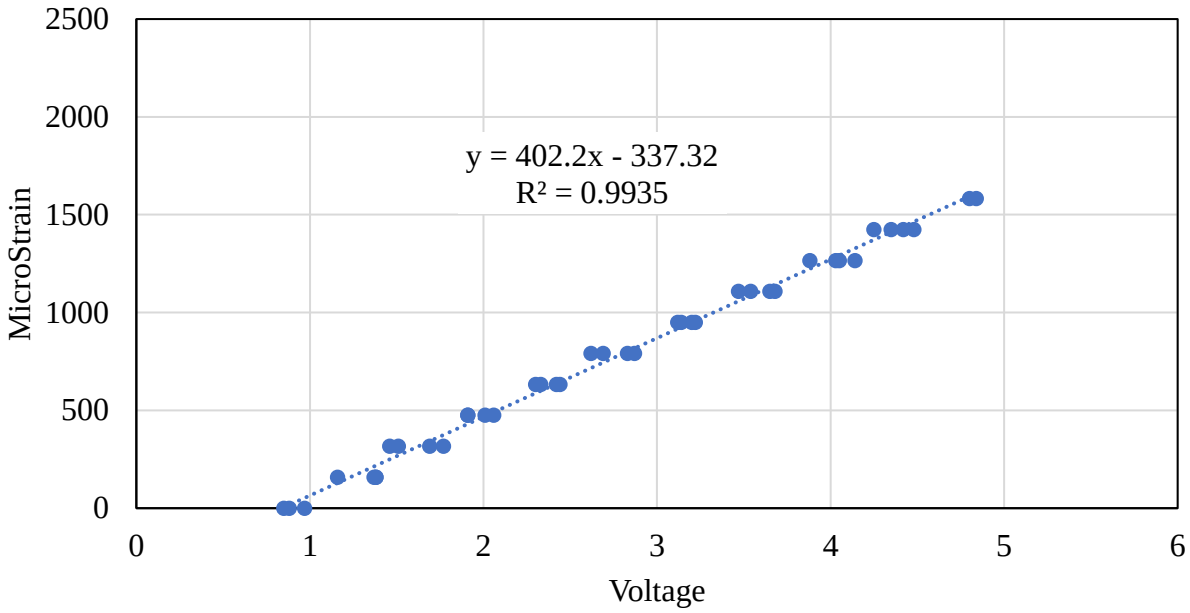

FIGURE A.8 ASG Channel 8 Calibration Graph.

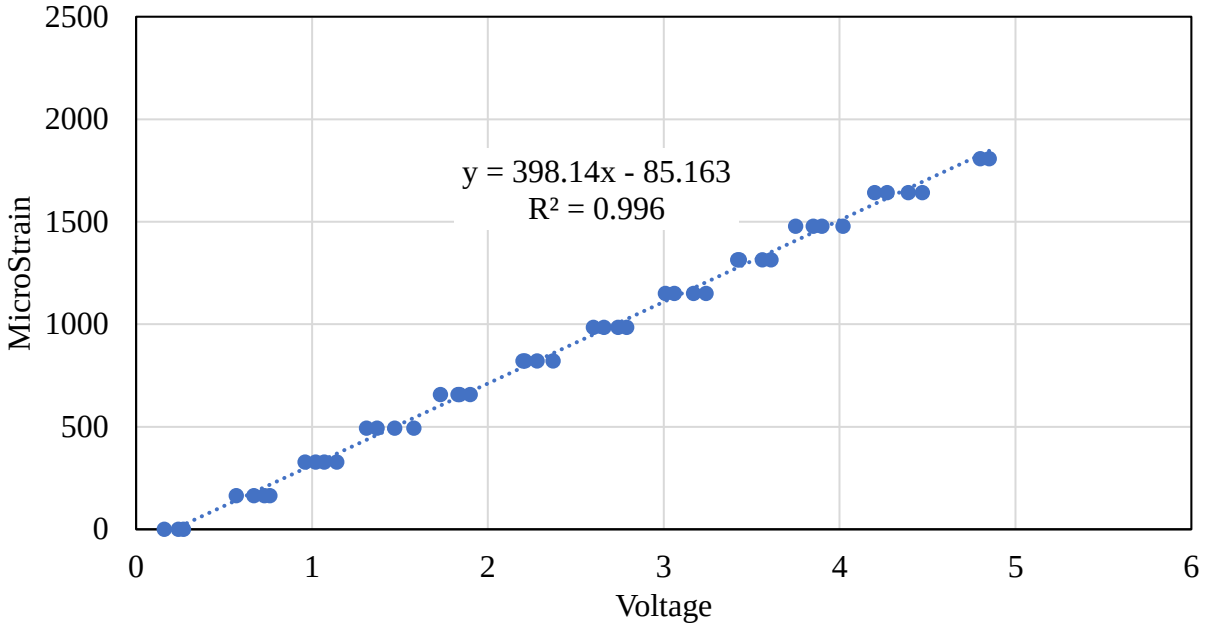

FIGURE A.9 ASG Channel 9 Calibration Graph.

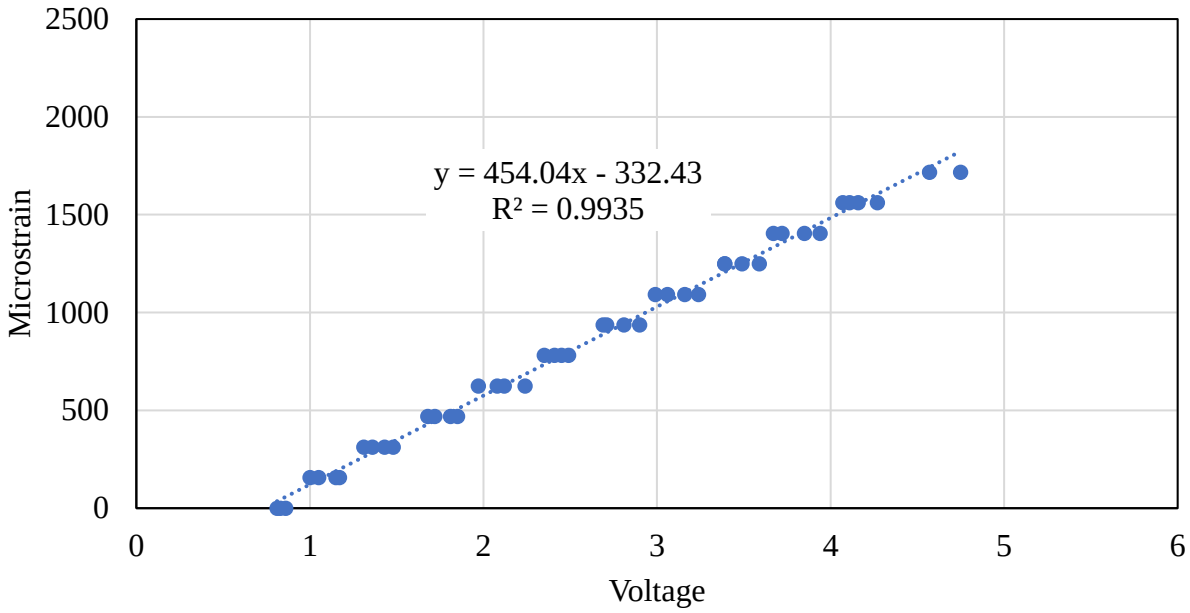

FIGURE A.10 ASG Channel 10 Calibration Graph.

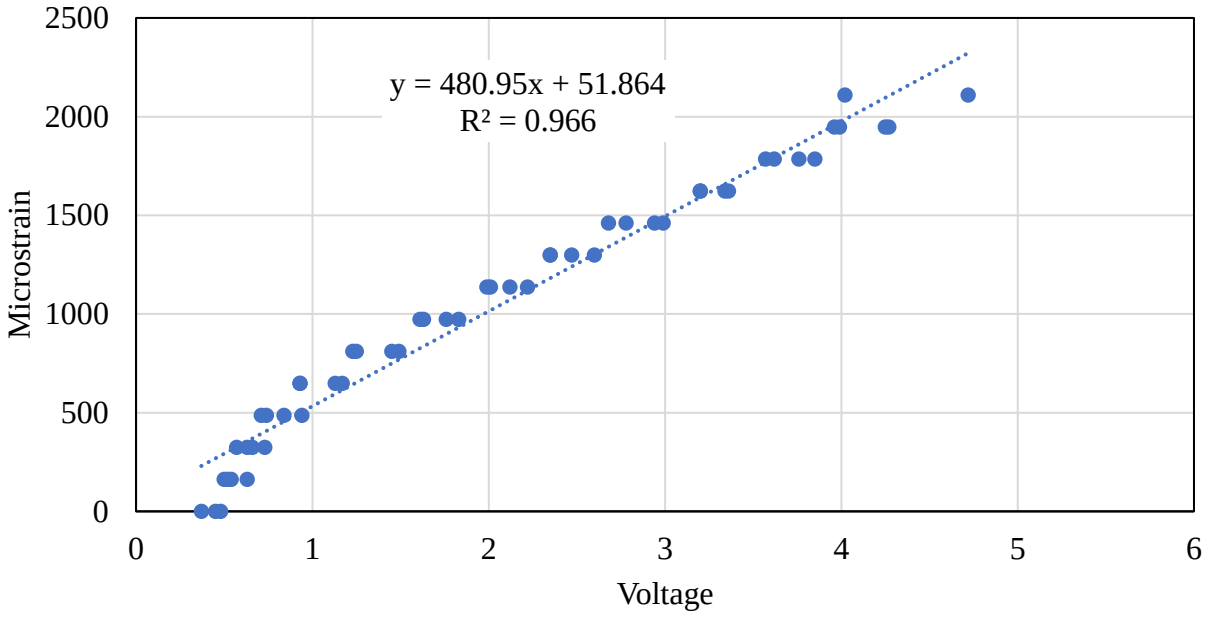

FIGURE A.11 ASG Channel 11 Calibration Graph.

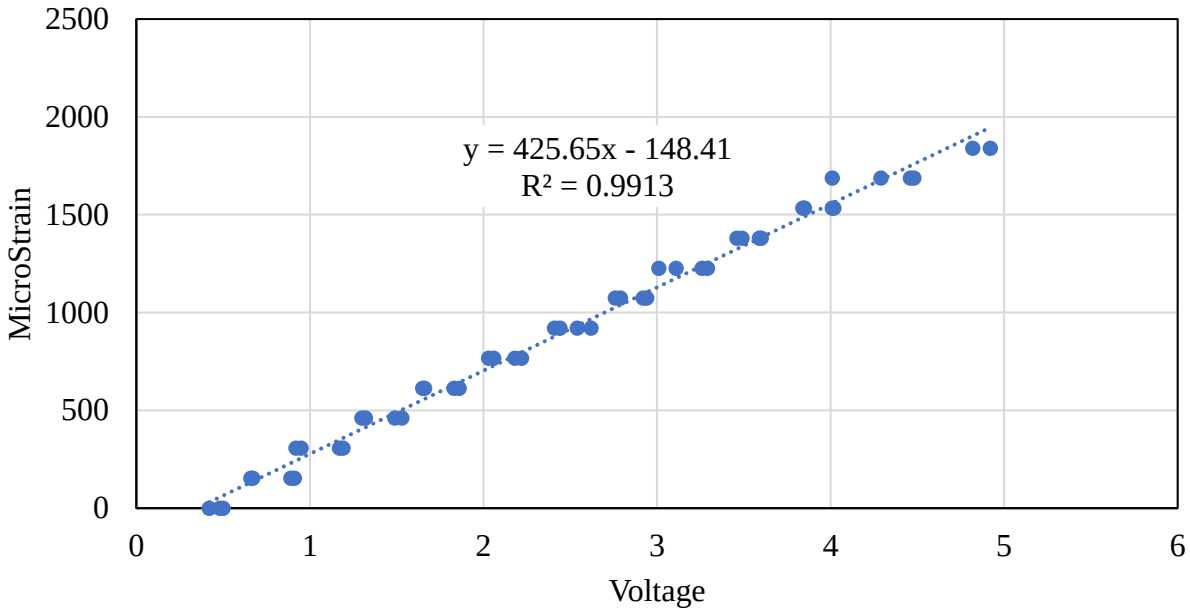

FIGURE A.12 ASG Channel 12 Calibration Graph.

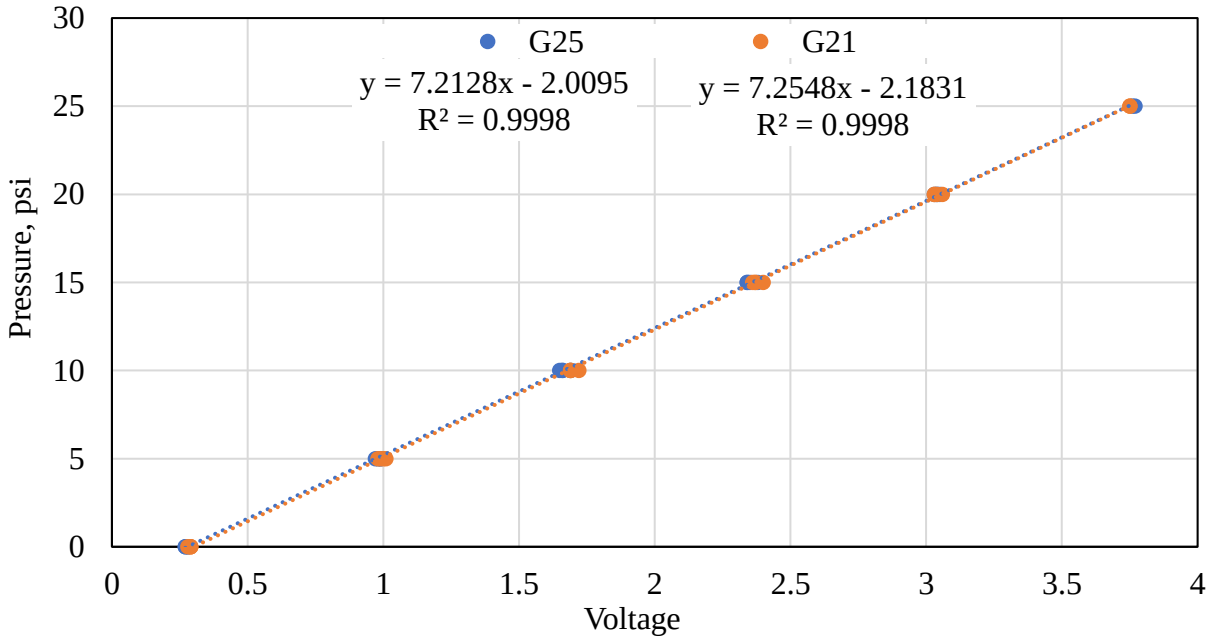

FIGURE A.13 EPC Channels 13 and 14 Calibration Graph.

APPENDIX B

ANOVA ANALYSIS RESULTS

Table B.1 Wheelpath I and O ANOVA Analysis

SUMMARY

Groups	*Count*	*Sum*	*Average*	*Variance*
ITempCorr	663	494134.1	745.3004	15449.95
OTempCorr	509	416091.3	817.4682	20704.48

ANOVA

Source of Variation	*SS*	*df*	*MS*	*F*	*P-value*	*F crit*
Between Groups	1499654	1	1499654	84.57617	1.65E-19	3.849419
Within Groups	20745742	1170	17731.4			
Total	22245396	1171				

Table B.2 Wheelpath O and B ANOVA Analysis

SUMMARY

Groups	*Count*	*Sum*	*Average*	*Variance*
OTempCorr	509	416091.3	817.4682	20704.48
BTempCorr	327	281575.8	861.088	14438.2

ANOVA

Source of Variation	*SS*	*df*	*MS*	*F*	*P-value*	*F crit*
Between Groups	378815	1	378815	20.75123	6.01E-06	3.852633
Within Groups	15224727	834	18255.07			
Total	15603542	835				

Table B.3 Wheelpath I and B ANOVA Analysis

SUMMARY

Groups	*Count*	*Sum*	*Average*	*Variance*
ITempCorr	663	494134.1	745.3004	15449.95
BTempCorr	327	281575.8	861.088	14438.2

ANOVA

Source of Variation	*SS*	*df*	*MS*	*F*	*P-value*	*F crit*
Between Groups	2935964	1	2935964	194.2274	1.95E-40	3.850888
Within Groups	14934722	988	15116.12			
Total	17870686	989				

APPENDIX C

SCDOT SPECIFICATIONS

Supplemental Technical Specification for

Material Properties for Asphalt Mixtures

SCDOT Designation: SC-M-402 (January 1, 2018)

1. SCOPE

1.1 Use the following specifications for preparing, constructing, and accepting Hot-Mix Asphalt (HMA) material properties. **NOTE: Refer to the Standard Specifications, Division 300 for HMA Base Courses and Division 400 for HMA Surface and Intermediate Courses for additional properties and specifications that are not included here.**

2. REFERENCED DOCUMENTS

2.1 SCDOT Standard Specifications

2.1.1 Division 300, Division 400, SC-M-407

2.2 AASHTO Standards

2.2.1 T85, T96, T104, T-312, T335, T340

2.3 SCDOT Test Methods

2.3.1 SC-T-77, SC-T-102

3. REQUIREMENTS FOR MIXTURES

3.1 Requirements for all HMA mixtures.

3.1.1 Have no more than 10% flat and elongated particles based on a 5:1 ratio based on SC-T-77.

3.1.2 Determine coarse aggregate Sodium Sulfate Soundness by AASHTO T 104.

3.1.3 Determine LA Abrasion by AASHTO T 96.

3.1.4 Determine Absorption by AASHTO T 85.

3.1.5 The composition limits are master ranges of tolerances. Conform to a closer control meeting the tolerance requirements as specified in Section 401.2.3.3.

3.1.6 VMA requirements for Surface and Intermediate Courses:

Nominal Max. Aggregate Size	Minimum, %
3/4"	13.5
1/2"	14.5
3/8"	15.5
No. 4	17.5

3.1.7 Use hydrated lime as an asphalt anti-stripping additive (ASA) in all mixes unless otherwise permitted in the following tables.

3.2 If crushed stone is required in the following tables, use crushed coarse aggregate meeting the following requirements:

3.2.1 Have 2 or more freshly mechanically-induced fractured faces meeting the percentage stated in each table based on count of the material retained on the No. 4 sieve as determined by AASHTO T-335.

3.3 Ensure rutting susceptibility is checked based on mix type as determined by AASHTO T340.

3.4 Ensure the Recycled Asphalt Pavement (RAP) conforms to Supplemental Technical Specification SC-M 407.

3.5 D/A Ratio requirements for Surface and Intermediate Courses:

D/A Ratio	**Mix Design Requirement (Washed Gradation)**	**Field Requirement (Dry Gradation) SC-T-102**
Range Limits	0.60 -1.20	0.40-1.00

3.2 Summary of Surface Course Requirements – Design Requirements*

Designation	Type A	Type B	Type C	Type D	Type E
System Application	Interstate Intersections	High Volume Primary	High Volume Secondary	Low Volume Secondary	Seal Course
Gradation Requirements					
1"			----	----	----
¾"	100.0	100.0	100.0	100.0	----
½"	95.0 –100.0	95.0 –100.0	97.0 – 100.0	97.0 – 100.0	----
3/8"	76.0 –100.0	76.0 –100.0	83.0 – 100.0	90.0 – 100.0	100.0
No. 4	52.0 – 75.0	52.0 – 75.0	58.0 – 80.0	70.0 – 95.0	90.0 – 100.0
No. 8	36.0 – 56.0	36.0 – 56.0	42.0 – 62.0	50.0 – 82.0	70.0 – 100.0
No. 30	16.0 – 36.0	16.0 – 36.0	20.0 – 40.0	20.0 – 50.0	36.0 – 70.0
No. 100	5.0 – 18.0	5.0 – 18.0	5.0 – 20.0	6.0 – 20.0	4.0 – 28.0
No. 200	2.00 – 8.00	2.00 – 8.00	2.00 – 9.00	2.00 – 10.00	2.00 – 10.00
Required Design Criteria					
Gyrations	75	75	50	50	50
Binder Limits, %	4.8 - 6.0*	4.8 - 6.0*	5.0 - 6.8*	5.0 - 6.8*	6.0 - 7.0*
Binder Grade	PG 76-22	PG 64-22	PG 64-22	PG 64-22	PG 64-22
Air Voids, %	3.0 – 4.0	3.0 – 4.0	3.5 – 4.5	4.0 – 9.0	NR
VFA, %	70.0 – 80.0	70.0 – 80.0	70.0 – 77.0	60.0 – 70.0	NR
Design D/A Ratio	0.60 - 1.20	0.60 - 1.20	0.60 - 1.20	0.60 - 1.20	NR
Min. Stability 150mm x 95mm (lbs.)					2500
ITS Testing Required?	Yes	Yes	Yes	No	No
Rutting Susceptibility (max mm)	3.0	5.0	NR	NR	NR
Liquid ASA Permitted	No	Yes	Yes	Yes	Yes
Required Aggregate Criteria					
Local Sand Allowed?	No	No	Yes	Yes	No
Crushed Coarse Aggr. Required? (% fractured faces)	Yes (90% min)	Yes (90% min)	Yes (70% min)	No	NR
Coarse Aggr. Max. % Passing No.200	1.50	1.50	1.50	1.50	NR
LA Abrasion (B), max %	55.0	55.0	60.0	60.0	60.0
Sodium Sulfate Soundness, max %	15.0	15.0	15.0	NR	NR
Crusher Run / Asphalt Sand Allowed?	No	No	Yes (25% max)	Yes (50% max)	No
Absorption, max. %	1.5	1.5	1.5	NR	1.5
Limestone Allowed? (CA / Screenings)	No / No	No / Yes	No / Yes	Yes / Yes	No
Slag Allowed?	No	No	Yes	Yes	No
RAP	Yes	Yes	Yes	Yes	Yes (-4)

Asphalt binder content may be increased based on percentage of aged binder in the mixture by OMR. AV and VFA limits will be allowed to extend outside of design ranges above once binder content is adjusted by OMR to assist with coating and provide additional cracking resistance.

3.3 Summary of HMA Intermediate Course Requirements – Design Requirements*

HMA Intermediate Courses				
Designation	**Type A**	**Type B**	**Type B Special**	**Type C**
System Application	New Construction	Interstates High Volume Primary FDP	Rehabilitation Repairs Interstates High Volume Primary FDP	Low Volume Primary Secondary Build up FDP
Gradation Requirements				
1"	100.0	100	100.0	100.0
¾"	90.0 – 100.0	98.0 - 100.0	98.0 - 100.0	90.0 – 100.0
½"	75.0 – 90.0	90.0 – 100.0	90.0 – 100.0	80.0 – 95.0
3/8"	64.0 – 80.0	72.0 – 90.0	72.0 – 90.0	68.0 – 87.0
No. 4	38.0 – 54.0	44.0 – 62.0	44.0 – 62.0	45.0 – 68.0
No. 8	22.0 – 36.0	23.0 – 43.0	23.0 – 43.0	30.0 – 46.0
No. 30	8.0 – 22.0	10.0 – 25.0	10.0 – 25.0	12.0 – 29.0
No. 100	3.0 – 10.0	4.0 – 12.0	4.0 – 12.0	4.0 – 13.0
No. 200	2.00 – 8.00	2.00 – 8.00	2.00 – 8.00	2.00 – 8.00
Required Design Criteria				
Gyrations	75	75	75	50
Binder Limits, %	4.0 – 5.5*	4.5 – 6.0*	4.5 - 6.0*	4.0 - 6.0*
Binder Grade	PG 64-22	PG 64-22	PG 64-22	PG 64-22
Air Voids, %	3.2 - 4.0	3.2 - 4.0	2.5 – 3.0	3.5 - 4.5
VFA, %	70.0 – 78.0	70.0 – 78.0	70.0 – 85.0	70.0 – 77.0
Design D/A Ratio	0.60 - 1.20	0.60 - 1.20	0.60 - 1.20	0.60 - 1.20
Min. Stability (lbs.)	No Requirement (NR)			
ITS Testing Required?	Yes	Yes	Yes	Yes
Rutting Susceptibility (max mm)	3.0	5.0	5.0	NR
Liquid ASA Permitted?	Yes	Yes	Yes	Yes
WMA Required?**	No	No	Yes	No
Required Aggregate Criteria				
Local Sand Allowed?	No	No	No	Yes
Crushed Coarse Aggregate Required? (% fractured faces)	Yes (90% min.)	Yes (90% min.)	Yes (90% min.)	No
Coarse Aggr. – max. % Passing No. 200	1.5	1.5	1.5	NR
LA Abrasion (B), max. %	55.0	55.0	55.0	60.0
Sodium Sulfate Soundness, max %	No Requirement (NR)			
Crusher Run / Asphalt Sand Allowed?	No	No	No	Yes (50% max)
Absorption, max. %	1.5	1.5	1.5	NR
Limestone Allowed? (CA / Screenings)	No / No	No / Yes	No / Yes	Yes / Yes
Slag Allowed?	Yes	Yes	Yes	Yes
RAP	Yes	Yes	Yes	Yes

Asphalt binder content may be increased based on percentage of aged binder in the mixture by OMR. AV and VFA limits will be allowed to extend outside of design ranges above once binder content is adjusted by OMR to assist with coating and provide additional cracking resistance.

****- Chemical process only***

3.4 Summary of HMA Base Course Requirements

HMA Base Courses					
Designation	**Type A**	**Type B**	**Type C**	**Type D**	**Shoulder Widening**
System Application	Interstates Primary	Secondary	Specialty	Specialty	Specialty
Gradation Requirements					
1 ½"	100.0	100.0	----	----	100.0
1"	85.0 - 100.0	85.0 - 100.0	----	----	80.0 - 100.0
½"	60.0 - 80.0	60.0 - 80.0	----	----	75.0 - 92.0
3/8"	----	----	100.0	----	
No. 4	40.0 - 55.0	40.0 - 55.0	90.0 – 100.0	----	45.0 - 65.0
No. 8	30.0 - 45.0	30.0 - 45.0	70.0 – 100.0	----	35.0 - 55.0
No. 30	----	----	36.0 – 70.0	----	
No. 100	----	----	4.0 – 28.0	----	
No. 200	----	----	2.00 – 10.00	----	
Required Design Criteria					
Gyrations	----	----	50	50	----
Binder Limits, %	4.0 - 5.5	4.0 - 5.5	4.3 - 5.7	3.8 - 5.2	3.8-5.2
Binder Grade	PG 64-22	PG 64-22	PG 64-22	PG 64-22	PG 64-22
Min. Stability, lbs.	NR	NR	2500	1500	NR
ITS Testing Required?	No Requirement (NR)				
Rutting Susceptibility (max mm)	No Requirement (NR)				
Liquid ASA Permitted	Yes	Yes	Yes	Yes	Yes
Required Aggregate Criteria					
Local Sand Allowed?	No	Yes	No	Yes	Yes
Crushed Coarse Aggregate Required? (% fractured faces)	Yes (90% min)	No	No	No	No
LA Abrasion (B), max. %	60.0	60.0	60.0	60.0	60.0
Sodium Sulfate Soundness, max %	No Requirement (NR)				
Crusher Run / Asphalt Sand Allowed?	Yes (50% max)	Yes (50% max)	No	No	Yes
Absorption, max. %	No Requirement (NR)				
Limestone Allowed? (CA / Screenings)	Yes / Yes	Yes / Yes	Yes / Yes	Yes / Yes	Yes / Yes
Slag Allowed?	Yes	Yes	Yes	Yes	Yes
RAP	Yes	Yes	Yes (-4)	Yes (-4)	Yes

APPENDIX D

SCDOT IRI SPECIFICATIONS

Table 1. Schedule For Adjusted Payment – New Construction and Multiple Lift Overlay on Interstate and Limited Access Segments	
Segment IRI (inches/mile)	**Price Adjustment – Asphalt Final Riding Course**
Less than 39	107%
39 – 43	105%
44 – 65	100%
66 – 70	95%
71 – 75	90%
76 – 80	80%
Greater than 80	For each additional increment of 5 inches per mile of roughness above 80 inches per mile, reduce payment by an additional 10% from 80% if the DCE determines the material may remain in place.

APPENDIX E

REGRESSION ANALYSIS RESULTS

SUMMARY OUTPUT –
Granular Base Modulus

Regression Statistics	
Multiple R	0.366008
R Square	0.133962
Adjusted R Square	0.112311
Standard Error	0.961636
Observations	42

ANOVA

	df	*SS*	*MS*	*F*	*Significance F*
Regression	1	5.721701	5.721701	6.187341	0.017135
Residual	40	36.98973	0.924743		
Total	41	42.71143			

	Coefficients	*Standard Error*	*t Stat*	*P-value*	*Lower 95%*	*Upper 95%*	*Lower 95.0%*	*Upper 95.0%*
Intercept	5.971058	0.604157	9.883286	2.71E-12	4.750011	7.192105	4.750011	7.192105
X Variable 1	-0.00019	7.51E-05	-2.48744	0.017135	-0.00034	-3.5E-05	-0.00034	-3.5E-05

SUMMARY OUTPUT – Soil
Subgrade

Regression Statistics	
Multiple R	0.699709
R Square	0.489592
Adjusted R Square	0.476832
Standard Error	1.890698
Observations	42

ANOVA

	df	*SS*	*MS*	*F*	*Significance F*
Regression	1	137.1582	137.1582	38.36873	2.52E-07
Residual	40	142.9896	3.57474		
Total	41	280.1479			

	Coefficients	*Standard Error*	*t Stat*	*P-value*	*Lower 95%*	*Upper 95%*	*Lower 95.0%*	*Upper 95.0%*
Intercept	29.23961	1.18785	24.61558	8.89E-26	26.83888	31.64035	26.83888	31.64035
X Variable 1	-0.00091	0.000148	-6.19425	2.52E-07	-0.00121	-0.00062	-0.00121	-0.00062